ELECTROMAGNETIC FLUX MONITORING FOR DETECTING FAULTS IN ELECTRICAL MACHINES

Doctoral Dissertation

Marian Dumitru Negrea

Helsinki University of Technology
Department of Electrical and Communications Engineering
Laboratory of Electromechanics

ELECTROMAGNETIC FLUX MONITORING FOR DETECTING FAULTS IN ELECTRICAL MACHINES

Doctoral Dissertation

Marian Dumitru Negrea

Dissertation for the degree of Doctor of Science in Technology to be presented with due permission of the Department of Electrical and Communications Engineering for public examination and debate in Auditorium S4 at Helsinki University of Technology (Espoo, Finland) on the 29th of November, 2006, at 12 noon.

Helsinki University of Technology
Department of Electrical and Communications Engineering
Laboratory of Electromechanics

Teknillinen korkeakoulu
Sähkö- ja tietoliikennetekniikan osasto
Sähkömekaniikan laboratorio

HELSINKI UNIVERSITY OF TECHNOLOGY P. O. BOX 1000, FI-02015 TKK http://www.tkk.fi	ABSTRACT OF DOCTORAL DISSERTATION

Abstract

The ability of the electromagnetic flux measured in various locations of a 35-kW cage induction motor to provide useful information about faults was investigated. The usefulness of this monitoring parameter was assessed in comparison with some other electrical parameters used for fault detection, such as stator phase current and circulating currents between the parallel branches of the stator winding.

The following faults were investigated in this thesis: a turn-to-turn short circuit in the stator winding; rotor cage-related faults (breakage of rotor bars); static and dynamic eccentricity, and bearing fault.

The relevant fault signatures of the studied electrical parameters were obtained from measurements and/or from numerical electromagnetic field simulations in steady state. These signatures were analysed and compared in order to deduce the most appropriate quantity for the detection of a specific fault. When and where possible, the accuracy of different fault signatures issuing from numerical electromagnetic field simulations was validated by experiments. This investigation is essential since, following a good agreement, it may be assumed that if a monitoring system cannot detect and diagnose an artificial fault from the virtual measurement signals, it is hardly likely to work with real electrical machines, either. In this respect, the numerical methods of analysis limited the present study to such faults that affect the electromagnetic field of a machine.

On the exclusive basis of data obtained from simulations, a study of the modifications brought by various stator winding designs to some of the asymmetrical air-gap electromagnetic flux density harmonics responsible for the detection of various faults was carried out.

The analysis of a core fault (insulation fault in the stator lamination) artificially implemented in the numerical electromagnetic model of the machine in terms of finding a suitable parameter to sense such a fault was also studied in this work.

PREFACE

Espoo, October 2006
Marian Dumitru Negrea

TABLE OF CONTENTS

READING INSTRUCTIONS

There are various ways of setting out references for scientific publications. In this thesis, the references to the literature are indicated using the Harvard (author-date) system. In this system, a textual citation generally requires only the name of the author(s) and the year of publication.

This may appear at the end of a sentence, before the full stop. Alternatively, the author's surname may be integrated into the text, followed by the year of publication in parentheses.

The full references are listed at the end of the work in alphabetical order and require the following details:

For an article
1. **name(s)** of author(s) of the article (surname and initials or given name)
2. **year** of publication
3. **title of article**, in single quotation marks
4. **title of periodical** (italicised)
5. **volume** number
6. **issue** (or part) number
7. **page number(s)**

For a book
1. **name(s)** of author(s), editor(s), or compiler(s) (surname and initials or given name) or the institution responsible
2. **year** of publication
3. **title** of publication and **subtitle** if any (all titles are italicised)
4. **series title** and individual **volume** if any
5. **edition**, if other than first
6. **publisher**
7. **place of publication**
8. **page number(s)** if applicable

For electronic resources
1. **name(s)** of author(s)
2. **date** of publication
3. **title** of publication
4. **publisher/organisation**
5. **edition**, if other than first
6. **type of medium**
7. **date item retrieved**
8. **name** or **site address** on internet (if applicable)

First level chapters are numbered consecutively (1, 2, 3, ...) and subchapters are numbered by chapters (1.1, 1.2,...,2.1, 2.1.1, 2.1.2, 2.2,...,).

The equations, figures and tables are numbered according to a similar rule: chapter_number.equation/figure/table number (i.e. 1.1, 1.2…)

LIST OF SYMBOLS

Symbol overview

$\boldsymbol{A}$, A magnetic vector potential; cross sectional area

$\boldsymbol{B}$, B magnetic flux density

B_r r - component of the magnetic flux density

B_φ φ - component of the magnetic flux density

a, b   points delimiting a short circuited section of the winding

$\boldsymbol{e_z}$ unit vector in the z-direction

f_s supply frequency

f_b mechanical frequency depending on the bearing characteristics

f_r rotational frequency

f_{bng} vibration bearing frequency

f_v characteristic vibration frequency

f_{brb} characteristic frequencies for the detection of broken rotor bar/s

f_{short} characteristic frequencies for the detection of inter-turn short circuits

f_{ecc} characteristic frequencies for the detection of eccentricity

$\boldsymbol{H}$, H magnetic field intensity

H_c coercive field

i electric current

I_c circulating current

$\boldsymbol{J}$, J electric current density

k constant

l length of the conductor

m constant

n constant

N number of turns

n_d eccentricity order

n_w order of the stator time harmonics

N_r number of broken rotor bars

p number of pole pairs; electric power

q constant

Q_2 number of rotor slots

R DC resistance of the conductor

r, φ, z coordinates of a circular cylindrical coordinate system

s slip

S integration surface

t time

u voltage

v reluctivity

σ conductivity

ϕ	electric scalar potential
φ_p, φ_w	phase angles
Ω	electric scalar potential
ω_1	fundamental angular frequency of the supply voltage
ω_r	rotor angular velocity

Abbreviation overview

MCSA	motor current signature analysis
MMF	magnetomotive force
AC	alternating current
DC	direct current
FE	finite element
rms	root mean square value
UMP	unbalanced magnetic pull
FFT	fast Fourier transformation
brb	broken rotor bars
ecc	eccentricity
NB	stator winding configuration consisting of no parallel branches (see Appendix II)
SB	stator winding configuration consisting of two parallel branches – special configuration (see Appendix II)
2B	stator winding configuration consisting of two parallel branches (see Appendix II)
4B	stator winding configuration consisting of four parallel branches (see Appendix II)
meas.	measurements
simul.	simulations
cf	core fault
$p\pm1$	search coils purposed to sense the air-gap electromagnetic flux

1 INTRODUCTION

1.1 Background and importance of fault diagnosis and condition monitoring

Electrical machines have been used extensively for many different industrial applications since several decades ago. These applications range from intensive care unit pumps, electric vehicle propulsion systems, and computer-cooling fans to electric pumps used in nuclear power plants. The electrical energy that is consumed in (induction) motors accounts for around 60% of the electrical energy that is consumed by industry in developed economies (Williamson 2004).

The present-day requirement for the ever-increasing reliability of electrical machines is now more important than ever before and continues to grow. Advances are continually being made in this area as a result of the consistent demand from the power generation and transportation industries. Because of the progress made in engineering and materials science, rotating machinery is becoming both faster and lighter, as well as being required to run for longer periods of time. All of these factors mean that the *detection*, *location*, and *analysis* of *faults* play *a vital role in the good operation of the electrical machine* and are essential for major concerns such as the *safety*, *reliability*, *efficiency*, and *performance* of applications involving electrical machines. Although continual improvement in design and manufacturing has become a priority task among contemporary manufacturers of electrical machines, faults still can and do occur.

Since the analysis and design of rotating machinery is critical in terms of the cost of both production and maintenance, it is not surprising that the fault diagnosis of rotating machinery is a crucial aspect of the subject and is receiving ever more attention. As the design of rotating machinery becomes increasingly complex, as a result of the rapid progress being made in technology, so *machinery condition monitoring strategies must become more advanced in order to cope with the physical burdens being placed on the individual components of a machine*.

When faults do occur and the machine fails in service, the result could, at best, be the loss of production and revenue, or, at worst, catastrophic for the industrial process and potentially dangerous to the operators.

The issues of *preventive maintenance, on-line motor fault detection*, and *condition monitoring* are of increasing importance, taking into consideration essential concerns such as:

- *ageing motors*,
- *lack of redundancy in the event of a machine failure*,
- *high-reliability requirements*,
- *cost competitiveness*.

During the past twenty years, there has been a substantial amount of research into the creation of new condition monitoring techniques for electrical machine drives, with new methods being developed and implemented in commercial products for this purpose (Chow 2000, Benbouzid 1999, Nandi et al. 2005). The research and development of newer and alternative diagnostic techniques is continuous, however, since *condition monitoring and fault diagnosis systems should always suit new, specific electric motor drive applications*. This continuous research and development is also supported by the fact that no specific system/technique may be considered generally the best for all the applications that exist, since *an operator must treat each motor drive as a unique entity*. In this respect, the *potential failure modes*, *fundamental causes*, *mechanical load characteristics*, and *operational conditions all have to be carefully*

taken into consideration when a monitoring system is to be designed or selected for a specific application (Thomson 1999).

The large amount of previous work carried out in the area of fault diagnosis and condition monitoring shows that there have been many challenges and opportunities for engineers and researchers to focus on. Various recommendations and solutions concerning condition monitoring technologies have been given in this area, mainly depending on the *machine type*, *size*, *operating conditions (loading)*, *available instrumentation*, *cost constraints* etc.

In order to allow analysts to correlate different aspects of each technology to troubleshoot symptoms and determine a course of action to avert failures, *several fields of science and technology*, such as *electrical*, *mechanical*, *thermal*, and sometimes *chemical engineering should be closely considered and combined whenever possible*. This is also a stringent requirement when aiming to build a competitive condition monitoring system.

1.2 Aim of the work

The main aim of this thesis is to *study the ability of electromagnetic flux to provide useful information about various faults in an induction machine*. The usefulness of this monitoring parameter will be assessed in comparison with some other electrical parameters used for fault detection, such as *stator phase current* and *circulating currents between the parallel branches of the stator winding* (if there are such).

Another aim of this thesis is to *validate by experiments*, when and where possible, *the accuracy of different fault signatures issuing from numerical electromagnetic field simulations*.

On the exclusive basis of data obtained from simulations, a *study of the modifications brought by various stator winding designs to some of the asymmetrical air-gap electromagnetic flux density harmonics responsible for the detection of various faults* will be carried out.

The *analysis of a core fault* (*insulation fault in the stator lamination*) artificially implemented in a numerical electromagnetic model of a machine, in terms of finding a suitable parameter to sense such a fault, is also studied in this work.

The area of interest for this thesis is restricted to induction machines but, the possibility of extrapolating the findings to other machine types is discussed at various points.

1.3 Scientific contribution

Scientific contribution of the author

First of all, this study represents a detailed analysis of the electromagnetic flux patterns that are supposed to provide potential useful information about a fault in an induction machine. For capturing such patterns, six search coils were employed in the measurements and four search coils in the simulations. The complexity of this sensor network for capturing the electromagnetic flux in various parts of the electrical machine and the critical comparative analysis of the indications provided by various fault indicators may be viewed as an important contribution to the existing state of the art in this research area.

The investigation carried out on finding the ability of electromagnetic flux eccentricity harmonics of the order "$p\pm1$" to detect machine abnormalities other than various types of eccentricity, both from measurements and simulations, is considered a new contribution.

This study also presents an attempt to implement in numerical simulations an insulation fault located in the stator lamination and to suggest an electrical fault indicator that may be confidently used to detect such an abnormality.

The investigations of the modifications brought by various stator winding designs to: 1) some of the asymmetrical air-gap electromagnetic flux density harmonics responsible for the detection of various faults, and 2) to the ability of stator branch currents and, also, circulating currents to sense such faults are considered to be further original contributions.

Contribution of other members of the research team

Most of the present research work was carried out as a part of a collaborative research project between the Laboratory of Electromechanics and Laboratory of Control Engineering of Helsinki University of Technology. The research project was entitled *"Fault detection and diagnosis for AC electrical machines"*. The industrial partners involved in this project were ABB Industry Oy, KCI Konecranes International Oyj, KONE Oyj, and Kuppari Mittaus Oy.

The main task of the Laboratory of Electromechanics was to develop simulation models and to carry out measurements for electrical machines working under both faulty and healthy conditions. Relying on the data provided by the Laboratory of Electromechanics, the main task of the Control Engineering Laboratory was to develop advanced signal processing techniques for fault diagnosis in electrical machines.

Antero Arkkio – played a very active role in providing comprehensive guidance and supervision throughout this work. Since he is the developer of the finite element electromagnetic field simulation code used in this work for modelling the electrical machinery, he made a major contribution by implementing the faults and by giving an insight into the capabilities and features offered by this tool.

Pedro Jover Rodriguez – made an important contribution in building and tuning the experimental measuring set-up. As a member of this project affiliated to the Laboratory of Electromechanics, he also contributed to this work with several comments on various aspects of the research.

A part of the results presented in this thesis were previously reported in conference and journal papers. Among the most representative of these papers are the followings: Negrea et al. (2002, 2004, 2005, 2006) and Pöyhönen et al. (2003). This thesis collects, unifies and summarises these previous reported results besides presenting the ones that were not yet reported in a publication.

1.4 Structure of the work

The structure of the research work is reflected in the divisions of the thesis:

1. Chapter 2 presents an *overview of the faults to be found in various types of electrical machines* together with a *description of the possible causes, failure mechanisms and symptoms produced by each fault*.

2. Chapter 3 offers a *general view of the fault indicators usually used for detecting faults in electrical machines*, with a special focus on current and electromagnetic flux monitoring, since this thesis relies only on the indications provided by these parameters.

3. Chapter 4 deals with the description of the methods of analysis used in this work: *numerical electromagnetic field analysis (simulations)* and *measurements.* Following a short history of the development of finite element methods in the area of electrical engineering, this chapter then describes the finite element analysis procedure used in the modelling of a cage induction motor. The faults implemented in the motor's structures and their modelling procedures are discussed. A description of the measurement set-up used for the validations of the results obtained from simulations and a brief presentation of the signal processing techniques used in the field of fault detection in electrical machines is also to be found in this chapter.

4. Chapter 5 reports the *results obtained from the simulations and measurements*.

5. Finally, the results obtained both from the simulations and measurements are discussed in Chapter 6, while Chapter 7 concludes by considering the most important findings of this work. The areas of the work which the author believes could be extended and improved in future research work are also discussed in Chapter 7.

2 FAULTS IN ELECTRICAL MACHINES

2.1 General

A *fault* in a component is usually defined as a condition of reduced capability related to specified minimal requirements and is the result of normal wear, poor specification or design, poor mounting (here also including poor alignment), wrong use, or a combination of these. If a fault is not detected or if it is allowed to develop further it may lead to a *failure* (Thorsen and Dalva 1999).

Several surveys have been carried out on the reliability of electrical machines. In such surveys, a large number of machine operators were usually questioned on the types and frequency of faults occurring in their plant. The largest of these surveys, carried out by the General Electric Company, was reported in an EPRI (Electric Power Research Institute) publication (1982) and covered about 5000 motors, approximately 97% of which were three-phase cage induction motors. According to this survey, Fig. 2.1 presents the distribution of faults occurring in the motors surveyed. It must be noted that Fig. 2.1 provides data from machines working in many different applications and in several different branches of industry. It is known that the occurrence of any of the fault types will depend heavily on the specific application of the machine. For example, it has been found that in cage induction machines, the incidence of rotor cage failures can be at least as high as stator winding failures in applications where the machine is continuously being stopped and restarted under a heavy load (drilling machines in the oil and mining industries).
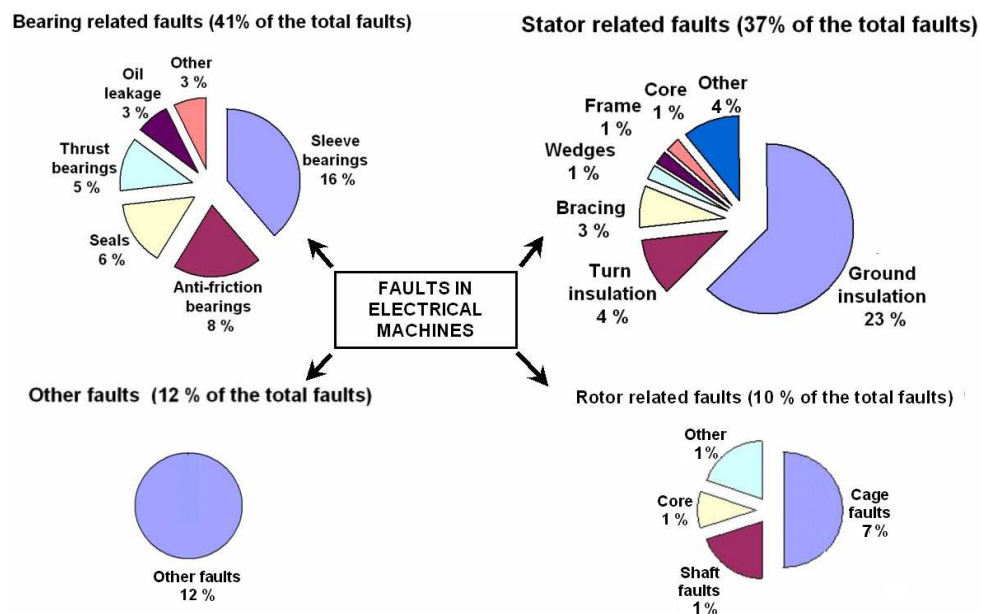
Fig. 2.1 Distribution of faults (EPRI 1982).
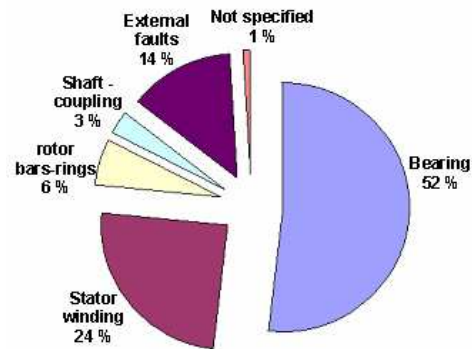
Fig. 2.2 Distribution of failures among failed components for electrical machines working in the petrochemical industry (Thorsen and Dalva 1999).

Based on the work of Thorsen and Dalva (1999), Fig. 2.2 is intended to highlight the failure distribution among failed components in 483 high-voltage induction motors working in the same branch of industry, i.e. the petrochemical industry. Such motors very often operate in extreme conditions within offshore activities. They are often started directly on-line, which leads to large starting currents and torque pulsation. These conditions are harmful for the motor, weakening different machine components in time. Comparing the results of this survey with the ones presented by EPRI (Fig. 2.1), it becomes clear that *the occurrence of a specific fault type depends considerably on the specific application of the machine and on the environment the machine is operating in.*

Since some electrical machines are subject to different environmental conditions (such as moisture intrusion in most offshore activities), it is important to have an idea about the dependence of the failure rate on the environment. In this respect, Thorsen and Dalva (1999) show that *the failure rate for motors situated outdoors in extremely tough conditions (in both onshore and offshore plants) may be 2.5 times higher than the failure rate for motors situated indoors.*

2.2 Fault types in electrical machines

This section presents a comprehensive description of the most common faults to be found in electrical machines. For each fault, the possible causes and mechanisms of failure are briefly outlined.

According to Nandi and Toliyat (1998), the major faults arising in electrical machines may generally be classified as:

- stator faults resulting in the opening or shorting of the winding,
- turn to ground faults,
- abnormal connection of the stator windings,
- a broken rotor bar or cracked rotor end-rings,
- static and/or dynamic air-gap irregularities,
- a bent shaft which results in rub between the stator and rotor, causing serious damage to the stator core and windings,
- shorted rotor field winding,
- demagnetisation of permanent magnets,
- bearing and gearbox faults.

2.2.1 Winding faults – Stator- and rotor-related

General

Industrial surveys and other studies have shown that a large percentage of failures in an electrical machine result from a fault related to the stator winding and core (EPRI 1982, IEEE 1985). Many works have indicated that the majority of motor stator winding failures result from the destruction of the turn insulation. In most cases, this failure starts as a *turn-to-turn fault* that finally grows and culminates in major ones such as *coil-to-coil*, *phase-to-phase*, or *phase-to-ground failure*, ultimately causing *motor breakdown* (Kliman et al. 1996).

Shorted turns in the stator winding belong to that class of faults that may often have a negligible effect on the performance of the machine but the presence of which may eventually lead to a catastrophic failure. Therefore, stringent demands for means to minimise the occurrence and mitigate the effects of turn insulation breakdown are highly desirable (Stavrou et al. 2001).

Causes

The stator winding of an electrical machine is subject to stresses induced by a variety of factors, including, among the chief ones, thermal overload, mechanical vibrations, and voltage spikes caused by adjustable-frequency drives etc. According to Tavner and Penman (1987), some of the most frequent causes of stator winding failures are:

- high stator core or winding temperatures,
- slack core lamination, slot wedges, and joints,
- loose bracing for end winding,
- contamination caused by oil, moisture, and dirt,
- short circuits,
- starting stresses,
- electrical discharges,
- leakages in the cooling systems.

Failure mechanisms and symptoms produced by the fault

Early investigations on failure mechanisms in motors (Crawford 1975) concluded that the great majority of failures seemed to be associated with wire insulation, resulting in low-power intermittent arcing, which causes erosion of the conductor until enough power is drawn to weld them. Crawford claims that once the welding has occurred, high induced currents in the shorted loops lead to rapid stator failure.

Short circuits in stator winding

In large generators and motors in power plants, the stator and rotor winding insulation is exposed to a combination of thermal, electrical, vibrational, thermo-mechanical, and environmental stresses during operation. In the long term**,** the multiple stresses cause ageing, which finally leads to insulation breakdown. For this reason, it is important to estimate the remaining insulation integrity of the winding after a period of operating time.

Deterioration of the winding insulation usually begins as an inter-turn fault involving a few turns of the winding. A turn fault in the stator winding of an electrical machine causes a large circulating current to flow in the shorted turns. Such a circulating current is of the magnitude of twice the locked rotor current; it causes severe localised heating and sustains favourable conditions for the fault to rapidly spread to a larger section of the winding (Kliman et al. 1996). The locked rotor currents are of the order of 6-10 times the rated current (Rotating

Electrical Machines Part 15 1995), (Wiedenbrug et al. 2003). If left undetected, turn faults can propagate, leading to catastrophic phase-ground or phase-phase faults.

Excessive heating caused by turn-to-turn shorts is the reason why motors in this condition will almost always fail in a matter of minutes, if not seconds. A basic rule of thumb to consider is that *every additional 10°C causes the winding to deteriorate twice as fast as when the operation takes place in the allowable temperature range*. Failure of the insulation between the winding and ground can cause a large ground current, which would result in irreversible damage to the core of the machine. This fault may be so severe that the machine might even have to be removed from service. If the fault is detected at an early stage, the machine can be put back into service by just re-winding the stator, while, on the other hand, replacing the whole motor means increased downtime (Tallam et al. 2003).

For high-voltage machines and large low-voltage machines, the development of a time delay between a direct turn-to-turn short circuit and ground insulation failure is very short, probably only a few seconds. For these types of machines, regular monitoring of the winding insulation condition utilizing on-line *Partial Discharge* analysis was successfully used since the '70s (Nattrass 1993). On-line monitoring of discharge activity in the structure of a stator winding produces an accurate indication of the deterioration process. Regular monitoring provides the opportunity for early detection of problems and possible remedial action thereby prolonging the life of the machine. For smaller machines, the development of a time delay between a direct turn-to-turn short circuit and ground insulation failure can be from some minutes up to as much as some hours, depending on the severity of the fault and the loading of the motor.

Another fault associated with the stator winding is called "*single-phasing*". In this case, one supply line or phase winding becomes open-circuited. The resulting motor connection has a line voltage directly across two phases (assuming a "star" connected machine) which is equivalent to a single-phase circuit.

The effect of an insulation fault between turns is to eliminate a turn or group of turns from the stator winding. This will be of little consequence but it will be quantifiable in the flux distribution in the air-gap (Penman et al. 1994).

Fig. 2.3 shows an inter-turn short circuit between two points, a and b, of a complete stator winding. The path to the circulating current between these points is closed and the path $A–A'$ can be expanded into two independent circuits. Fig. 2.3 shows that the two currents, the phase current and the current which flows in the short circuited part, produce opposite MMFs. Therefore, inter-turn short circuits have a cumulative effect in decreasing the MMF in the vicinity of the short-circuited turn(s). Firstly, when a short circuit occurs, the phase winding has less turns and, therefore, less MMF. Secondly, the short-circuit current MMF is opposite the MMF of the phase winding. The circulating current I_c is a result of the galvanic contact between points a and b but also due to the contribution brought by the transformer effect or mutual induction.
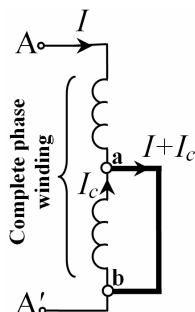
Fig. 2.3 Inter-turn short circuit.

2.2.2 Stator core-related faults

General

Stator core problems are rare (1% of all faults, according to Fig. 2.1) compared to stator winding problems and such problems are not usually a major concern for small machines. However, the repair/rebuild process is more costly in the case of a stator core failure, since it usually requires the entire core to be replaced. Therefore, there has been interest in identifying the causes of core problems and finding ways of monitoring the core in order to detect and prevent stator core failure, especially in the case of large machines, where the cost of repair and outage can be significant (Tallam et al. 2003).

Tavner and Anderson (2005) stated that such faults are relatively rare, even for large electrical machines. The same authors claim that on many occasions the details of such failures assume major commercial significance, and therefore failure investigations have, of necessity, to be handled in a confidential manner, touching as they do on the design, manufacture, operation, and insurance of large electrical plant. This may be one of the reasons why no literature on core faults has been published but the scientific principles of the mechanisms at work have been studied in considerable detail and papers published on those principles in the international literature.

Causes

The stator cores of electrical machines are built from thin insulated steel laminations with the purpose of minimising the eddy current losses for higher operational efficiency. In the case of medium/large machines, the core is compressed after the core laminations are stacked in order to prevent the individual lamination sheets from vibrating and to maximise the thermal conductance in the core.

According to Tavner and Penman (1987) and Kliman et al. (2004), the main causes of stator core failure are:

- core end-region heating resulting from axial flux in the end-winding region,
- core melting caused by ground fault currents,
- lamination vibration resulting from core clamping relaxation,
- loosening of core-tightening at the core end resulting from vibration during operation,
- relaxation of lamination material resulting from the compression of insulation material with time and temperature,
- manufacturing defects in laminations – non-uniform thickness within lamination sheets causes cumulative non-uniform pressure distribution,
- inter-laminar insulation failure,
- mechanical damage to the inner surface of the stator during assembly, inspection, re-wind, and re-wedge,
- heat, chemicals, or mechanical force applied when stripping the winding during rewind,
- stator-rotor rub during assembly and operation,
- arcing from winding failure,
- foreign particles introduced during assembly, inspection, or repairing,

Inter-laminar faults are very difficult to monitor on-line since the fault causes only localised flux re-distribution and heating. The core of a large machine is usually inspected during or after manufacturing, during regular maintenance, and after repair. Before any thermal or electromagnetic techniques were developed for detecting inter-laminar insulation failure, the detection of core faults relied on visual inspection (Lee et al. 2005).

Mechanisms of failures and symptoms produced by the fault

If laminations are shorted together for one of the reasons above, a circulating eddy current larger than that found in normal operation is induced in the fault loop. The circulating fault current causes additional power loss in the core and results in localised heating, which may grow in severity and eventually cause the laminations to burn or melt. As a result, the stator insulation and windings can also be damaged, causing ground current through the stator core, which may potentially cause machine failure.

2.2.3 Rotor-related faults

General

Because of different rotor constructions, consisting of:
  - rotor bars − for cage induction machines,
  - rotor windings−for conventional synchronous machines and slip-ring induction machines,
  - rotor permanent magnets − for permanent magnet machines,

and constituent materials:
  - aluminium (copper, steel) for cage rotor bars,
  - permanent magnets for rotors of permanent magnet machines,
  - copper wires for the wound rotor of synchronous machines,

rotor faults may be considered to be more complex and various than stator-related ones.

Following the previous description of the rotor configurations and constituent materials, the most common rotor faults an electrical machine may encounter may be classified as:

  - fractures (breakage) of rotor bar and/or end-ring in cage induction motors,
  - short-circuits in the field winding occurring in conventional synchronous machines with a wound rotor,
  - demagnetisation of the permanent magnets in permanent magnet machines,
  - rotor pole displacements in permanent magnet machines and synchronous machines.

Short circuits in rotor winding - failure mechanisms

Short-circuited turns in power generator rotor windings cause operational problems, such as high vibration levels; therefore, early detection is essential.

Similarly to the case of stator winding-related faults, inter-turn short circuits usually appear because of mechanical, electromagnetic, or thermal stress conditions.

Normally, the resistance of the windings on opposite poles is identical. The heat produced by Joule's effect is distributed symmetrically about the rotor forging. If the inter-turn insulation is damaged in such a way that two or more turns of the winding become short-circuited, then the resistance of the damaged coil diminishes and, if the poles are connected in series, less heat is generated than in the symmetrical coil on the opposite pole. The rotor body thus experiences asymmetric heating, which produces a thermal bow in the rotor body, causing vibration. The unbalanced magnetic forces on the rotor produced by the change in the magneto-motive force (MMF) from the winding contribute to increased vibration (Ramirez-Nino and Pascacio 2001).

Rotor failures of the induction machines - physical structural damages

General

Unlike stator design, cage rotor design and manufacturing has undergone little change over the years. As a result, rotor failures now account for around 10% of total induction motor failures (EPRI 1982, Kliman et al. 1996). However, in the field of fault diagnosis and the condition monitoring of electrical machines, most of the research presented in the literature deals with induction motor rotor failures, while bearing-related failures, which account for 40-50% of motor failures, are not so widely discussed. Rotor cage-related faults perhaps received so much attention in the literature as a result of their well-defined associated fault frequency components.

Causes

Manufacturing process defects

For a rotor cage, physical damage faults can arise at the manufacturing stage through defective casting in the case of die-cast aluminium rotors, or through poorly welded or brazed bar-to-end-ring joints in the case of fabricated rotor cages. A defective cast aluminium rotor may have air bubbles within the casting, thus increasing the resistances of the rotor bars and consequently resulting in hot spots in the bars where the resistance is greatest and which could lead to a complete fracture of the bar (Paterson 1998).

Severe operational conditions

Under normal operating conditions, large mechanical and thermal stresses are present, especially if the machine is being continually stopped and restarted or if the machine is heavily loaded. It is well known that the rotor current during starting can be as much as ten times the normal full load current and that the effects of these large currents are represented by very large thermal stresses in the rotor circuit. The starting period is also characterised by minimal cooling and maximum mechanical forces, which over-stress the rotor bars.

Mechanisms of failures and symptoms produced by the fault

The sequence of events following the cracking of a rotor bar is described as follows: the cracked bar will increase in resistance and will overheat at the crack. The bar will break completely and arcing will occur across the break. This arcing will then damage the rotor laminations around the faulted bar. The neighbouring bars will carry an increased current and will be subject to increased stresses, eventually causing these bars to fail. Finally, the broken bars may lift outwards because of centrifugal forces and could catastrophically damage the stator windings (Paterson 1998).

Eccentricity

General

Machine eccentricity is defined as a condition of the *asymmetric air-gap that exists between the stator and rotor* (Vas 1993). The presence of a certain level of eccentricity is common in rotating electrical machines; some manufacturers and users specify a maximum permissible level of 5 percent, whereas in other cases, a maximum level of 10 percent of the air-gap length is allowed by the user (Thomson and Gilmore 2003). However, manufacturers normally try to keep the total eccentricity level even lower in order to reduce vibration and noise and minimise unbalanced magnetic pull (UMP) (Nandi and Toliyat 1998). Since the air-gap of an induction machine is considerably smaller than in other types of machines with a similar size and performance, this type of machine is more sensible to changes in the length of the air-gap.

There are two types of air-gap eccentricity: *static air-gap eccentricity* and *dynamic air-gap eccentricity* (Fig. 2.4). In the case of static air-gap eccentricity, the position of the minimal radial air-gap length is fixed in space, while in the case of dynamic eccentricity, the centre of the rotor is not at the centre of the rotation and the position of the minimum air-gap rotates with the rotor. However, the static and dynamic eccentricities are basic classifications, since varieties and modifications such as unilateral eccentricities, as well as angular and radial misalignments, are just as possible.

a) concentric   *b) static eccentricity*   *c) dynamic eccentricity*
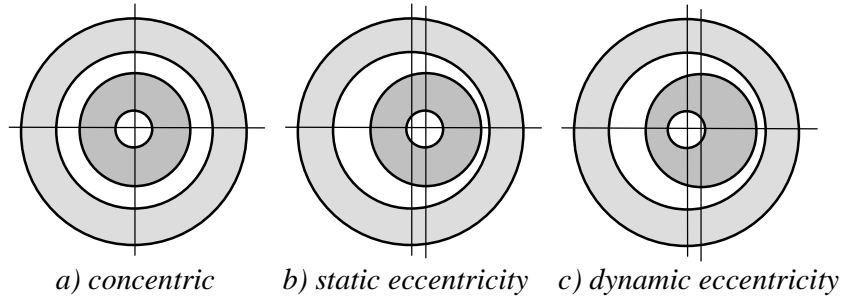
Fig. 2.4 Eccentricity types.

Causes

Static eccentricity may be caused by the ovality of the stator core or by the incorrect positioning of the rotor or stator at the commissioning stage. Assuming that the rotor-shaft assembly is sufficiently stiff, the level of static eccentricity does not change.

The *dynamic eccentricity* may be caused by several factors, such as manufacturing tolerances, wear of bearings, or misalignment, mechanical resonance at critical speed, and incorrect manufacture of the machine components. Rotor "*whirl*" near a critical speed is another source of dynamic eccentricity and is an important consideration in larger, flexible-shaft machines.

Mechanisms of eccentricity production and symptoms produced by the fault

In reality, both *static* and *dynamic eccentricities* tend to *co-exist*. An inherent level of static eccentricity exists even in newly manufactured machines as a result of manufacturing and assembly methods. This causes a steady UMP in one direction and with usage this may lead to a bent rotor shaft, bearing wear and tear etc., resulting in some degree of dynamic eccentricity. Unless detected early, the eccentricity becomes large enough to develop high unbalanced radial forces that may cause stator-to-rotor rub, leading to a major breakdown of the machine (Barbour and Thomson 1997).

2.2.4 Bearing faults

General

Because of the close relationship between motor system development and bearing assembly performance, it is difficult to imagine the progress of modern rotating machinery without considering the wide application of bearings. As reported by Kliman et al. (1997) and EPRI (1982), bearing faults may account for 42%-50% of all motor failures. Motor bearings may cost between 3 and 10% of the actual cost of the motor, but the hidden costs involved in downtime and lost production combine to make bearing failure a rather expensive abnormality (Barker 2000).

Bearing faults might manifest themselves as rotor asymmetry faults, which are usually included in the category of eccentricity-related faults. Otherwise, ball bearing-related defects can be categorised as outer bearing race defects, inner bearing race defects, ball defects, and train defects. Figure 2.5 presents the artificially created outer bearing race fault studied in this work.

Causes, mechanisms of failure, and symptoms produced by faults

Different stresses acting upon a bearing may lead to excessive audible noise, uneven running, reduced working accuracy, and the development of mechanical vibrations and, as a result, increased wear. As long as these stresses are kept within the design capabilities of the bearing, premature failure should not occur. However, if any combination of them exceeds the capacity of the bearing, then the lifetime may be drastically diminished and a catastrophic failure could occur.

More than twenty years ago, few bearing failures were electrically induced but at the beginning of the '90s a study by Kerszenbaum (1992) showed that bearing failures are about 12 times as common in converter-fed motors as in direct-on-line motors. This relatively high percentage of electrically induced motor bearing failures is due to the modern high-frequency switching power devices that were rapidly developing in that period. Such devices, employing, for instance, bipolar junction transistors (BJTs) and faster (shorter rise time as a result of fast switching) insulated gate bipolar transistors (IGBTs) produce unintended consequences for peripheral equipment, generally described as electromagnetic interference (EMI) (Busse et al. 1997). Concerning this issue, relying on simulations, analytical expressions, and experiments, Mäki-Ontto presents some methods for the mitigation of shaft voltages and bearing currents in frequency converter-fed AC motors (Mäki-Ontto 2006).

However, Barker (2000) claims that mechanical issues remain the major cause of bearing failure. The same author provides a list of reasons and mechanisms that usually cause bearing failures:

- thermal overloading,
- misalignment of the shaft,
- excessive loading (both static and/or dynamic), (axial/radial combined),
- mechanical overload,
- excessive shock and vibration,
- inappropriate shaft fit,
- machining defects,
- bad handling and/or mounting,
- improper application,
- improper installation,

Fig. 2.5 Artificially created bearing fault studied in this work.

- heavy radial and axial stresses caused by shaft deflection,
- lifetime load profile,
- environmental/external problems,

  - contamination and corrosion caused by pitting and the sanding action of hard and abrasive minute particles or corrosive action of water, acid, etc.
  - improper lubrication, including both over- and under-lubrication, causing heating and abrasion

- bearing currents,
- shear stress.

3 FAULT INDICATORS FOR ELECTRICAL MACHINES

3.1 General

The history of fault diagnosis, condition monitoring, and protection is as old as technical devices themselves. Generally, *on-line condition monitoring and diagnostics requires the sensing and analysis of such signals that contain specific information (symptoms) which is characteristic of the degradation process, problem, or fault to be detected.* Various factors need to be considered when selecting the most appropriate monitoring technique for application in an industrial environment. The most important factors, according to Thomson (1999), are listed below:

1. *the sensor should be non-invasive*,
2. the *sensor and instrumentation system must be reliable*,
3. *the diagnosis must be reliable*,
4. *the severity of the problem should be quantified*,
5. *ideally, an estimation of the remaining run-life should be given*,
6. *ideally, a prediction of the fundamental cause(s) of the fault should be provided via on-line information from sensors etc*.

It is extremely difficult and, in most cases, impossible to satisfy all the above criteria, mainly because of the complexity of the degradation mechanisms, abnormalities, and nature of the fault. Because of the world-wide interest in the condition monitoring and diagnostics of drive systems, substantial advances have been made during the last fifteen years and in many cases it is possible to achieve Criteria 1 to 4. However, Criteria 5 and 6 are extremely difficult to achieve.

3.2 Potential fault indicators for a technical device

Because of the wide variety of physical phenomena to be found in a technical device, several fields of science and technology need to be considered when designing and developing competitive monitoring and diagnosis systems. As an example, Fig. 3.1 illustrates the complexity of the interactions of physical phenomena characteristic for a general electromagnetic energy converter structure.
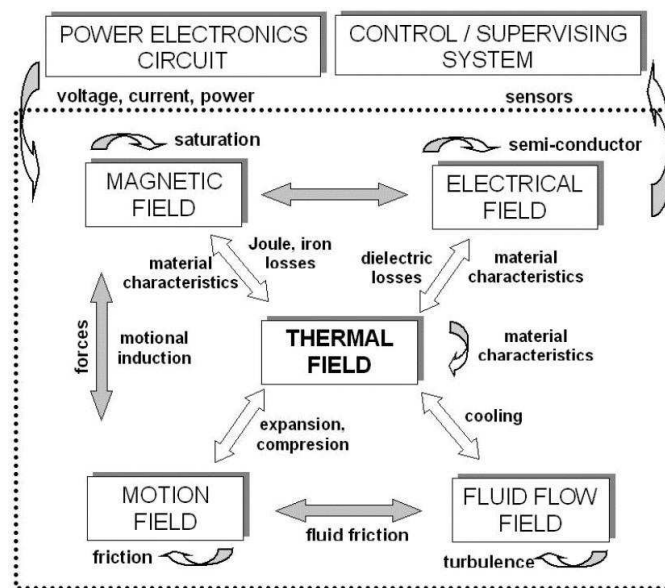

Fig. 3.1 Interactions of physical phenomena characteristic for a general electromagnetic energy converter structure (Driesen 2000).

Different fields of physics, such as *electrical*, *mechanical*, *thermal*, *fluid flow*, and *motion* interact in a complex manner, as depicted in the previously mentioned picture. Various parameters belonging to these fields may be found to be suitable potential fault indicators for the technical device. The control system that governs the overall system and the power electronic system specialised in translating its commands into energetic signals supplied to the device may together be considered the core of a condition monitoring and fault diagnosis scheme.

3.3 Potential fault indicators for electrical machines

3.3.1 General

It was previously claimed that the monitoring and diagnosis of electrical machines is a very popular topic, since it corresponds with industrial requests for an increasing number of applications for which reliability is the key point. In this respect, sensor implementation is fundamental for the development of industrial methods at a cost compatible with the applications in which monitoring and diagnosis are necessary.

In order to ensure safe and reliable operation, the manufacturers and users of electrical machines initially relied on simple protections such as over-current, over-voltage, or earth-fault. However, as the tasks performed by electrical machinery grew more complex, improvements were also sought in the area of fault diagnosis (Nandi and Toliyat 1999).

A number of potential measurement parameters are likely to provide nowadays useful condition-indicating information for possible failure modes in any electrical machine. Thorsen and Dalva (1999) categorise mainly these parameters as *mechanical,* like vibrations, acoustic, speed fluctuations, and *electromechanical,* like currents, electromagnetic leakage fluxes, surges, and partial discharges. In addition, come *temperature*, *oil particle* and *gas analysis*.

Following, a short description of the most popular mechanical parameters, temperature, oil particle and gas analysis based methods is presented. The electromechanical parameters used in the field of fault diagnosis and condition monitoring of electrical machines will be discussed in more detail in the following sections of this thesis.

Acoustic emission monitoring works with ultrasonic but also with audible frequencies, and is particularly promising for detecting bearing faults. The contact between rolling elements with and without cracks generates waves that propagate through the machine with the speed of sound. The waves have little energy, but their high frequencies can be detected by piezoelectric transducers. Rienstra and Hall (2004) present a study on the basic principles of the acoustic monitoring and on the industrial use of this technique for bearing fault detection. However, the acoustic monitoring has also proven feasible in the attempt to identify electrical faults, such as loose stator coils (Gaylard et al. 1995). In this case, the identification procedure was performed automatically by a neural network.

Nau and Mello (2000) indicate the causes of acoustic noise in induction motors and present methods to reduce the noise before and after the motors are manufactured.

Vibration monitoring uses vibration transducers such as measuring accelerometers of piezoresistive types with linear frequency spectrum. Vibrations are caused by magnetic, mechanical and/or aerodynamic forces. The measuring parameters can be *displacement*, *velocity* and *acceleration*. Vibrations are measured directionally, e.g. radially or axially, and the transducers are often placed on the bearings for detecting mechanical faults (Wang and Gao 2000). However, by placing probes on the stator, it is also possible to detect non-even air gap (Cameron et al. 1986), stator-winding or rotor faults (Trutt et al. 2002), asymmetrical

power supply (Chow 1996) and unbalances in the driven load (Obaid and Habetler 2003), (Leonard and Thomson 1986).

The users of electrical machinery pay a special attention to the *temperature monitoring* since the basic rule of thumb claiming that '*every additional 10°C causes a winding to deteriorate twice as fast as when the operation takes place in the allowable temperature range*' represents a very serious concern for the good operation of their machinery. Other components of electrical machinery may be irreversibly affected by higher temperatures; the case of *permanent magnets* found in the structure of a permanent magnet machine rotor is a good example in this respect. The *magnetic characteristics* of permanent magnets are *temperature-dependent* and a high temperature may lead to *irreversible demagnetisation* of the permanent magnets. Negrea et al. (2001) present a study dealing with the temperature distribution in a permanent magnet synchronous motor used for ship propulsion drives. More specifically, the transient thermal behaviour of the motor under fault conditions, i.e. during short circuits occurring in the terminals of the test motor is studied, and various considerations on the issues of stator winding and permanent magnets protection are presented.

Temperature monitoring devices installed to monitor bearing temperatures are also often used. Remembering that bearing failures cause the majority of motor failures, many maintenance departments utilize thermal image scanning to look for abnormally hot spots on in-plant inspections (Malinowski and McCormick 2002).

For figuring out ventilation malfunctions, the *coolant bulk outlet temperature* is monitored, particularly when the machine is stressed beyond its rated data.

Gas in oil analysis is the traditional way to monitor insulation condition. Dissolved gases in the oil produced by thermal ageing can provide an early indication of an incipient fault. Gases normally analyzed are hydrogen, oxygen, carbon monoxide, carbon dioxide, methane, ethane ethylene, and acetylene. The *gas in oil analysis* together with the *oil particle*, and other methods relying on *chemical analysis*, are extensively presented by Tavner and Penman (1987).

Table 3.1, based on Payne et al. (2002), briefly presents:

- what type of instrumentation is required to monitor some of the most popular machine parameters used in fault detection in the case of a transverse flux motor,
- the degree of accuracy of fault indication that may be obtained when relying on a specific parameter,
- the level of expertise an operator needs in order to interpret the recorded data,
- how invasive a dedicated sensor for each fault indicator would be,
- possible means of analysis (signal processing techniques).

Even though the content of Table 3.1 refers to a transverse flux motor, which is not typical of industrial drives, this may also be considered as being representative of any type of electrical machine, since the same potential measurement parameters are presented by other research as likely to provide useful condition-indicating information for possible fault modes.

From the multitude of previously-mentioned machine parameters, some authors claimed that on-line technologies based on *temperature*, *axial flux*, and *shaft current/voltage* measurements present enough ability to protect the motor against fault conditions which were previously difficult or impossible to detect (Bowers and Piety 2001). These measurements are known as *proactive.* A *proactive* concept may be defined as the capability of controlling a situation by controlling a situation capable of causing a fault rather than waiting to respond to it after it happens.

Table 3.1 Fault indicators in electrical machines (Payne et al. 2002),

Parameter	Measurement device	Potential information richness	Intrusive to electrical machine	On/off line	Operator skill required	Measurement frequency	Measured as part of control strategy	Possible means of analysis
Current	Hall effect transducer	Average	No	On	High	Continuous	Yes	RMS trending, phase relationship, spectrum analysis, statistical methods
Voltage	DVM	Average	No	On	High	Continuous	Yes	RMS trending, phase relationship, spectrum analysis, statistical methods
Flux	Search coil / Hall effect device	Very high	Yes and no	On	High	Hourly	No	RMS trending, time analysis, spectrum analysis, statistical methods
Force	Dynamometer	Very high	No	On	High	Continuous	No	RMS trending, time analysis, spectrum analysis, statistical methods
Vibration	Accelerometer	High	Yes and no	On	Expert	Hourly	No	spectrum analysis, statistical methods
Acoustics	Microphone	High	No	On	Expert	Hourly	No	RMS trending, spectrum analysis, statistical methods
Temperature	Hand-held probe	Low	Yes and no	Off	Low	Monthly or on suspected deterioration	No	Trending
	Thermal paint		Yes					Visual interpretation
	Thermocouple	Average	Yes		Average	Continuous	Yes	Trending
	Infra-red camera	High	No	On	Expert	Monthly or on suspected deterioration	No	Visual interpretation and trending
Instantaneous angular speed	Encoder	Average	No	On	high	Continuous	Yes	Peak to peak variation
Torque	Torque sensors (magnetoelastic, piezoelectric, strain gauge)	High	No	On	Expert	Continuous	Yes and no	RMS trending, spectrum analysis, statistical methods

3.3.2 Indicators for detecting winding-related faults

The detection of stator winding faults in low-voltage motors during operation has been a problem, mainly because such a fault is not always distinguishable when the stator current is monitored (Joksimovic and Penman 2000). A large amount of work has been carried out on developing condition monitoring techniques based on other machine parameters such as:

- axial leakage component of the electromagnetic flux (Penman et al. 1994),
- electrically excited vibrations (Trutt et al. 2002),
- negative-sequence impedance (Kohler et al. 2002), (Melero et al. 2003),
- instantaneous power (Legowski et al. 1996),
- partial discharge testing (Green et al. 2005),
- electromagnetic torque (Hsu 1995).

Frequent changes in the temporal behaviour of the power supply cause unbalance, which in turn obscures the fault signature, resulting in false alarms. Such a false alarm could lead one to detect the presence of a stator fault, even though the root cause of the problem is supply unbalance. Similar arguments could be made regarding the impact of low-frequency load variations and load changes on mechanical fault detection and the effectiveness of various methods in detecting such problems (Parlos and Kim 2001).

To detect shorted turns in the rotor windings, several methods have been used, such as the air-gap search coil technique (Connolly et al. 1985, Ramirez-Nino and Pascacio 2001), the monitoring of the circulating stator current in double-circuit machines (Muhlhaus et al. 1985), measurement of the rotor shaft voltage, or monitoring the harmonic components present in the generator excitation current for synchronous generators (Penman and Jiang 1996).

3.3.3 Indicators for detecting rotor-related faults

The consequences of faulty rotors are poor starting performance, excessive vibration, and higher thermal stresses. All these contribute to the further deterioration of the rotor, as well as to secondary failures of the stator.

Various methods have been proposed for the detection of rotor faults, relying on monitoring motor torque (Thomas et al. 2003), rotor speed (Hargis et al. 1982), electromagnetic flux (Elkasabgy et al. 1992, Penman et al. 1994), vibrations in the machine stator housing (Cameron et al. 1986), and stator current (Kliman 1988, Benbouzid 2003). The analysis of the current spectrum is the most popular, because of its simple way of recording the stator input current while the motor is running under load hence no interruption to the machine operation being required.

Relying on extensive experiments carried out on an induction motor with various rotor faults and under various load conditions, Trzynadlowski and Ritchie (2000) have shown the usefulness of the instantaneous power as diagnostic media for rotor faults in induction machines. The stator current, which is regularly used in motor signature analysis, yielded inferior results.

3.3.4 Indicators for detecting bearing faults

Bearing faults may lead to increased vibration and noise levels. Considering these symptoms, it is easy to understand why previous research has found out that bearing faults are best detected by monitoring vibrations, shock pulses, and acoustic emissions. However, many of the previous investigations and methods proposed to detect bearing faults are based on the spectral analysis of electrical quantities (Schoen et al. 1995, Cardoso and Saraiva 1993, Obaid

et al. 2000). They have the advantage that they work with standard current sensors that are already available in most drive applications and may provide the same indications without requiring access to the motor by correlating the characteristic bearing frequencies to the spectral components of the stator currents (Kliman and Stein 1990). The fault spectral lines in the current can be determined on the basis of the bearing geometry and the rotational speed (Schoen et al. 1994).

However, a fault signature is detectable in the stator current only if the bearing fault causes a displacement of the rotor within the air-gap, resulting in a distortion of the air-gap field. Hence, it is hard to obtain a reasonable signal-to-noise ratio at an early stage of bearing fault.

For a 15 kW four pole induction motor, Lindh et al. (2003) have investigated the use of stator current signal for the detection of an outer ring defect of a ball bearing with normal radial clearance. It was found that the stator current measurement as a bearing fault indicator is not adequate for this motor type since the modification produced by the radial movement of the rotor was found very small if the radial movement was restricted with bearing with small radial clearance. An outer race defect was clearly indicated only in the case of the large internal radial clearance of the bearing.

Obaid et al. (2003) claim that the main disadvantage of using the current for monitoring the condition of bearings comes from the difficulty of distinguishing bearing fault signatures from non-fault components or noise in the stator current.

Stack et al. (2004) also claim that, the main disadvantage of stator-current-based bearing fault detection is that the effects of a bearing fault are often subtle and difficult to predict. This is the reason why they propose a modeling technique where the changes in the stator current spectrum are compared to a baseline spectrum, rather than searching for specific fault components. These changes in spectral content are then used to identify developing faults. Before this modeling technique is applied, the stator current should be filtered to remove the significant non-bearing fault components such that only changes in bearing health are tracked. Stack et al. (2004) claim and there are no bearing fault detection techniques in industry that are current-based.

Additional methods based on special sensors placed in the machine in order to detect shaft voltages or axial magnetic flux caused by a bearing defect have also been reported (Ong et al. 2000). Besides an increase in costs, the mounting of additional sensors is, however, also a practical problem in terms of motor design and approval by the manufacturer, operator, or safety legislation authorities.

Kliman et al. (1997) claim that bearing faults may also produce small torque perturbations. These perturbations are major for some types of faults (such as a pit in the race), resulting in predictable frequencies, but very small for other types, such as a dented cage or damaged balls. Therefore the necessity arises that a monitoring system must be able to resolve very small components of the spectrum, even when their frequencies are not definitely known, and recognise when they differ from a nominal or healthy motor. In this respect, Schoen et al. (1994) use neural network techniques with the purpose of characterising the spectra of the stator current that are associated with the normal state of a motor and load and then determining when the spectra have changed significantly from the nominal to indicate a fault.

Li et al. (2000) used the commercially available Machinery Fault Simulator (SpectraQuest) to obtain vibration data from bad bearings to train a neural network with the purpose to identify fault severity. Both simulation and real-world testing results obtained indicate that neural networks can be effective agents in the diagnosis of various motor bearing faults through the measurement and interpretation of motor bearing vibration signatures

3.3.5 Indicators for detecting eccentricity

If a certain level of eccentricity between the rotor and the stator occurs in an electrical motor, whatever its origin, it causes new air-gap field harmonics to appear and/or an increase in the amplitude of the previously existing harmonics. Then, it produces a global effect that stimulates the development of the following side effects (Duque et al. 2004):

- unbalanced magnetic pull,
- parasite torque,
- intensification of vibration and noise levels,
- decrease in the rotor speed,
- electric current flowing through the bearings.

Many surveillance schemes determine the Fourier spectrum of a single line current in order to monitor the condition of the motor (Thomson 1994, Nandi and Toliyat 2002). These schemes evaluate additional fault specific harmonics that are due to rotor misalignment. The location of these harmonic waves is given by the number of rotor bars and the actual slip (Hirvonen 1994, Barbour and Thomson 1997, Dorrell 1997). It is very important to sense the misalignment between the motor and mechanical load, since this may initiate a radial force, which pushes the rotor to the side and can produce higher eccentricity ranges.

Vibration signals can also be monitored in order to detect eccentricity-related faults. Cameron (1986) gives the high-frequency vibration components to be monitored for detecting static or dynamic eccentricity. The relationship of the vibration of the bearing to the stator current spectra can be determined by remembering that any air-gap eccentricity produces anomalies in the air-gap flux density. Most bearing defects produce a small radial motion between the rotor and stator of the machine that may be perceived as a form of eccentricity.

Mechanical unbalances give rise to two first-order current harmonics. Because of the interaction of the currents and voltages, both these current harmonics are also reflected by a single harmonic component in the frequency spectrum of the electric power. It is claimed that this single component is easier to assess than both the current harmonics (Kral et al. 2004, Liu et al. 2004).

Eccentricity-specific signals are also present in the electromagnetic flux, which can be measured by search coils which sense the axial leakage flux and the electromagnetic flux from the air gap (Früchtenicht et al. 1982, Tenhunen et al. 2003, Dorrell et al. 1995).

Other schemes evaluate mechanical (Dorrell et al. 1997) or acoustic vibrations caused by mechanical unbalances, torque signatures (Wieser et al. 1999), and radial forces (Smith and Dorrell 1996, Arkkio 1996).

Cardoso et al. (1997) use a detection technique that evaluates space phasors calculated from two or three measured currents. This technique analyse the characteristic patterns of the locus diagram of the current phasor.

3.4 Current monitoring

This section presents the state of the art for different monitoring techniques based on motor current signature analysis (MCSA) that are used to detect and, eventually, localise different faults in electrical machines.

Why current monitoring?

Vibration measurements have historically been the foundation of most on-line condition monitoring programs, but new techniques such as those involving spectral analysis of the electric line current powering the motor are becoming of significant interest. The main problem concerning the monitoring methods based on, for instance, measurement of the rotor speed, vibration, and fluxes is that they are essentially invasive, requiring transducers to be fitted in or around the machine, with an obvious interruption to operation. Besides the increase in costs, the mounting of additional sensors is also a practical problem in terms of motor design and approval by the manufacturer, operator, or safety legislation authorities.

The condition monitoring schemes that rely on the analysis of the motor current are the most attractive, as the current sensors are usually installed by default in the motor control centre for other control or protection purposes. As a consequence, a variety of methods are applied to today's cost-effective microprocessor hardware platforms in order to accurately diagnose impending failures of electrical machines and many commercial products rely on integrated packages incorporating analysis techniques based only on the voltages and currents available.

The MCSA technique is applied to machines operating under steady state conditions and has a basic requirement that for reliable diagnosis a substantial current must flow; i.e. the motor must be operating at or near full load conditions. There are certain situations, however, when this requirement is impractical, i.e. if the motor has been removed from service and taken to a workshop for repair. Under such circumstances, the motor can only be tested under no-load conditions (Burnett et al. 1995).

The current monitoring method is highly likely to meet Criteria 1-4, which were previously mentioned in Section 3.1 and depicted again in Fig. 3.2.
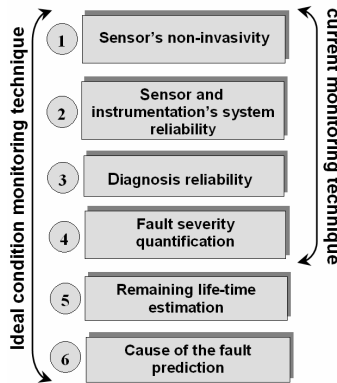

Fig. 3.2 Factors to be considered when selecting the most appropriate monitoring technique for application in an industrial environment (Thomson 1999).

3.4.1 Phase current

Stator winding faults

Some diagnostic methodologies have been proposed to detect stator short circuits that rely on the fact that stator asymmetry causes an increase in the space harmonics. The interaction

between the electrical quantities at the supply frequency and the different space harmonics produces additional time harmonic components in the stator and rotor currents. As a consequence, the space harmonics of the air-gap flux density may be considered useful to obtain reliable results. Thomson et al. (1998) and Filippetti et al. (2000a) claim that the harmonic components of the stator currents caused by the rotor slotting can be used for diagnostic purposes.

On the other hand, Joksimovic and Penman (2000) state that as a result of the nature of the rotor, no new frequency components of the line current spectra can appear as a consequence of the fault in the stator winding of an electrical machine. For the case of a turn-to-turn short circuit in the stator winding, only a rise in some of the frequency components which already exist in the line current spectra of a healthy machine was observed both from their experiments and simulations.

It is well known that degradation of the insulation between stator winding turns introduces a dissymmetry in the first harmonic components of the currents and consequently a so-called negative sequence component. It was suggested that this effect may be used for the detection of an insulation failure (Vas 1993).

Rotor related faults

When used properly, the analysis of the electric current signature of the motor has proven to be very reliable for quantifying broken rotor bars.

Supposing that the current in a healthy motor has the fundamental supply frequency f_s, changes in the load of the motor modulate the amplitude of the current to produce sidebands besides this fundamental frequency component. Broken or fractured rotor bars generate a sideband below the supply frequency, which is displaced by twice the slip frequency ($2sf_s$) from the supply frequency. This cyclic variation in the current reacts back to the rotor to produce a torque variation at twice the slip frequency, giving rise to a speed variation twice the slip frequency. This speed effect reduces the lower sideband $f_s(1-2s)$ and produces an upper sideband at the frequency $f_s(1+2s)$. It was found that the magnitudes of these sidebands are affected by the motor-load inertia (Thomson 1999, Filippetti et al. 1996). Concluding, the characteristic fault sideband components f_{brb} around the fundamental for detecting broken bar faults are given by:

$$f_{brb} = (1 \pm 2ks)f_s \qquad k = 1, 2, 3... \qquad (3.1)$$

Deleroi (1982) suggests that additional spectral components should be observed in the stator line current with the purpose of detecting rotor-cage-related faults:

$$f_{brb} = f_s \left[\left(\frac{k}{p} \right)(1-s) \pm s \right] \qquad (3.2)$$

where k has the integer values 1, 2, 3..., p is the number of pole-pairs, s is the per unit slip and $k/p=1, 3, 5…$

The most prominent sideband frequency is the one that appears at twice the slip frequency below the line frequency. The ratio of this lower sideband amplitude to the main supply frequency component gives an estimation of the severity of the fault, indicating the amount of broken or fractured bars (Hirvonen 1994, Kliman et al. 1988). Besides the sideband components at twice the slip frequency, current components near the rotor-slot harmonic frequency may be found. In the case of broken rotor bars, the modulation of the stator current at twice the slip frequency can be found on the spectrum by analysing the slot frequencies:

$$f_{\text{brb}} = f_{\text{s}} \cdot \left[\frac{N_r(1-s)}{p} \pm 2n \right] \pm 2sf_{\text{s}}$$

<div align="right">(3.3)</div>

where $n = 0, 1, 2\ldots$ and N_r is the number of broken rotor bars.

Other techniques, such as those based on monitoring the torque and instantaneous power, have been shown to be sensitive to rotor bar faults, but have not been proved to be as reliable or to provide a quantitative estimate of broken bars. In this respect, a comparison and performance evaluation of different diagnostic procedures that use input electric signals to detect and quantify rotor breakage in induction machines supplied by the mains was achieved by Bellini et al. (2000). This work proved that the current signature analysis provides the information to diagnose the rotor breakage accurately and quantitatively by retrieving an effective diagnostic index that sums the amplitudes of the two sideband components in the current spectrum given by Eq. 3.1. Alternative diagnostic methods that use current space vector modulus, as well as instantaneous power, or instantaneous torque, lose information and thus do not allow an accurate quantification of the breakage, since they are affected twice by the speed reaction.

Siau et al. (2003) claim that it is difficult to detect partial rotor bar breakages or make accurate estimates of the number of broken rotor bars using the current spectrum alone. A possible solution for improving the accuracy of rotor fault detection and estimation of severity would be to combine the information from the current and flux signals.

Burnett and Watson (1995) presented a methodology to find the location of broken bars within a rotor of an induction motor. The technique used to detect the location of broken bars involved using the stator windings as reference locations within the motor from which the distance travelled by the broken bar can be computed. This technique was found to be dependent on the successful detection of the frequency components given by Eq. 3.2.

A drawback of the diagnostic procedure based on MCSA is the possible confusion with the motor current modulation produced by other events, such as pulsating load, undesired interaction between the motor and the train equipment, and particular rotor design, which also cause sideband current components. If the load variation frequency is near, the resulting current spectrum is similar to that of a faulted rotor (reflected as two anomalous lines in the current spectrum $2sf$ from the supply frequency line), but previous experiences showed that the two causes can still be distinguished (Filippetti et al. 1998). However, a particular rotor structure design, such as a spidered structure with the same number of legs and poles as are found in large motors, may produce a magnetic asymmetry whose effect is the same as rotor electrical asymmetry (Thomson 1992).

Bearing faults

Generally, the bearing condition monitoring techniques rely on the indications provided by the motor current and vibration. The efficacy of current monitoring for bearing fault detection by correlating the relationship between vibration and current frequencies caused by incipient bearing faults was investigated by Schoen et al. (1994). In this respect, it was experimentally proven that there is a relationship between the vibrational and current frequencies, since the stator current signature can be used to identify the presence of a bearing fault. This combined analysis is supported by the fact that the mechanical vibrations are associated with variations in the physical air-gap of the machine. When ball bearings support the rotor, any bearing defect will produce a radial motion between the rotor and stator of the machine. Such variations cause the air-gap flux density to be modulated and the stator currents to be

generated at predictable frequencies related to the electrical supply and vibrational frequencies.

Vas (1993) and Schoen et al. (1994) suggest that the mechanical damages referred to bearing faults introduce harmonic components in the current spectrum at the frequencies

$$f_{bng} = f_s \pm f_b \tag{3.4}$$

where f_s is the supply frequency and f_b is a mechanical frequency depending on the type of fault and on the bearing characteristics. Other components at different frequencies can be introduced by load anomalies and it should be noted that they can cause misunderstandings, because these components can be confused with those caused by machine faults.

Schoen and Habetler (1997) present a method for removing the load effects from the monitored quantity of the machine. The methods compares the actual stator current to a model reference value which includes the load effects and the difference between these two signals provides a filtered quantity, independent of variations of the load, that allows continuous on-line condition monitoring to be conducted without concern for the load condition. Simulation and test results presented the effects on the spectrum of the monitored quantity for both constant and eccentric air gaps when in the presence of an oscillating load.

Eccentricity

Variation in the air-gap length because of static or dynamic eccentricity leads to variations in the air-gap flux density. As induced stator currents are affected, many of their frequency components can help to identify both static and dynamic eccentricity.

Vas (1993) claims that, generally, the presence of static and dynamic eccentricity can be detected using MCSA. Cameron et al. (1986) found that static eccentricity can be identified by changes in the mechanical vibrations caused by the rotor-slot harmonics, and dynamic eccentricity is characterised by the appearance of unique frequency components in both the current and frame vibration signals. The same authors claim that static eccentricity variations result in the introduction of dynamic eccentricity components in the current and vibration, thus indicating that dynamic eccentricity is a by-product of static eccentricity.

According to Cameron (1986), the frequencies of the harmonics resulting from the asymmetries caused by the slotting and eccentricity can be calculated according to:

$$f_{ecc} = f_s \left[\left(kQ_2 \pm n_d \right) \frac{(1-s)}{p} \pm n_w \right] \tag{3.5}$$

where f_s denotes the machine supply frequency and Q_2 gives the number of rotor slots, $n_d = 0$ in the case of static eccentricity, and $n_d = 1, 2, 3\ldots$ in the case of dynamic eccentricity (n_d is known as eccentricity order), s is the slip, p is the number of pole-pairs, k is any integer, and n_w is the order of the stator time harmonics that are present in the power supply driving the motor ($n_w = \pm 1, \pm 2, \pm 3, \pm 5$, etc.). In the event that one of these harmonics is a multiple of three, it cannot exist in the line current of a balanced three-phase machine. However, it has been shown by Nandi and Toliyat (1998) that only a particular combination of a machine pole-pair p and a rotor slot number Q_2 will give rise to significant components related only to static or only to dynamic eccentricity. This relationship for a three-phase machine is given by

$$Q_2 = 2p \left[3(m \pm q) \pm r \right] \pm k \tag{3.6}$$

where $m \pm q = 0, 1, 2, 3$, and $r = 0$ or 1, $k = 1$.

According to Obaid et al. (2000), Dorrell et al. (1995), and Nandi and Toliyat (1998), the effects of combined static and dynamic eccentricity cause characteristic sideband currents in the current spectrum given by

$$f_{ecc,i} = f_s \left(1 \pm k \frac{1-s}{p} \right)$$ (3.7)

where k is the order number and is an integer. The interaction of these harmonics with the mainly sinusoidal supply voltage causes eccentricity-specific harmonics in the power and torque spectrum at:

$$f_{ecc,p} = f_s k \frac{1-s}{p}$$ (3.8)

These low-frequency components also give rise to high-frequency components, as described by Penman et al. (1994). However, these components are strong only for machines whose pole-pairs and rotor slot numbers are given by Eq. 3.6, where $k = 1$, while for machines with $k = 2$ these frequency components are rather weak. Since a changing load torque may also result in current harmonics similar to those calculated with the above equations, a constant load is usually assumed. Schoen and Habetler (1995 and 1997) found that the magnitudes of the frequency components caused by load changes are always larger than those of eccentricity harmonics.

Another motor current-related approach for the detection of eccentricity in induction motors was suggested by Cardoso and Saraiva (1993) and consists of monitoring the Current Park's Vector.

3.4.2 Circulating current

In many electrical machines (usually, but not only, in large synchronous generators), the stator/rotor windings are parallel-connected in order to deliver the rated required characteristics at the terminals of the machine.

The additional (parallel) connections serve to generate an MMF which counteracts the asymmetrically distributed magnetic field in the air-gap resulting from the asymmetrical construction or assembly of the machine, especially the off-centre position of the rotor in the stator bore. Such an asymmetrical magnetic field induces mechanical vibration in the rotor and stator (with the attendant increased load on the bearings), as well as an unbearable noise. Equalising currents between winding coils are responsible for the drastic reduction of radial forces and ensure almost vibration-free operation (Berman and Erlicki 1991).

Concerning the use of circulating currents in fault diagnostics, it was claimed that for stator winding short circuits in double-circuit machines, the measurement of the differential current between the parallel connected half-phases represents an accurate way to detect a fault (Penman and Jiang 1996, Tavner and Penman 1987). Single-winding stators present a more intractable problem, although it has been observed that there are some harmonic changes in line current under such conditions. The computation of the circulating current under faulty conditions such as eccentricity and short circuits in the rotor winding of large synchronous generators was also discussed by Foggia et al. (1999).

3.4.3 Shaft currents

Irregularities in the magnetic circuits of electrical machines may result in unwanted voltages that lead to shaft currents through the shaft, bearings, bearing supports, and closing through

the machine framework. The IEEE Standard Test Procedure for Polyphase Induction Motors and Generators (IEEE 2004) discusses the shaft current and presents a measurement method for recording either the voltage across the ends of the shaft or the current.

Ong et al. (1997) claim that only the Rogowski coil measurement yields accurate measurements of shaft currents, whereas the other method either yields inaccurate measurements or may result in other problems for the machine's integrity.

3.4.4 Current monitoring - drawbacks

Taking into consideration the following potential drawbacks of a condition monitoring system relying only on current monitoring, the motivation for approaching and relying on additional fault indicators seems to be clear and realistic:

- For multiple faults or different varieties of drive schemes, MCSA may not provide enough ability to discriminate between different faults, since such abnormalities and time harmonics may end up generating similar signatures.

- The current spectrum is influenced not only by fault conditions but also by other factors, including the supply, static and dynamic load conditions, noise, machine geometry, and fault conditions, and these conditions may lead to errors in fault detection.

- When a commercial diagnostic system has to operate between a few kW up to MW range of different designs and driving a wide range of mechanical loads, providing a diagnosis from sensing only the current and its subsequent analysis becomes much more complex than is at first apparent (Thomson 1999).

- In order to facilitate the successful detection of rotor faults during steady state operation, a large supply current needs to flow. This large current is usually obtained by monitoring the motor while it is running under full load conditions. The necessity of requiring a large current may not be appropriate nor achievable in some cases if, for example, the motor has been taken off-line or removed to a workshop environment. In addition to requiring a large current, it was found that these monitoring techniques also have difficulty in detecting other common rotor faults over and above simple broken bars. These faults include damaged end-rings or broken bars within a double-bar rotor machine (Burnett and Watson 1995).

- It is very important to bear in mind that the MCSA techniques are not able to detect all of the possible faults in an induction machine. In this respect, many researches, including this work, were aimed to transfer a part of the MCSA knowledge to techniques that monitors the signatures produced by the fault to the electromagnetic flux signals.

39

3.5 Magnetic flux monitoring

Why flux monitoring?

As previously shown, electrical motors experience a wide range of mechanical problems common to most machinery, such as unbalance, misalignment, bearing faults, and resonance, but electrical motors also experience their own specific set of problems, which are a result of electro-magnetically generated fields in the stator and rotor. In this respect, monitoring devices relying on the information provided by the electromagnetic fluxes produced by any small unbalance in the magnetic or electric circuit of motors may be efficiently used in addition to or as alternatives to the widely-used current monitoring. An example of such a combined current-magnetic flux analysis was carried out by Kliman et al. (1988), where, based on an evaluation of numerous test runs, the stator current and external leakage flux were selected as the most practical signals containing the needed information for the detection of broken bars.

Generally, it may be claimed that a monitoring technique based on magnetic flux measurement is highly likely to meet Criteria 1-4 (Fig. 3.2).

3.5.1 General principles, comparisons, sensor-measuring technologies

There are many ways to sense magnetic fields, most of them based on the strong interaction between magnetic and electric phenomena. Magnetic sensing techniques exploit a broad range of physics and chemistry disciplines. In this respect, Lenz (1990) presents some of the most common magnetic sensor technologies used in different fields of science (Table 3.2). This table compares approximate sensitivity ranges; in some cases the projected ranges based on further improvements are indicated by dashed lines. It is very important to bear in mind that the electronic measurement devices considerably influence the sensitivity range for each concept. There are many other factors to be considered when deciding what type of sensor is best suited for a specific application. Among these factors, the *frequency response*, *size*, and *power* should be carefully taken into account.

More information on the general characteristics of magnetic fields and magnetic field meters that are typically used in electrical machines, on calibration methods for magnetic field meters, and on the sources of measurement uncertainty can be found in the specifications for magnetic flux density and electric field strength meters provided by IEEE (IEEE 1994).

3.5.2 Sensors used for condition monitoring in electrical machines – the search coils

General

When the stator phase current is used for the monitoring of rotor faults (such as broken rotor bars in cage induction machines), *the stator winding is used as a search coil for problems associated with the rotor. The converse of this concept* is that the *rotor may be used as a search coil for stator faults*. For example, the axial magnetic leakage flux sensing is a similar technique but detects changes in the line current harmonics indirectly via the axial flux spectrum.

Search coils are employed to capture flux signals from inside and outside the machine. Such coils are able to provide electrical *"quality" signatures* sensitive to conditions which alter the electrical characteristics of the motor, such as broken rotor bars, eccentricity, unbalance between phases, and stator faults. The voltage pick-up of such coils is directly proportional to the rate of change of the flux.

Table 3.2 Magnetic sensor comparison (Lenz 1990)

Magnetic Sensor Technology	Detectable Field (G) $(1T = 10^4 G = 10^9 \gamma)$				
	10^{-10}	10^{-6}	10^{-2}	10^2	10^6
1. Search–Coil Magnetometer					
2. Flux–Gate Magnetometer					
3. Optically Pumped Magnetometer					
4. Nuclear-Precession Magnetometer					
5. SQUID Magnetometer					
6. Hall-effect Sensor					
7. Magnetoresistive Magnetometer					
8. Magnetodiode					
9. Magnetotransistor					
10. Fiber-–Optic Magnetometer					
11. Magneto-Optical Sensor					

The occurrence of a fault in an electrical machine results in a change in the air-gap space harmonic distribution. A search coil is able to detect the time harmonics but is not able to capture the space harmonics. Space harmonics in the stator cause time harmonics in a rotating rotor. By choosing the search coil properly, the number of space harmonics to be monitored may be restricted.

3.5.3 Electromagnetic flux regions to be monitored in electrical machines

General

In the industrial environment, the flux measurements are preferably taken with the flux coil placed outboard in the axial direction, since it is easier to take readings in the *axial* direction in order to ensure the repeatability of the flux coil position. On the other hand, the recommended mounting location for some monitoring units is *radial* for the optimal location to detect temperature and vibration (Burnett 2002).

The use of internally mounted search coils is highly invasive and is not a practical option for machines already installed. However, when the fault information is more valuable than that provided by only one fault indicator (for example, current monitoring), such search coils have to be confidently implemented. For example, the technique of using air-gap search coils has been proved to be more sensitive than the stator current in detecting faults such as broken damper bars or short-circuited turns in power generator rotor windings (Ramirez-Nino and Pascacio 2001, Connolly et al. 1985, Karmaker 2003).

Fig. 3.3 presents some of the most comprehensively studied magnetic fluxes for the identification of particular fault components produced by different stator- or rotor-related faults.

The axial flux appears in all electrical machines and is produced because no machine can be constructed perfectly symmetrically; it will be always present in electrical machines as a result of the small asymmetries on both the rotor and stator sides. Since asymmetries are coming from both the rotor and stator sides, the axial leakage flux contains a component caused by the stator currents and a component caused by the rotor currents.

The axial flux measurements are a potential method for monitoring the condition of the stator and rotor winding of induction motors during operation. The axial flux analysis has also been found to be able to identify rotor asymmetries, shaft misalignments, and bearing faults (Tavner and Penman 1987, Vas 1993).
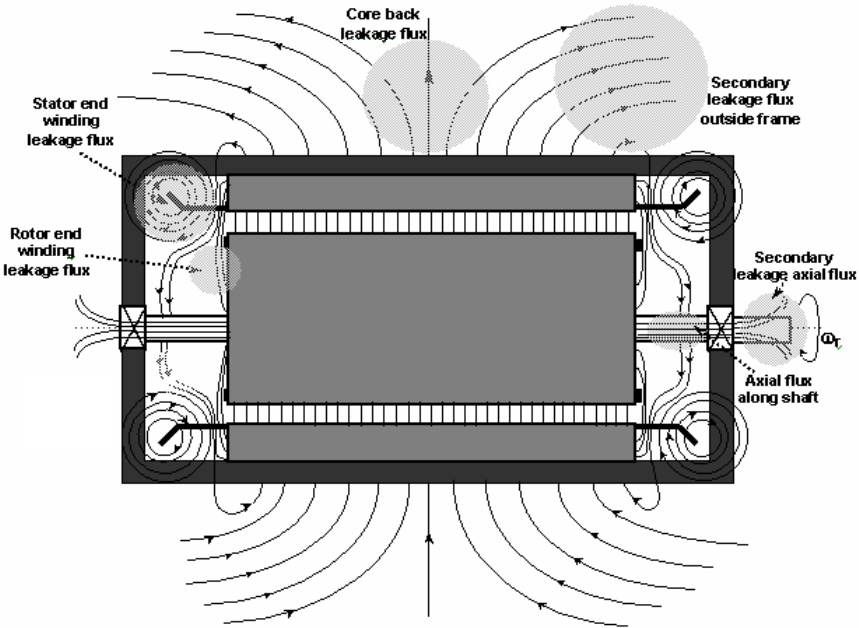
Fig. 3.3 Schematic of flux regions used for fault detection and condition monitoring of electrical machines (Thomson 1999).

Increments in the amplitudes of specific fault sideband frequencies are indicative of such abnormalities. The axial leakage flux trajectory is not clearly defined in electrical machines, but usually this is associated with the shaft. In practice, the detection of axial leakage flux is relatively straightforward. The technique of measuring the axial leakage flux is simple and non-invasive. All that is required is a search coil placed concentrically with the drive shaft of the motor. Some authors claim that, typically, there is sufficient axial leakage flux that it is possible to mount the coil, or coils, external to the machine case (Kokko 2003).

End winding leakage fluxes are the main cause of the axial leakage flux, which is measured using axial leakage flux measurements.

A source of troublesome eddy currents in the stator core end regions of large machines is caused by the "back-of-core leakage flux", which is the small component of armature flux that is not contained by the core and which permeates the space behind the core and tends to be drawn into circumferential members of the core frame. The axial members of the core frame are exposed to this leakage flux and act as a squirrel cage, with the circumferential members of the core frame at the ends of the machine providing return paths (Anderson).

Electromagnetic flux regions to be monitored for the machine under study in this work

In this thesis, the search coils presented in Figs. 3.4–3.5 were studied both by means of measurements (carried out for a 35-kW cage induction motor) and simulations (when possible) in order to find out their ability to sense specific machine faults:

- "1" internal search coil mounted around one stator tooth; wave winding formed of a conductor 1.7 mm in diameter,
- "2" external search coil formed of 200 turns, with its length equal to the active axial length of the machine and width equal to 2 pole pitches; the conductor used is 0.2 mm in diameter,
- "3" search coil formed of 200 turns mounted in the non-drive end (ventilator side); the conductor used is 0.2 mm in diameter,
- "4" search coil formed of approximately 300 turns mounted around the motor shaft (internal), the conductor used is 0.2 mm in diameter,
- search coils sensing the electromagnetic flux harmonics of the order "$p\pm1$"; wave windings formed of a conductor 1.7 mm in diameter and placed in the slot openings of the stator slots.

When the end connections of the coils are spread apart a *wave* or *series winding* is formed. In a wave winding there are only two paths regardless of the number of poles.

The external search coil, with its width equal to 2 pole pitches and the search coils purposed to sense the electromagnetic flux harmonics of the order "$p\pm1$", are chosen with the purpose of eliminating the main symmetrical air-gap field. In this way, only those spatial harmonics that appear during a working condition that affects the symmetry of the machine are to be displayed. In the simulations, the indications provided by these search coils should be ideally zero for healthy operation as a result of the perfect machine symmetry, which will not be the case for the measurements obtained with tests on a real machine because of inherent constructional asymmetries. The search coils intended to sense the axial flux were chosen with it being borne in mind that any asymmetry, whether coming from the rotor or from the stator side, in an electrical machine is reflected in this flux.
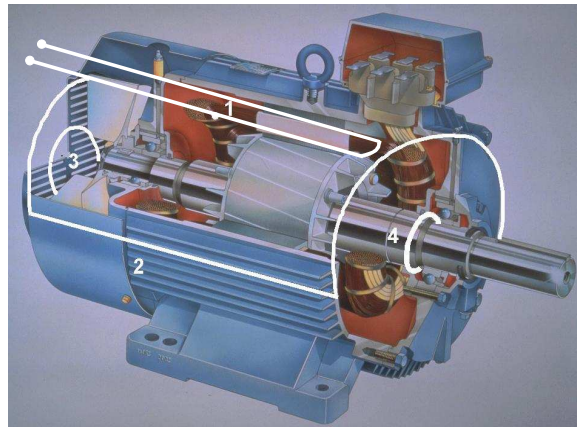

Fig. 3.4 Search coils used for the electromagnetic flux monitoring.

3.5.4 Electromagnetic flux harmonics of order "$p \pm 1$" used for fault detection

As will be shown in the following sections of this work, there is a stringent need to look for a fault indicator that is able to point out eccentricity-related abnormalities and bearing faults. In this respect, the electromagnetic flux eccentricity harmonics of the order "$p \pm 1$" that interact with the fundamental harmonic of the machine and generate the forces will be studied to find out their ability to detect machine abnormalities other than various types of eccentricity; this approach is a novelty in the field of fault diagnosis in electrical machines. The electromagnetic flux eccentricity harmonics of the order "$p \pm 1$" were determined by analytical means and are of the following form (Früchtenicht et al. 1982, Tenhunen et al. 2003):

$$b_{p \pm 1}(x,t) = B_{p \pm 1} \cos\left[\left(p \pm 1 \right)x - \left(\omega_1 \pm \omega_w \right)t - \left(\varphi_p \pm \varphi_w \right) \right] \qquad (3.9)$$

where p is the pole-pair number of the motor, ω_1 is the fundamental frequency, ω_w is the whirling frequency, and φ_p and φ_w are phase angles.

Dorrell et al. (1995) have shown that dynamic eccentricity produces air-gap field components rotating at $f_s \pm f_r$ Hz (where f_s is the supply frequency and f_r is the rotational frequency of the rotor) with corresponding $p \pm 1$ pole-pairs in addition to the usual p pole-pair field. It can be seen that both static and dynamic eccentricity produce their own "$p \pm 1$" field components and these field components may be used for monitoring purposes.

Fig. 3.5 presents the positioning of the search coils used for the detection of the "$p \pm 1$" eccentricity harmonics in the electromagnetic flux. Basically, the balanced pair(s) of the search coils in the air-gap are so arranged that the main symmetrical air-gap field is eliminated and only the lack of symmetry resulting from the flux associated with a fault is to be displayed. The three search coil pairs placed 120° apart in the air-gap (Fig. 3.5.b) are connected in series.
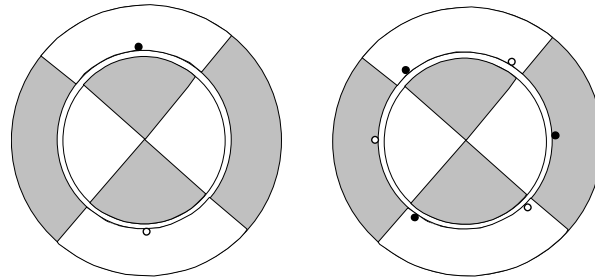
a) search coil "p-1"　　　　*b) search coil "p+1"*

Fig. 3.5 Search coils positioning for measuring the "p±1" harmonics (the test motor has p=2).

3.5.5 Turn-to-turn (inter-turn) short circuit fault detection in stator windings

In the case of a stator winding-related fault, there is a strong need for techniques that would not only detect the occurrence of the fault but would also locate its position in the winding while the motor is operating. Since the effect of a turn-to-turn short circuit will be to increase asymmetry and consequently modify axial flux, a possible method to locate the position of the shorted turn is based upon localised measurement of the magnetic field symmetry disruption in the end-winding region of the motor.

Penman et al. (1994) tested a technique based on axial leakage flux. A large coil wound concentrically around the shaft of the machine has the ability to sense a fault in the winding while the motor is operating. The set-up needed with this method for the fault location procedure consists of four coils symmetrically mounted in the four quadrants of the motor at a

radius of about half the distance from the shaft to the stator end winding (Fig. 3.6). The frequency components to be detected in the axial flux component are given by

$$f_{\text{short}} = f_s \left(k \pm n \frac{(1-s)}{p} \right)$$ (3.10)

where p is the number of pole-pairs, f_s is the supply frequency, $k = 1, 3$ (order of the supply time harmonics), s is the slip, and $n = 1, 2, 3, \ldots (2p\text{-}1)$.
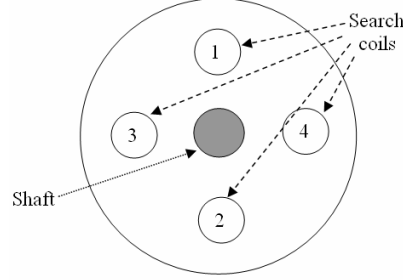
Fig. 3.6 Coil geometry arrangement for reliable turn fault location (Penman et al. 1994).

3.5.6 Broken rotor bars detection

Elkasabgy et al. (1992) present different techniques for the detection of broken rotor bars in the cage rotor of an induction machine. Among these techniques, those involving the study of voltages induced in search coils appeared to provide the most useful, reliable, and cost-effective diagnostic techniques. It was found that an external search coil placed against the casing is just as effective as an internal coil mounted around a stator tooth tip for the detection of a rotor fault. The characteristic frequencies at which the rotor fault would become distinguishable are given by:

$$f_{\text{brb}} = f_s \left[\left(\frac{k}{p} \right)(1-s) \pm s \right]$$ (3.11)

with $k = 1, 2, 3$.

Techniques relying on the indications provided by internally mounted search coils proved to sense well enough rotor faults such as broken damper bars (Karmaker 2003).

Following the work of Penman et al. (1986), the detection of rotor bar faults is also possible by frequency domain analysis of the axial leakage flux, which is monitored by using an external search coil wound around the shaft of a machine. The frequency components are still given by (3.11) with $k = 1, 2, 3$.

Other characteristic frequencies at which rotor faults would become distinguishable are given by Vas (1993):

$$f_{\text{brb}} = sf_s$$ (3.12)

$$f_{\text{brb}} = f_s (2s \pm 1)$$ (3.13)

3.5.7 Bearing fault detection

The voltages resulting from the irregularities in the magnetic circuits of motors lead to shaft currents through the shaft, bearings, bearing supports, and closing through the machine framework. The procedure of measuring the shaft current has already been discussed in Section 3.4.3.

3.5.8 Eccentricity detection

Air-gap eccentricity induces harmonics in the air-gap flux. These harmonics give rise to axially directed flux and the amplitude of axially directed flux harmonics is proportional to the amount of air-gap eccentricity.

Rankin et al. (1995) have demonstrated that the shaft voltage's AC component can be used as an indicator to static eccentricity in the stator to rotor air-gap of a diesel driven salient pole alternator.

Summary

Chapter 3 has presented a general view of the fault indicators used for electrical machines, with a special focus on the ones of an electrical nature – current in the stator winding and electromagnetic flux captured in various machine locations.

The possible signatures to be produced by various faults were presented and will be resorted to in Chapter 5 that deals with the presentation of the results obtained form experiments and simulations.

However, it is very important to bear in mind that the MCSA techniques are not able to detect all of the possible faults in an induction machine and many research, including this work, are aimed to transfer a part of the MCSA knowledge to techniques that monitors the signatures produced by the fault to the electromagnetic flux signals.

4 METHODS OF ANALYSIS

4.1 Finite element analysis

4.1.1 Finite elements methods – general description, areas of application

The *finite element method* is a technique used to solve complex problems, which are represented by differential equations. It effectively transforms the problem into a series of algebraic problems, which are much easier to compute. Electromagnetic problems are described by *Maxwell's equations* (Maxwell 1865), which relate electric fields to magnetic fields.

The finite element method splits the problem domain into a large number of small elements. The elements are typically triangular or quadrilateral in shape. Different techniques exist for the derivation of the algebraic equations from the initial problem region. The two most widely used methods are the *Variational Method* (Binns et al. 1992, Silvester and Ferrari 1996, Jiamning 1993), such as the Rayleigh Ritz method, and the method of *Weighted Residuals*, such as the Galerkin Method (Binns et al. 1992, Salon 1995). Both types have advantages, depending on the particular problem to be solved.

In order to solve a problem, the following information is required:

- the problem geometry must be specified and split into many small regions (elements),
- the material properties are required, i.e. the conductivity, permeability, and so on,
- the excitations in the problem region must be known (normally current densities in conducting regions),
- any constraints which include boundary conditions must be specified.

The first published paper to use the term "*Finite Elements*" was published by Clough in 1960. However, similar techniques were used as far back as 1943 by Courant.

The technique was initially used in civil engineering and aeronautical problems, especially by the large aircraft companies, which could afford the powerful computers required for carrying out stress analysis work on aircraft designs. Since then, the method has increased in popularity, mainly because of rapid advances in computing power and speed. *Finite element analysis techniques* are now used in a wide variety of engineering problems, including *mechanical stresses*, *electric and magnetic fields*, *heat transfers*, and *fluid flows*. The advantages offered by the finite element method over more traditional methods are that complex geometries can be represented accurately, material properties and forcing functions can be modelled accurately, and material non-linearity can be accounted for.

4.1.2 Numerical electromagnetic field analysis for electrical machines

History

The potential of using finite element methods for analysing the magnetic field distribution in electrical machines was identified in the early '70s (Chari and Silvester 1971). As well as fixed mesh models, where the actual model is stationary and the rotating fields and current distributions are modelled by complex number representation, time-stepping techniques have been developed (Arkkio 1988), where the rotor is physically rotated inside the stator to give a more realistic representation of machine operation.

With the finite element method of modelling an electrical machine, the complex geometry of the machine and the magnetic non-linearity of the core regions can be accurately represented, allowing the effects of saturation to be modelled. The induced currents in the rotor cage, for instance, allowing for skin effects, can also be modelled accurately.

Three-dimensional finite element modelling has been discussed since the early '80s (Chari et al. 1982), but because of the even greater computational burden this involves, the extent of its use was rather limited until the mid-2000s.

Application to fault diagnostics and condition monitoring

The basis of any reliable diagnostic method is an understanding of the *electric*, *magnetic*, and *mechanical behaviour of the machine in a healthy state and under fault conditions*. As a consequence of electrical or mechanical faults which may arise during the operating period, many electrical machines are operating under *asymmetrical conditions*. In this respect, the study of the asymmetrical magnetic field of the electrical machine is an inseparable part of the diagnostic procedure.

The magnetic field distributions and operating characteristics provided by computer simulations are essential in foreseeing the *changes of motor performance* resulting from the parameter changes that appear as the consequence of different faults. Computer simulations based on mathematical models represent an *effective* and *inexpensive method* for studying the influence of different motor faults on drive performance. Simulation results represent a contribution to the correct evaluation of the measured data in diagnostic procedures, which are an important part of a supervision system based on expert systems and artificial intelligence methods (Vas 1999).

Numerical modelling and simulation can provide *virtual measurement data* from machines that have faults implemented in their structures. Then, modern signal processing techniques can be used to convert the simulation results into a form from which faults can easily be detected. It is very important to bear in mind that *if a monitoring system cannot detect and diagnose an artificial fault from the virtual measurement signals, it is hardly likely to work with real electrical machines, either.*

The electromagnetic model is valid for studying only those *faults which modify the magnetic field distribution in the machine*. It is not suited to studying, for instance, partial discharges in the winding's insulation or small mechanical vibrations caused by a fault in the bearings.

4.1.3 Description of the numerical electromagnetic field simulation tool used in this thesis

The numerical electromagnetic field simulation tool used in this thesis was developed in the Laboratory of Electromechanics of Helsinki University of Technology and was originally presented by Arkkio (1987).

By using this simulation tool, one may take full advantage of the possibility to monitor a wide variety of electrical parameters (and not only) and to implement various fault types characterised by specific severity degrees. This method of analysis is based on the *combined solution of the magnetic field equations and the circuit equations of the windings. The equations are discretised by the finite element method.* In order to keep the amount of computation at a reasonably low level, several simplifications were made:

- the magnetic field in the core of the machine is assumed to be two-dimensional.
- the three-dimensional end region fields are modelled approximately by constant end-winding impedances in the circuit equations of the windings.
- the current density in the stator conductors is constant, meaning that the skin effect in the stator is neglected.

-   the laminated iron core is treated as a non-conducting, magnetically non-linear medium, and the non-linearity is modelled by a single valued magnetisation curve.

The three-dimensional effects of the stator and rotor end winding leakage reactances are accounted for by their inclusion in equivalent circuits inside the finite element model.

The *magnetic vector potential A* satisfies the equation

$$\nabla \times (v\nabla \times A) = J \tag{4.1}$$

where v is the reluctivity of the material and J is the current density. The current density can be expressed as a function of the vector potential and the electric scalar potential ϕ

$$J = -\sigma \frac{\partial A}{\partial t} - \sigma \nabla \phi \tag{4.2}$$

where σ is the conductivity of the material. In the two-dimensional model, the vector potential and the current density have only the z-components

$$A = A(x, y, t)e_z$$
$$J = J(x, y, t)e_z \tag{4.3}$$

The scalar potential ϕ has a constant value in the cross-section of a two-dimensional conductor, and it is a linear function of the z-coordinate. The gradient of the scalar potential can be expressed with the aid of the potential difference u induced between the ends of the conductor. By substituting (4.2) in (4.1), the field equation becomes

$$\nabla \times (v\nabla \times A) + \sigma \frac{\partial A}{\partial t} = \frac{\sigma}{l}ue_z \tag{4.4}$$

where l is the length of the conductor. A relation between the total current i and the potential difference u is obtained by integrating the current density (4.2) over the cross-section of the conductor

$$u = R\,i + R\int_S \sigma \frac{\partial A}{\partial t}\,dS \tag{4.5}$$

where R is the DC resistance of the conductor. The circuit equations for the rotor cage are constructed by applying Kirchhoff's laws and (4.5) for the potential difference. The details of the construction of the circuit equations have been presented by Arkkio (1987).

Time dependence

A *time-dependent field* is solved by discretising the time at short time intervals Δt and evaluating the field at the times t_1, t_2, t_3, ($t_{k+1} = t_k + \Delta t$). The time-dependence of the field is modelled by the Crank-Nicholson time-stepping method. In this method, the vector potential at time t_{k+1} is approximated as following

$$A_{k+1} = \frac{1}{2}\left\{\left.\frac{\partial A}{\partial t}\right|_{k+1} + \left.\frac{\partial A}{\partial t}\right|_k\right\}\Delta t + A_k \tag{4.6}$$

By adding the field equations written at the times t_k and t_{k+1} together and substituting the sum of derivatives from (4.6), the following expression is obtained:

$$\nabla \times (v_{k+1} \nabla \times A_{k+1}) + \frac{2\sigma}{\Delta t} A_{k+1}$$

$$= \frac{\sigma}{l} u_{k+1} e_z - \left\{ \nabla \times (v_k \nabla \times A_k) - \frac{2\sigma}{\Delta t} A_k - \frac{\sigma}{l} u_k e_k \right\} \qquad (4.7)$$

The potential difference equation (4.5) is discretised in the same way as the field equation, the result being

$$\frac{1}{2}(u_{k+1} + u_k) = \frac{1}{2} R(i_{k+1} + i_k) + R \int_S \sigma \frac{A_{k+1} - A_k}{\Delta t} \cdot dS \qquad (4.8)$$

Eqs. (4.7) and (4.8) form the *basic system of equations in the time-stepping formulation.* Starting from the initial values and successively evaluating the potentials and currents of the next time-steps, the time variation of the quantities is worked out.

Motion of the rotor

In a general time-stepping analysis of a running motor, the equations for the rotor and stator fields are written in their own co-ordinate systems. The solutions of the two field equations are matched with each other in the air-gap. The rotor is rotated at each time-step by an angle corresponding to the mechanical angular frequency. The rotation is accomplished by changing the finite element mesh in the air-gap.

Numerical solution

The construction of the circuit equations and the details of the numerical solution of the coupled field and circuit equations have been presented by Arkkio (1987). The finite element discretisation leads to a non-linear system of equations in which the unknown variables are the nodal values of the vector potential and the currents or potential differences of the windings. The system of equations is solved by the Newton-Raphson method.

Evaluation of operating characteristics

The magnetic field, the currents, and the potential differences of the windings are obtained in the solution of the coupled field and circuit equations as discussed above. Most of the other machine characteristics can be derived from these quantities.

The calculation of the *electromagnetic torque* is computed using the method developed by Coulomb (1983). This method is based on the principle of virtual work, for calculating the forces from a finite element solution. In this method, the force is calculated as a partial derivative of the coenergy functional with respect to virtual movement.

Finite element mesh

The *magnetic field* of a *healthy electrical machine is periodic in space*, *typically from one pole-pair to the next one*. In order to reduce the complexity of the geometry and the number of nodes of the finite element mesh, the calculations are usually performed over the smallest symmetrical part of the motor model. However, a fault in the machine disturbs the symmetry, and the whole machine cross-section has to be modelled.

For fault detection purposes, the interest is focused more on qualitative than exact quantitative results, i.e. *more focused on detecting how the monitored parameter behaves as a function of time and not so much in magnitude*. In this respect the finite element meshes to be used can be relatively sparse, as long as the geometric symmetry is the same as for the faulty machine and the time dependence of the parameters is modelled properly. In this study, triangular first-order finite elements are used, and the finite element meshes typically contain 6000-8000 elements.

In the numerical simulations, during *healthy motor operation*, *the symmetry forbids the flux linkage through the search coils "p±1" and through the one externally wound around two pole pitches of the test motor*. In a faulty machine, a flux linkage through these search coils may be detected.

The input for the finite element code may be represented by the voltage waveforms measured via a transient recorder directly from the frequency converter or by various other supply sources. In this thesis, the simulation models were tested with the voltage waveforms measured from the frequency converter but also with a sinusoidal supply. During the simulations, the speed of the rotor was kept constant since the objective of the thesis was to study only the operation at steady state.

4.1.4 Fault modelling procedure

The test motor used in this thesis is a cage induction motor whose main parameters are presented in Table 4.1. Table 4.2 presents the faults taken into consideration in this work both from experiments and simulations.

Table 4.1 Main parameters of the test motor.

Number of poles		4
Parallel branches in stator winding		2
Turns/coil in stator winding		11
Stator connection		star
Rated slip	[%]	3
Rated power	[kW]	35
Rated frequency	[Hz]	100
Rated voltage	[V]	400
Rated current	[A]	64
Number of stator slots		48
Number of rotor slots		40

Table 4.2 Faults studied in the numerical simulations and in the measurements.

Fault	Simulations	Experiments
Shorted turn in stator winding	yes	yes
Broken rotor bar/s	yes	yes
Static rotor eccentricity	yes	yes
Dynamic rotor eccentricity	yes	yes
Bearing fault	no	yes
Core faults	yes	no

Shorted turns

To model a *shorted turn*, the sides of this turn in the finite element mesh are substituted by conductors in a perfect short circuit. There is no galvanic contact between the reduced phase winding and the new, shorted conductors. A shorted coil is treated in a similar manner. Fig. 4.1 presents a simple description of the turn-to-turn short circuit implemented in the simulations.

In measurements, the turn-to-turn short circuit was implemented between two adjacent turns of the stator winding (see Fig. 4.1), was initiated and cleared from outside the motor, and did not comprise any resistor specialised in limiting the effects of such an operating state. By using a switcher, the duration of this faulty condition was limited to about one second. However, the measurements at full load were not carried out, since the main concern was to keep the test machine healthy for further tests and not to expose it to extreme conditions.
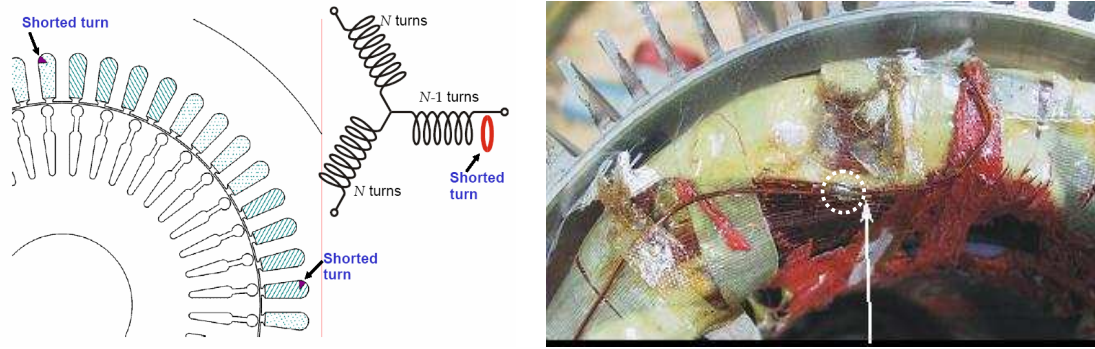
Fig. 4.1 Description of the turn-to-turn short circuit implemented in the simulations (left figure) and measurements (right figure).

Static and dynamic eccentricity

Static eccentricity is obtained by shifting the rotor by 30% of the radial air-gap length and rotating the rotor around its centre point in this new position. *Dynamic eccentricity* is obtained by shifting the rotor by 33% of the air-gap length, but rotating it around the point that is the centre point of the stator bore.

Experimentally, a dynamic eccentricity of 33% was obtained by fitting non-concentric support parts between the shaft and bearing (see Fig. 4.2). In order to create an artificial static eccentricity in the test motor, the inner diameter of the motor end-shields was reduced by about 0.6 mm (the size of the machine air-gap is 0.8 mm). Both end-shields were then shifted in the same direction in order to obtain a static eccentricity of around 30%.
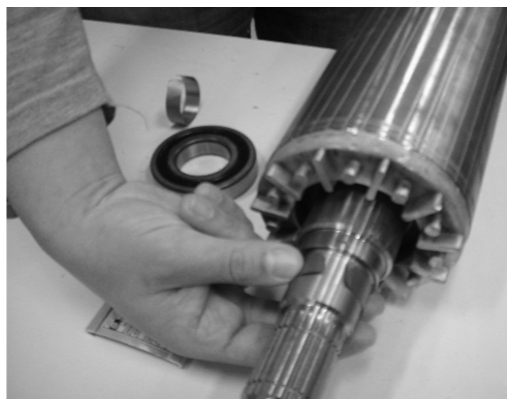
Fig. 4.2 Artificially created dynamic eccentricity.

Broken rotor bars

Fig. 4.3 presents how the circuit equations of the cage windings are composed of the potentials of the bars inside the rotor core, bar ends outside the core, and end-ring segments connecting the bars. When modelling a *broken bar*, the resistance of the bar end outside the core is increased to a value 1000 times the DC resistance of the whole bar. When modelling a *broken end-ring*, the resistance of an end-ring segment between two bars is increased to a value 1000 times the original resistance of the segment. In addition to the description of the model implemented in the simulations for the study of various rotor cage-related failures, Fig. 4.3 also presents the artificially created rotor cage faults obtained by drilling holes in the rotor bars.
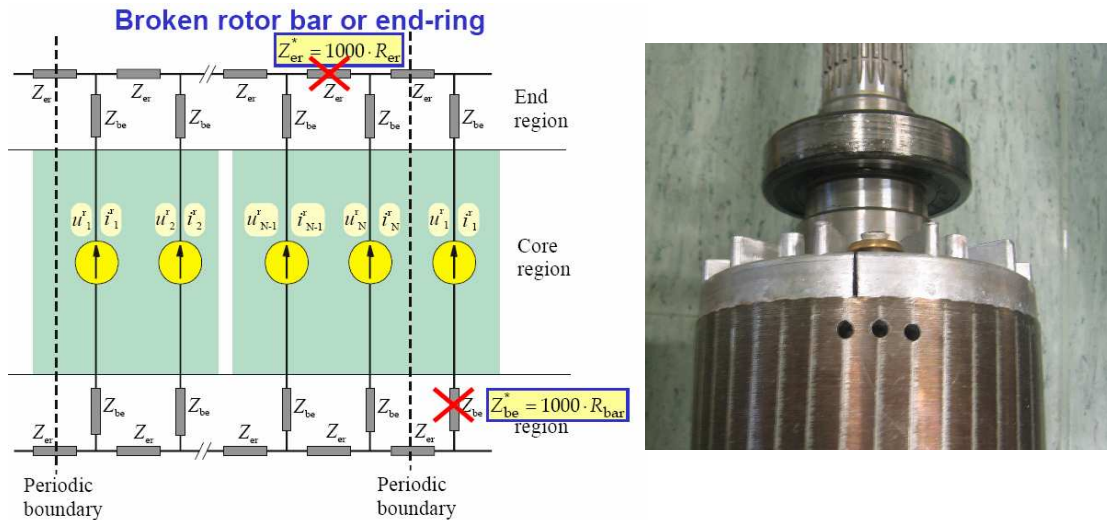
Fig. 4.3 Description of the rotor cage-related faults implemented in simulations (left figure) and artificially created in measurements (right figure).

Core faults – fault in core insulation

To model a fault in sheet insulation on a tooth-top surface, a current is allowed to flow along the tooth-top and return back into the frame. A similar fault can also be created in several adjacent teeth. Fig. 4.4 presents a description of the core fault implemented in the simulations.

Table 4.3 is intended to offer a view of the magnitude of the various fault levels implemented in the simulations ("cf1" – "cf9" were used to indicate various degrees of core fault; see Fig. 4.4). The various stator winding configurations studied and referred to in this table as "NB" (no parallel branches), "SB" (special configuration), "2B" (two parallel branches – this is the original configuration to be found in the motor tested experimentally), and "4B" (four parallel branches) are described in detail in Appendix II.
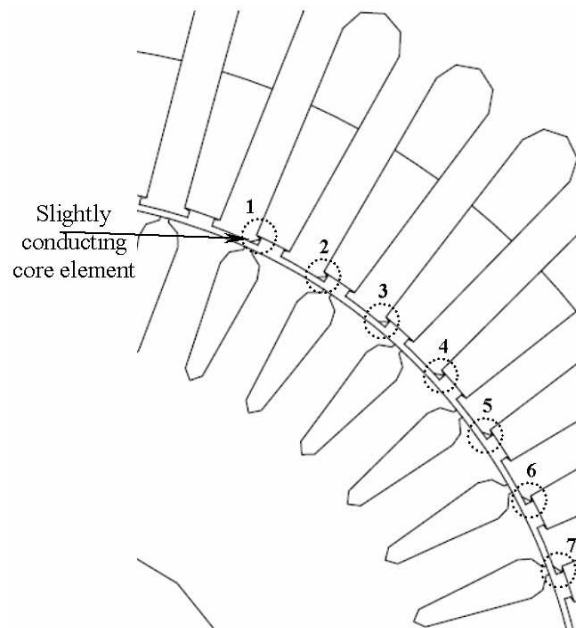
Fig. 4.4 Description of the core fault implemented in the simulations.

Table 4.3 Eddy current losses at the fault location and corresponding total electromagnetic loss following the core fault implementation.

|	Stator winding configurations – losses [W]				Total electromagnetic losses [W]		
	"NB"	"SB"	"2B"	"4B"	"NB" "2B" "4B"		"SB"
cf1	31	29	32	31	3106		2830
cf3	94	87	94	93	3260		2900
cf6	188	173	188	187	3347		2980
cf9	281	260	281	279	3426		3068

4.2 Method of measurements

The test cage induction motor described in Table 4.1 was fed from an inverter that had a switching frequency of 3 kHz. A DC generator was used for loading the motor. The currents, voltages, power and supply frequency, were measured using a wide band power analyser. The measurements were carried out for three different load conditions. Figs. 4.5-4.7 present the measuring set-up. A detailed description of a few of the devices used in this set-up is to be found in Appendix II. The current and voltage waveforms were recorded with a transient recorder. Hall sensors (LEM) were used as current transducers, and the voltages were measured through an isolation amplifier. The sampling frequency was 40 kHz and a typical number of samples was 20000. The recording system was calibrated using the measurements from the power analyser. The measurements were carried out only for the original stator winding topology, consisting of 2 parallel branches.
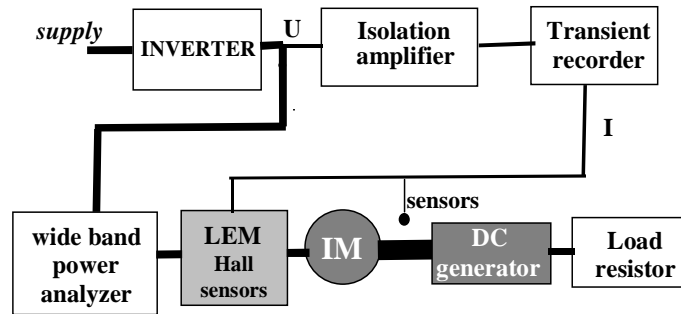
Fig. 4.5 Schematic of the measuring set-up.
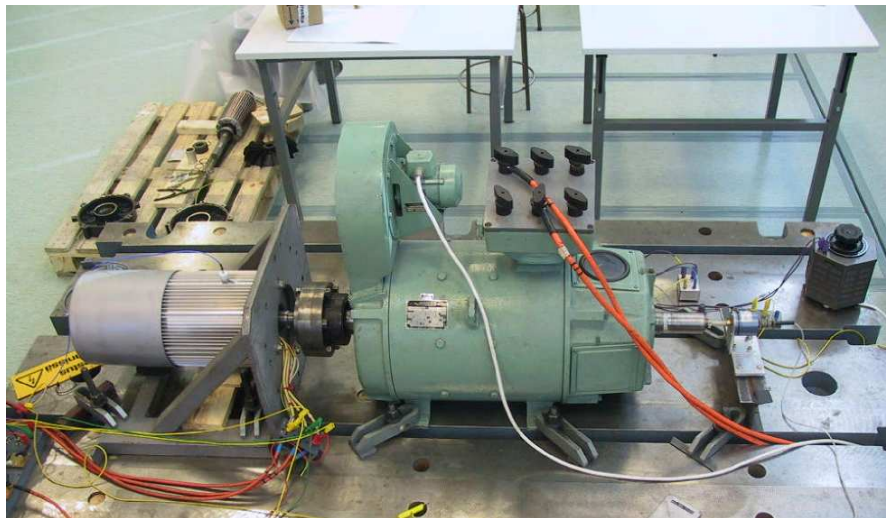
Fig. 4.6 Test induction motor (left) and DC generator used as load.

From the beginning, it is important to specify that the induction machine used in the measurements has a skewed rotor but the simulated machine has a non-skewed one. Because of this, some differences between the measured and simulated results should be expected, especially in the magnitude of the rotor-slot harmonics.

Fig. 4.8 presents the cross-sectional geometry of the machine and the magnetic field distribution at rated load operating conditions for healthy operation.

Fig. 4.7 Measurement devices. From top to bottom: transient recorder, keyboard, power analyser, isolation amplifier, and connection box.
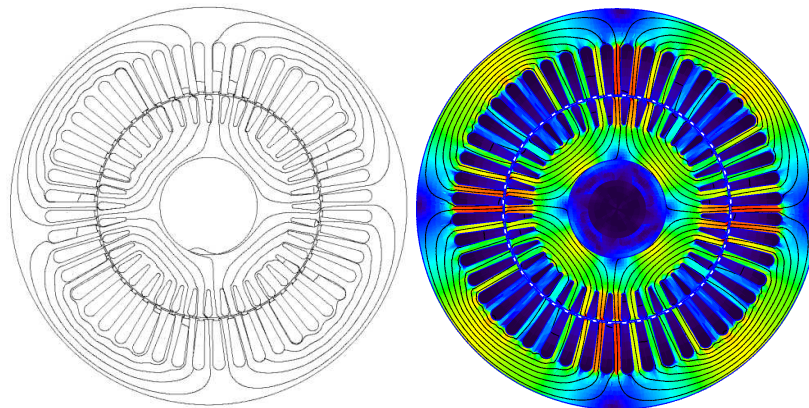
Fig. 4.8 Cross-sectional geometry of the test motor and the electromagnetic field distribution for healthy operation at rated load.

4.3 Signal processing methods

4.3.1 General

With advances in digital technology over the last several years, adequate data processing capability is now available on cost-effective, microprocessor-based, protective-relay platforms to monitor motors for a variety of abnormalities in addition to the normal protection functions.

Various electromechanical operational parameters able to provide rich information for diagnosis are analysed in steady state but also in transient state (especially at no-load starting) using approaches such as:

- frequency-domain analysis,
- time-domain analysis,
- time-frequency domain analysis,
- neural network,
- model-based techniques.

4.3.2 Analysis in steady state

The *frequency-domain analysis* for the detection and localisation of abnormal electrical and mechanical conditions in electrical machines is widely used and accepted in the industrial environment. This popularity is due to the availability of the *Fourier transform technique*, as the characteristics of the studied signals are more easily noticed in the frequency domain than in the time domain.

Advanced signal processing techniques, such as *high-resolution spectral analysis* are also used since they may lead to a better interpretation of the spectra characteristic to specific machine abnormalities. In this respect, it was experimentally proved that stator current high-resolution spectral analysis is very sensitive to induction motor faults modifying main spectral components, such as voltage unbalance and single-phasing effects (Benbouzid et al. 1999). *Bi-coherence spectra* were used by Li et al. (1995) to derive features that relate to the condition of a bearing. The application of *bi-spectral* and *tri-spectral* analysis to the vibration monitoring was also discussed by McCormick and Nandi (1999).

4.3.3 Transient state analysis

Elder et al. (1989) developed a technique which allows the detection and identification of specific faults within induction motors during the starting transient. During this short period the machine is under conditions of severe and electrical stress. This type of analysis at transient state is important especially for the detection of eccentricity since any UMP is a maximum at starting.

Since under transient conditions the frequency components indicative of faulty operations are non-stationary in both the time and frequency domains, other signal processing strategies applicable to time variants need to be applied. Time-frequency domain techniques use both time and frequency domain information, allowing for the investigation of transient features. A number of time-frequency domain techniques that have been proposed in literature are summarised by Ocak and Loparo (2001) as following:

- Short Time Fourier Transform (STFT),
- Spectogram - a representation of frequency components versus time (Burnett et al. 1995),
- Wigner Ville Distribution (Burnett et al. 1995),
- Wavelet Decomposition (Douglas et al. 2005, Yen and Lin 2000).

Since in both the measurements and simulations the signals studied as possible fault indicators were captured in steady state, only the traditional signal processing technique based on Fourier transformation (FFT) was used in this thesis.

4.3.4 Artificial intelligence techniques

The condition monitoring and fault detection of electrical machines have moved in recent years from traditional techniques to Artificial Intelligence (AI) techniques. In the AI-based systems, several quantities are utilized as input signals such as, stator currents and voltages, electromagnetic fluxes, frame vibrations, etc. The AI techniques have numerous advantages over conventional fault diagnostic approaches; besides giving improved performance, these techniques are easy to extend and modify, and can be made adaptive by the incorporation of new data or information. The AI-based techniques may use *expert systems*, *artificial neural networks*, *fuzzy logic*, *fuzzy-neural networks*, *genetic algorithms*, *support vector machines*, etc.

A review of the developments in the field of AI-based diagnostic systems in electrical machines and drives is provided by Vas (1999) and Filippetti et al. (2000b). Siddique et al. (2003) focus their review of various AI techniques to the induction motors, aiming more specifically to the stator winding fault detection.

From the multitude of AI-based diagnostic systems, the neural networks have a wide industrial applicability (Meireles et al 2003). A representative work dealing with the application and design of artificial neural networks for electrical motors fault detection is the one of Chow et al. (1993). Following, there will be presented few references to contributions dealing with the detection of various faults using the neural network approach.

Salles et al. (2000), show that a neural network approach is able to distinguish between *load anomalies* (oscillation torque, repetitive dip of torque) and *rotor asymmetries* (*broken bars*) of cage induction motors. This is a very important issue since a load anomaly causes a sequence of speed and current spectral components that can be confused with the one produced by a cage-related fault.

Filippetti et al. (2005) report an induction machine *rotor fault* diagnosis based on a neural network approach. After the neural network was trained using data achieved through experimental tests on healthy machines and through simulation in case of faulted machines, the diagnostic system was found able to discern between "healthy" and "faulty" machines.

Tallam et al. (2000), present an on-line neural network based diagnostic scheme, for induction machine *stator winding turn fault* detection. This scheme is claimed to be insensitive to unbalanced supply voltages or asymmetries in the machine and instrumentation. In addition, it is claimed that a turn fault can be detected in the early stage of development.

Huang et al. (2004) propose a scheme to monitor voltage and current space vectors simultaneously in order to monitor the level of *air gap eccentricity* in an induction motor. For the amplitudes of eccentricity related components that change non-monotonically with the operating conditions, an artificial neural network is used to learn the complicated relationship and estimate corresponding signature amplitudes over a wide range of operating conditions.

Li et al. (2000) use neural networks to perform motor *bearing fault* diagnosis based on the extracted bearing vibration features. Computer-simulated data were first used to study and design the neural network motor bearing fault diagnosis algorithm. Actual bearing vibration data collected in real-time were then applied to perform initial testing and validation of the

approach. The results show that neural networks can be effectively used in the diagnosis of various motor bearing faults through appropriate measurement and interpretation of motor bearing vibration signals.

Support Vector Machine (SVM) is a novel machine learning method introduced in early 90's and it has been successfully applied to numerous classification and pattern recognition problems such as text categorization, image recognition and bioinformatics. SVM based classification scheme were designed for different tasks in cage induction motor fault diagnostics and for partial discharge analysis of insulation condition monitoring and were found highly competitive with, e.g., neural networks, which are widely studied also in the area of condition monitoring and fault diagnosis of electrical machines (Pöyhönen et al. 2002a, Pöyhönen et al. 2002b, Pöyhönen 2004).

5. RESULTS OBTAINED FROM EXPERIMENTS AND SIMULATIONS

First of all, the relatively good agreement between the computed and measured total electromagnetic losses is presented in Fig. 5.1. These machine quantities are responsible for the correct evaluation of the motor performance and are considered very important for the procedure of validating the simulated data.

Once more, it should be mentioned that the measured machine has a skewed rotor, while the rotor of the simulated one is unskewed. The main effect of slot skew that is the filtering of high frequency harmonics may be observed in the waveforms of various simulated motor parameters characterised by higher ripple content in comparison with the similar measured ones (i.e. Fig. 5.2.1, etc.).
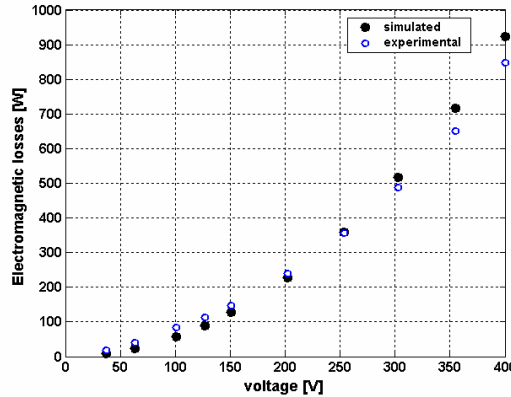

Fig. 5.1 Experimental and simulated total electromagnetic losses.

5.1. Current monitoring

5.1.1. Stator winding currents

First of all, the ability of the phase current to detect specific faults will be tested, since it was shown that monitoring this parameter is the most convenient (non-invasivity) and cheapest way to sense a fault in terms of expense caused by any additional sensors. For all the current spectra presented in this section, the supply frequency component (100 Hz) has been normalised to be set at 0 dB.

On the basis of the measurements, no new frequency components of the line current spectra appeared as a consequence of the inter-turn short circuit in the stator winding; only a rise of 15 dB in the amplitude of the 3rd harmonic component and of 3 dB in the magnitude of the fundamental was observed from experiments. This amplitude change is independent of the machine loading (half load or no load). With reference to the case of healthy operation, irrespective of the machine loading, an increase of around 6 dB in the amplitudes of the rotor-slot harmonics was found. The rotor-slot harmonics were calculated according to Eq, 3.5 where k and n_w are 1 and n_d is 0.

Based on simulations, Fig. 5.1.1 presents the modifications produced in the frequency spectrum of the branch currents by the inter-turn short circuit. These new components are according to Eq. 3.10 (Penman et al. 1994, Thomson 2001) and are of about the same amplitude for all the configurations studied except the "SB" one (Appendix II), where the amplitudes are 25 dB higher. Minor modifications (increment of about 2-3 dB) in the magnitude of the rotor-slot harmonics were observed, irrespective of the stator winding configuration and machine loading. The magnitude of the fundamental frequencies suffers similar changes to the ones mentioned before (3.5 dB for "4B" and "SB", 1.6 dB for the "2B" stator winding type).
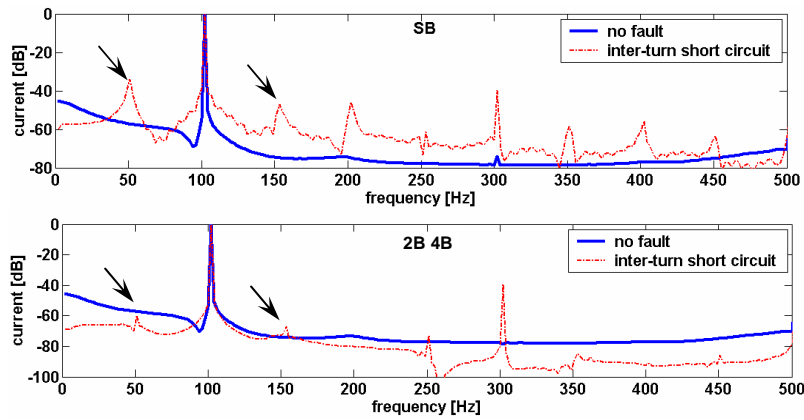
Fig. 5.1.1 Frequency spectrum of the branch current – inter-turn short circuit – simulations at full load.

In the measurements, an inter-turn short circuit in the stator winding was best reflected in the unbalance of the stator winding currents (Fig. 5.1.2). A work dealing with the detection of stator-related faults based on current amplitudes has been presented by Jover and Arkkio (2003).

It came out from both the simulations and experiments that the eccentricities, bearing-related faults, and major rotor cage faults do not result in any unbalance of the stator currents; spectral analysis then becomes indispensable when attempting to detect such faults.

From the simulations, it was found that the static eccentricity is not reflected in the indications of the branch currents in any of the configurations that were studied. The measurements revealed increases of around 6-8 dB in the amplitudes of the rotor-slot harmonics, irrespective of the machine loading. Modifications of similar magnitudes are to be found in the case of a bearing fault. However, these modifications are not very specific and it would be quite difficult to rely confidently on them for claiming the presence of a fault and, moreover, distinguishing between various faults.

Fig. 5.1.3 presents the frequency spectra of the stator winding branch current for healthy operation and for abnormal operations provoked by rotor cage faults. A rotor cage fault is clearly visible when the sideband components closest to the fundamental given by Eqs. 3.1 and 3.2 are checked. For a rated slip of 3%, according to Eq. 3.1 these side bands are situated at 94 Hz and 106 Hz, and at 45.5 Hz and 51.5 Hz, etc., according to Eq. 3.2. The results obtained from simulations stand for the original "2B" winding configuration. They look similar to the ones obtained from a motor equipped with a "4B" winding configuration that are not presented here.
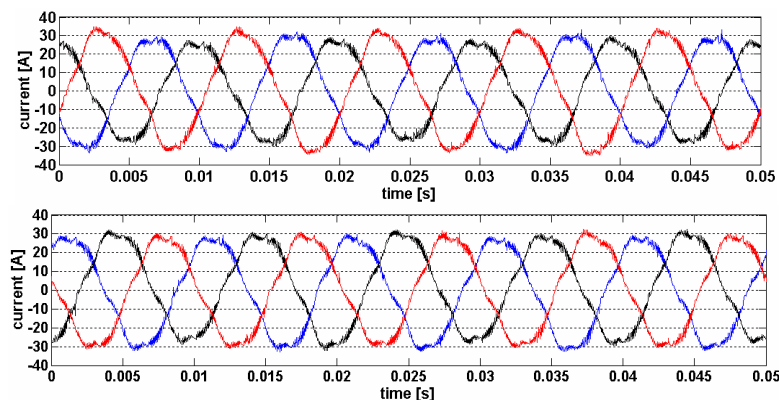

Fig. 5.1.2 Stator winding branch currents – inter-turn short circuit (top) and no fault (bottom) – measurements at half load.
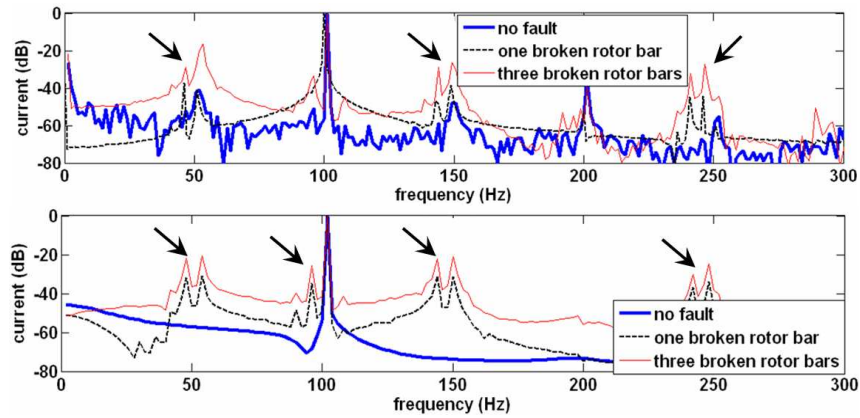
Fig. 5.1.3 Frequency spectra of the branch current – rotor cage faults – measurements (top) and simulations (bottom) at full load.

Fig. 5.1.4 presents the distortions produced by a major rotor cage-related fault (three broken rotor bars) in the stator winding branch current spectrum for the stator winding configurations "NB" and "SB". It is clear that for the stator winding configurations "NB" and "SB" a rotor-cage-related fault does not produce similar modifications in the indications of the branch currents as is the case with the "2B" and "4B" winding configurations; the distortions according to Eq. 3.2 are not found any more.

Fig. 5.1.5 offers a quantitative view of the magnitude of the distortions produced by various degrees of severity of the fault at full load. The measurements (marked by dots) reveal a good agreement with the simulations in terms of new frequency components detected as a result of a rotor cage fault. Simulations and measurements at half load do not cause major changes to the magnitude of the frequency components characteristic of this fault, but the distortion content is poorer than the one that is clear at full load (the frequency components around the fundamental according to Eq. 3.1 are not found any more in the cases of the "2B" and "4B" configurations). At no load it is almost impossible to detect a rotor cage fault, since most of the characteristic frequency components responsible for the fault detection are missing or are characterised by a dramatic change in magnitude (less than 50 dB) with reference to the fundamental.
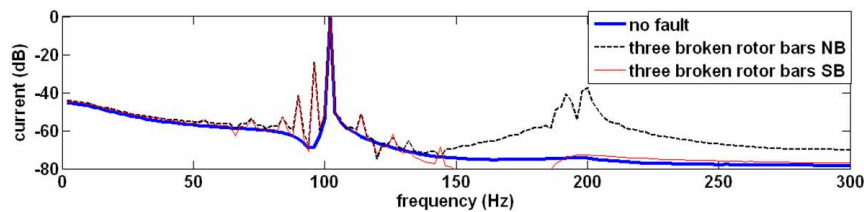
Fig. 5.1.4 Frequency spectra of the branch current – rotor cage fault – simulations at full load.
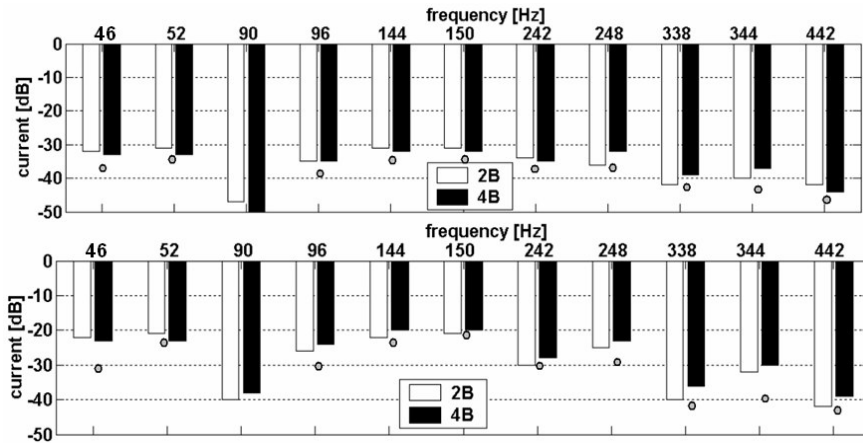
Fig. 5.1.5 Characteristic fault frequencies produced by rotor cage-related faults in the stator winding branch current spectrum – simulations (represented by bars) and measurements (represented by dots) at full load. One broken rotor bar (top) and three broken rotor bars (bottom).

On the basis of the simulations, the dynamic eccentricity is not reflected in the indications of the branch currents for the cases of the "NB" and "SB" stator winding configurations. For the "2B" stator winding configuration, Fig. 5.1.6 presents the distortion produced by dynamic eccentricity in the branch current spectrum. For the "2B" and "4B" stator winding configurations, Table 5.1 presents a summary of the most important modifications considered useful for the detection of such asymmetry (according to Eq. 3.5). No relevant modifications in comparison with the case of healthy operation were found in the magnitudes of the rotor-slot harmonics.

The relatively good agreement between the measurements and simulations in terms of ability to predict the location of the frequency sidebands responsible for the detection of this fault is shown by arrows.
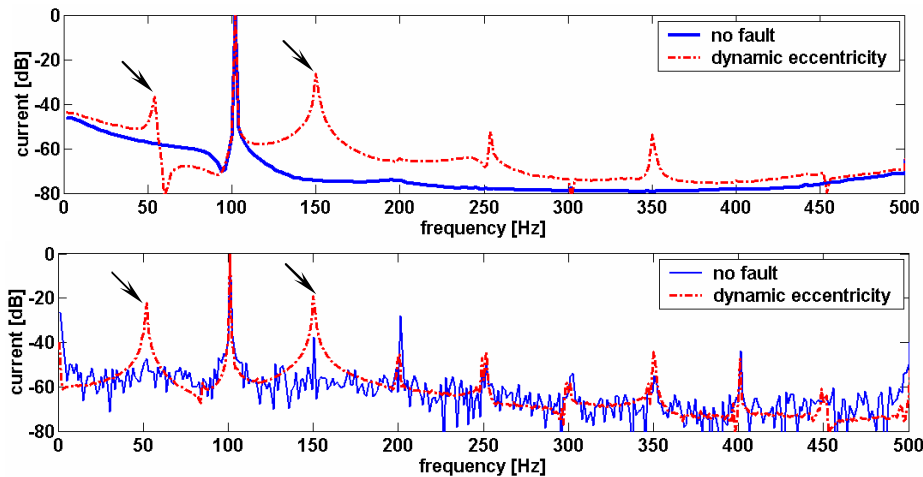
Fig. 5.1.6 Spectrum content of the stator winding branch current – dynamic eccentricity – simulations (top) and measurements (bottom) at half load. Figure corresponding to the operation of a motor equipped with the original stator winding configuration of type "2B".

Table 5.1 Modifications in the spectrum of the branch current caused by dynamic eccentricity [dB].

| f [Hz]	Full load Simul.		Full load Meas.	Half load Simul.		Half load Meas.	No load Simul.		No load Meas.
	"2B"	"4B"		"2B"	"4B"		"2B"	"4B"	
51.5	-33	-34	-28						
50.7				-27	-28	-22			
50							-18	-22	-9
148.5	-23	-23	-26						
149.2				-20	-20	-19			
150							-12	-13	-5
1991.5	-62	-50	-60						
1918.5				-43	-41	-56			
1949.5							-44	-44	-30
2088.5	-41	-36	-56						
2118.5				-42	-54	-58			
2149.5							-32	-46	-18

5.1.2. Circulating current between parallel branches

Since the stator winding phase of the test induction motor consists of two half-phases (branches) connected in parallel and these phases are accessible from outside the motor, the analysis of the differential *circulating current* between the half-phases is also performed with the purpose of fault detection. Figs. 5.1.7-5.1.8 present the measured and simulated waveforms of the circulating currents between stator winding parallel branches for healthy machine operation and for the faults under study.

For a machine which has its stator winding distributed in parallel branches, it is quite clear that by monitoring the circulating current one could easily identify both a major rotor fault (such as a rotor bar breakage) and a stator-related fault (such as an inter-turn short circuit). The circulating current may then be used as an additional diagnostic medium when aiming to sense a stator-related fault or as a first sign of other abnormal operation, since it would be easier to sense the current unbalance in the parallel branches than compute the current frequency spectra.

However, it appears difficult to discriminate between different fault conditions and between a fault and a healthy motor condition on the sole basis of the magnitudes of the circulating currents. In this respect, it was found that a static eccentricity level of 30% is reflected in the circulating current almost identically as a bearing fault and the magnitude of the circulating current in these cases is almost the same as that which is characteristic of healthy machine operation.

The relatively clear agreement between the predicted and measured circulating currents is noteworthy. In simulations, the stator winding branch currents are equal (perfect balance) for healthy operation and their difference is zero.
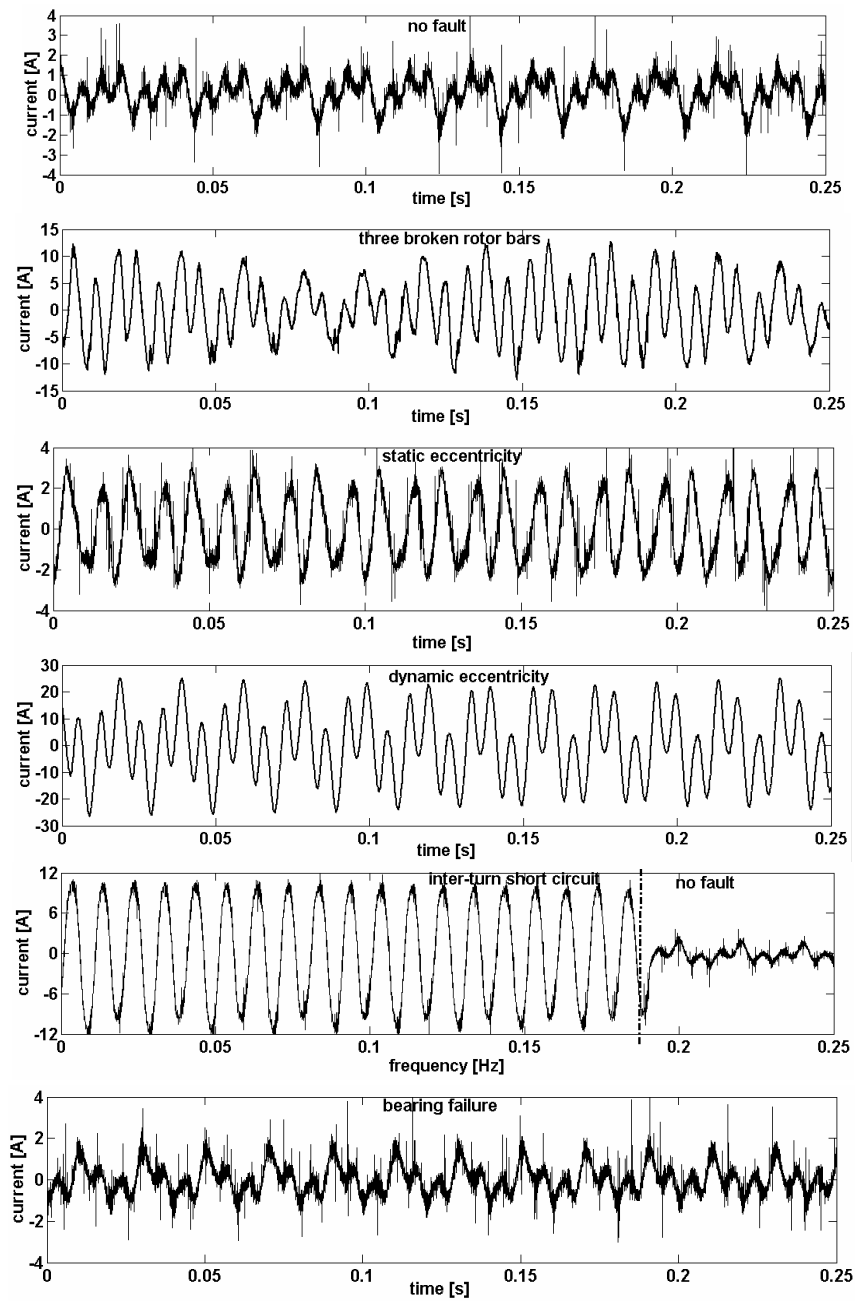
Fig. 5.1.7 Measured circulating currents.
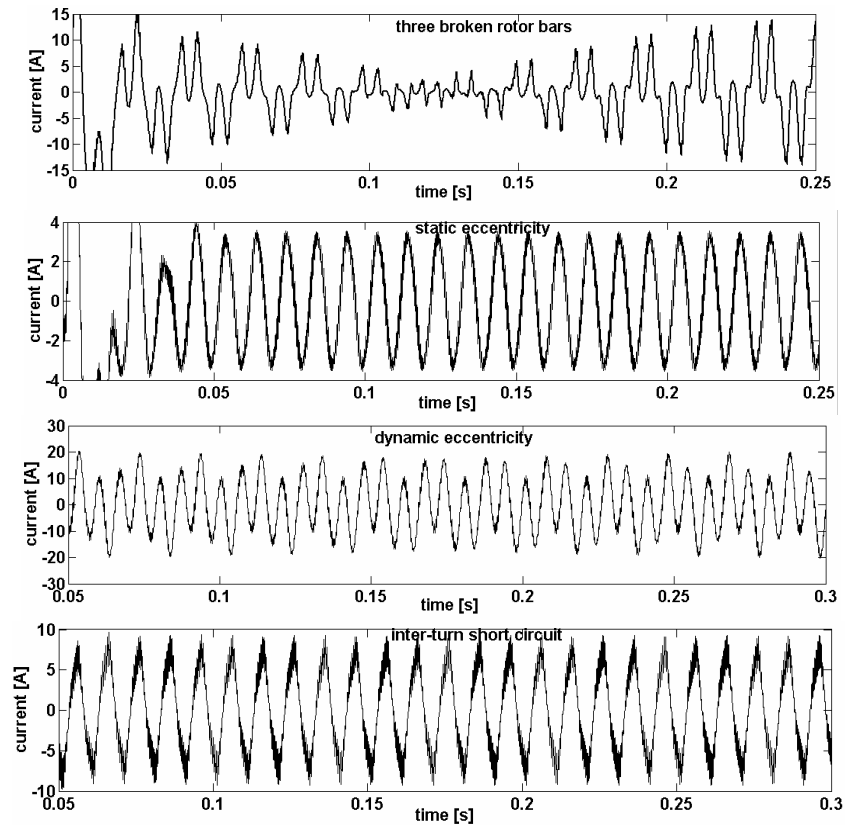
Fig. 5.1.8 Simulated circulating currents for the test motor equipped with the original stator winding configuration of type "2B".

Discussion

Inter-turn short circuit

On the basis of the measurements, no new frequency components in the line current spectra appeared as a consequence of a fault in the stator winding of an electrical machine. For the case of a turn-to-turn short circuit in the stator winding, only a rise in the amplitude of the 3rd harmonic component and of the fundamental was observed from the experiments. This change in amplitude was independent of the machine loading. With reference to the case of healthy operation, irrespective of the machine loading, an increase of around 6 dB in the amplitudes of the rotor-slot harmonics was found.

The monitoring of the 3rd harmonic of the motor supply current was also found to be an effective method for the detection of the presence of stator faults by other authors (Cruz and Cardoso 2004). The only drawback of a technique relying on sensing this frequency component is that low-voltage motors, especially random-wound motors, usually have appreciable levels of inherent asymmetries and it may be possible that the residual asymmetries of the motor may lead to the appearance of the 3rd harmonic component in the supply currents, even when no faults are present in the motor.

The simulations were in relatively good agreement with the measured results. In comparison with similar signatures produced by other faults, the new frequency sidebands produced in the frequency spectrum of the branch currents by the inter-turn short circuit are so small that they may be considered non-existent. For the "4B" and "2B" winding configurations, the

magnitude of these new frequency components is about 60 dB lower with reference to the fundamental, while for the "SB" configuration these components are only 35 dB lower with reference to the fundamental. The simulations also predicted minor modifications (increment of about 2-3 dB) in the magnitude of the rotor-slot harmonics and in the magnitude at the fundamental frequency (3.5 dB for "4B" and "SB", 1.6 dB for the "2B" stator winding type).

The simulated and experimental results obtained for a motor equipped with a stator winding configuration of type "2B" are in accordance with those presented by Joksimovic and Penman (2000). They have also shown that no new frequency components of the line current spectra can appear as a consequence of an inter-turn short circuit, but only a rise in some of the frequency components which already exist in the line current spectra of a healthy machine can be observed. These harmonics were the ones caused by rotor slotting.

The inability of the measured stator current to clearly detect a turn-to-turn fault was mentioned by Henao et al. (2003). In this work, in the case of six turns short-circuited in a phase of an 11-kW cage induction machine, the stator current was found not to be sensitive to this fault. However, the stray flux, which was studied in parallel with the stator current, was found to be affected by the fault being studied.

An increase in the magnitude of the rotor-slot harmonics produced by an inter-turn short circuit was also observed by Stavrou et al. (2001). In this work, with a 150-kW slip ring induction motor and a 30-kW cage induction motor, it was shown that the most reliable indicators of the presence of the fault were the lower sideband of the field rotational frequency with respect to the fundamental, together with some of the components that are related to slotting.

However, the experimental results obtained in this section are in contradiction with the results presented by Thomson (2001). In this work, relying on measurements carried out on a few low-voltage cage induction motors of 2 and 4 poles respectively, it was found that certain current components are clearly produced by inter-turn fault. The reasons for differences between the results presented in this thesis and the ones presented by Thomson (2001) are unclear. However, one may suspect that the stator winding configuration of the test machine represents a cause for the pronounced nature of some specific frequency sideband components produced by an inter-turn short circuit.

Yazidi et al. (2004) observed that the techniques relying on the stator winding current analysis are not always reliable, especially when the number of shorted turns is small compared to the total number of turns in a phase winding. Following a comparative investigation, the leakage flux was found to be a more effective way to detect the stator fault than the stator current in terms of specific frequency components at 750 Hz and 850 Hz (15th and 17th harmonic) which are excited increasing their magnitude to a level of 20 dB.

Concerning the use of the rotor-slot harmonics as potential indicators of a fault in the stator winding, Nandi and Toliyat (2000) claimed that although MCSA can detect these components, they may be confused with voltage unbalance in machines. In this respect, it was claimed that these harmonics can be unambiguously detected at the terminal voltages of the machine just after it has been switched off, since the supply voltage is absent and the voltage unbalance cannot influence the detection process.

The behaviour of induction machines affected by stator short circuits by assuming the dominant slot harmonic components of the stator currents as diagnostic indexes was also investigated by Gentile et al. (2003). The results obtained from the simulations of different asymmetric machines using the space vector approach confirm that the main harmonic components of the stator currents resulting from the rotor slotting of eighteen motors may be

considered a reliable diagnostic index. However, contrary to the results obtained by Nandi and Toliyat (2000), it was shown that these harmonic components are almost completely insensitive to possible supply voltage asymmetries.

In accordance with the results presented in this section, following a study on fault diagnosis in the stator windings of a low-voltage induction motor fed by PWM inverters, Villada et al. (2003) also found only a small increase in some components of the stator current spectrum which are difficult to detect. Nevertheless, the vibration and axial leakage flux frequency spectra experienced measurable differences at many frequencies. Therefore, for a better indication of a stator winding fault, a combined analysis of these signals was recommended.

In conclusion, it may be stated that monitoring the stator current does not always provide useful and sufficient information for the detection of a stator winding fault. Moreover, the possible reflections of the turn-to-turn short circuit in the stator currents are also characteristic of other faults and the probability of discriminating clearly between various faults remains small. The circulating current between parallel branches and the unbalance in the phase currents are suitable indicators for confidently claiming a turn-to-turn fault, but this is only true in the case of a symmetrical supply.

Rotor cage fault - broken rotor bars

A rotor cage-related fault appears in a different manner for motors equipped with various stator winding configurations. The distortions according to Eq. 3.1 are to be found in all of the cases under study but those according to Eq. 3.2 only hold true for motors equipped with a stator winding configuration of types "2B" and "4B". However, the new frequency sideband components given by Eq. 3.2 provide a precise signature of the rotor cage fault which is not the case for those given by Eq. 3.1, which may also appear as a result of pulsating loads, interactions between the motor and the train equipment, and particular rotor designs (Thomson 1992).

Simulations and measurements at half load do not produce major changes to the magnitude of the frequency components characteristic of this fault but the distortion content is poorer than that found at full load. At no load it is almost impossible to detect a rotor cage fault since most of the characteristic frequency components responsible for the fault detection are missing or are characterised by a dramatic change in magnitude (less than 50 dB) with reference to the fundamental. This conclusion is in accordance with those obtained by other researchers, who also claim that in order to facilitate the successful detection of rotor faults during steady-state operation a large supply current is required to flow.

Static eccentricity, dynamic eccentricity, and bearing fault.

Previously, it was shown that an inter-turn short circuit in the stator winding was best reflected in the unbalance of the stator winding currents. It emerged from both simulations and experiments that the eccentricities under study and bearing-related fault do not result in any major visible unbalance of the stator phase currents. It appears, then, that spectral analysis becomes indispensable when attempting to detect such faults.

However, relying on both experiments and simulations, this section concludes that the static eccentricity being studied does not bring any major modification to the spectral content of the branch current (in simulations, the same conclusion is valid for the case of static eccentricity, irrespective of the stator winding configurations). Moreover, not even the circulating current between the parallel stator winding branches is able to offer useful information about the fault

(the magnitude of these currents during such asymmetries is not very different from that corresponding to healthy operation). A similar conclusion may be drawn for the case of a bearing fault.

Considering only the experimental data, it was also found that the case of a bearing fault does not produce any major distortion in the spectral content of the branch current but only increases of around 6-8 dB in the amplitudes of the rotor-slot harmonics, irrespective of the machine loading; similar modifications were found for the case of static eccentricity. However, these are not clear signs to be used for an accurate detection of the implemented static eccentricity and bearing fault.

The difficulty to sense a bearing fault from the stator current was also mentioned by other authors.

> Kim et al. (2003) found it very difficult to sense any important distinction between the spectrum of a healthy motor current and the spectrum of the current corresponding to a motor operating with a damaged bearing. The same conclusion was valid for two cases of an eccentric air-gap (1 - condition of moving the rotating centre 25% upward at the end of the inboard shaft and 2 - condition of moving the rotating centre at the end of the outboard shaft 20 % downward and 10% right).

> Lindh et al. (2003) have investigated the use of the stator current signal for detection of an outer ring defect of the ball bearing with normal radial clearance of a 15 kW four pole induction motor. It was found that the stator current measurement as a bearing fault indicator is not adequate for this motor type since the modification produced by the radial movement of the rotor was found very small if the radial movement was restricted with bearing with small radial clearance. The outer race defect was clearly indicated only in the case of a large internal radial clearance of the bearing.

> Obaid et al. (2003) also showed that detecting the characteristic frequencies of a bearing fault in the motor current is difficult, even when the corresponding fault frequencies are prominent in the motor vibration. Only a very big window (a drilled hole) artificially created in the inner race showed some modifications in the stator current.

The results obtained for the case of dynamic eccentricity both from experiments and simulations are in accordance with the results obtained by most of the other research in this field.

> Tsoumas et al. (2005) also showed that motor current signature analysis is able to detect an air-gap eccentricity of 30% for a slip-ring asynchronous induction motor by monitoring the characteristic sideband frequency components given by Eq. 3.7.

> The investigations carried out by Nandi et al. (1997) confirmed the presence of harmonics as described by Eq. 3.5 in the presence of air-gap eccentricity. The dynamic eccentricity (obtained by replacing the good bearings with bad ones and running the machine at load) was reflected in an increase in the magnitude (about 3 times in comparison with healthy operation) of the components provided by Eq. 3.5. New characteristic frequency components were also found during the dynamic eccentricity.

> Nandi et al. (2002) showed that a link exists between the low- (Eq. 3.7) and high-frequency (Eq. 3.5) elements of the harmonics in the line-current spectrum in the presence of eccentricity. For various levels of mixed eccentricity in a four-pole, 3-hp cage-induction motor, the air-gap flux density components around the fundamental and rotor-slot

harmonics were found in the line current. However, it was proven that not all machines produce strong high-frequency components.

Studying the stator current spectra for both symmetrical and dynamically eccentric rotors, Joksimovic et al. (2000) also observed that in the symmetrical condition only the base frequency exists, while for the dynamic eccentricity condition, sideband frequencies around the base frequency appear at specific frequencies (Eq. 3.7).

Dorrell et al. (1997) studied the effects of combined dynamic and static rotor eccentricity on air-gap fields without recourse to slotting effects. Lower-frequency components in the current and vibration spectra were identified as being suitable for monitoring to assess the degree and type of rotor eccentricity present.

Another interesting conclusion drawn from the simulations is that the dynamic eccentricity is not reflected in the indications of the branch currents in the cases of the "NB" and "SB" stator winding configurations.

5.2. *Electromagnetic flux monitoring*

5.2.1. Inter-turn short circuit in the stator winding

In the following sections, only the most representative figures for fault detection and discrimination that correspond only to a specific loading of the test motor will be presented. However, for some specific cases figures will be presented that correspond to more than one loading point. A summary of the main results obtained from the studies carried out under all the loading conditions under study will always be presented.

The measurements for the case of the inter-turn short circuit in the stator winding at full load are not available, since the main concern was to keep the test machine healthy for further tests and not to expose it to extreme conditions.

For each of the search coils under study, the time-domain and frequency-domain representation of the voltages induced during the inter-turn short circuit in the stator winding from both the measurements and simulations will be shown.

In the simulations, the indications provided by all the search coils studied, with the exception of the one wound around a stator tooth, are ideally zero for healthy operation because of the perfect machine symmetry, which is not the case for the real machine tested in the measurements. However, in most of the cases the time representation of the measured signals for the case of healthy motor operation are not presented here since the changes caused by the fault are not easy to distinguish from such a representation.

SEARCH COIL AROUND STATOR TOOTH

Fig. 5.2.1 presents, both from the measurements and simulations, the time-domain representation of the voltages induced in the search coil placed around a stator tooth for the case of the inter-turn short circuit in the stator winding. The measured waveform corresponding to the healthy operation was not included in this figure since it looks almost identical with the one corresponding to the studied fault.

In the beginning, two search coils wound around different stator teeth (situated about 45° left and right, respectively, of the fault locations) were used, with the aim of verifying if the position of the shorted turn with respect to the search coil produces different indications about the fault. This may happen because this search coil is not purposely intended to make use of the machine symmetry for capturing various flux harmonic components (see the external search coil around two pole pitches and internal search coils for monitoring the "$p\pm1$" harmonic components). However, the indications provided by both of these coils seemed to be identical.

From the measurements it was found that the indications provided by the search coil around a stator tooth are of no major relevance when aiming to detect a stator winding fault. The paucity of the information provided by this search coil refers mainly to the absence of the new frequency sideband components characteristic of a stator fault (see Section 3.5.5). Choosing the fundamental frequency as reference, the only significant changes in comparison with healthy operation were observed at 500 Hz (10-dB increase at half load and 6-dB at no load) and at 900 Hz (10-dB increase both at half-load and no load). The changes corresponding to the half load operation are presented in Fig. 5.2.2. In the high-frequency range, no modifications were found in the amplitudes of the slot harmonics.
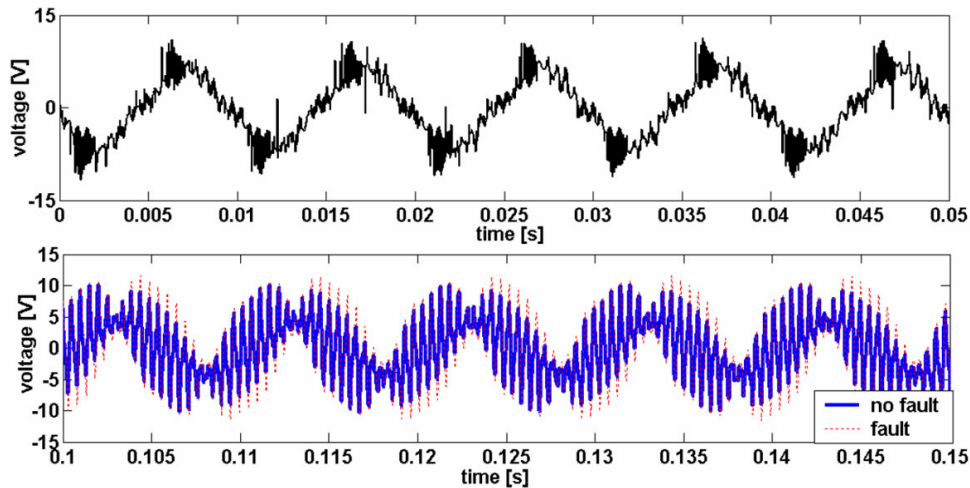
Fig. 5.2.1 Time-domain representation of the voltages induced in the search coil placed around stator tooth – inter-turn short circuit in the stator winding – measurements (top) and simulations (bottom) taken at half load.

Fig. 5.2.3 presents the frequency-domain representation of the voltages induced in the search coil wound around a stator tooth for the case of the inter-turn short circuit based on data gathered from simulations of the test motor equipped with various stator winding configurations. It may be observed that this type of fault introduces new characteristic fault sideband frequencies only for the winding configurations of the types "NB" and "SB". The new relevant frequencies for detecting this fault are according to Eq. 3.10 (Melero et al. 2003, Penman et al. 1994) and are indicated by arrows. This is in agreement with the results obtained from the measurements of the test motor equipped only with a stator winding consisting of 2 parallel branches, where no new frequency sideband components characteristic of a stator winding fault were found.
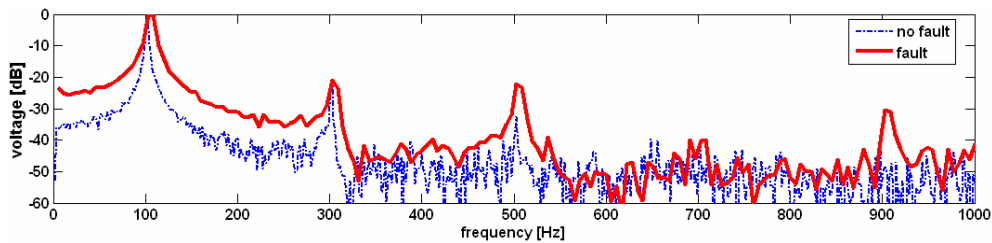
Fig. 5.2.2 Frequency-domain representation of the voltages induced in the search coil wound around a stator tooth during the inter-turn short circuit – measurements at half load.
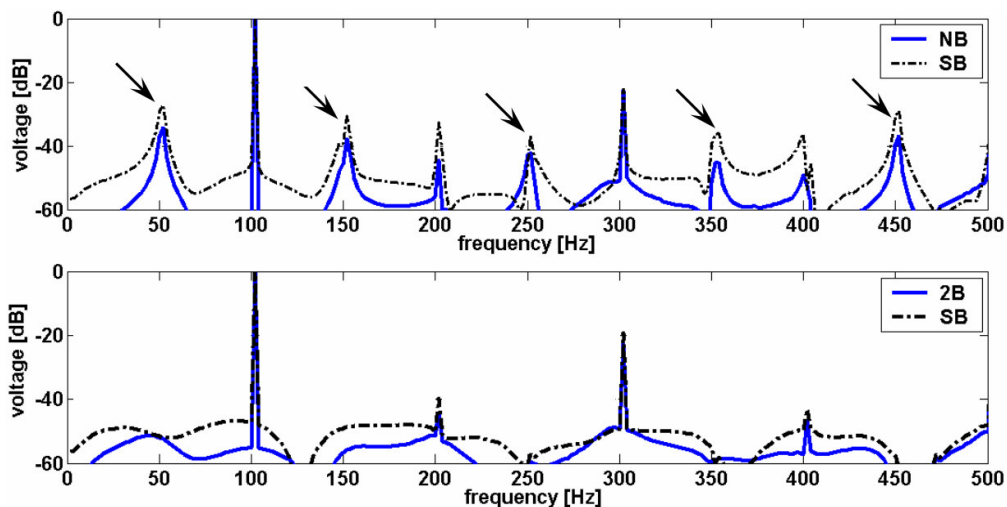

Fig. 5.2.3 Frequency-domain representation of the voltages induced in the search coil wound around a stator tooth during the inter-turn short circuit – simulations at half load.

Relying on simulations at full load, Fig. 5.2.4 presents the magnitudes of the new frequency sideband components found to be characteristic of the inter-turn short circuit. The fundamental frequency of 100 Hz is the reference at which these components are reported. This type of fault remains relatively easy to identify at half load (the magnitudes of the new frequency sideband components do not vary much from the ones presented in Fig. 5.2.3), but at no-load operation there are no longer any clear signs of such new components (most of the magnitudes of the sidebands of interest fall below the level of 40 dB).
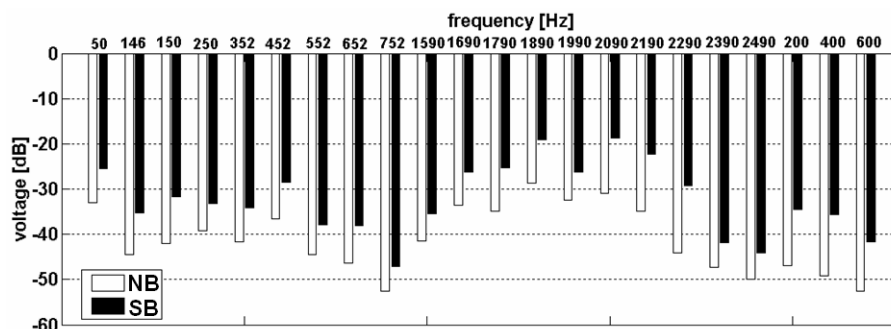

Fig. 5.2.4 Characteristic frequency sidebands produced by the inter-turn short circuit in the indications provided by a search coil wound around a stator tooth – simulations at full load.

Table 5.2.1 presents the changes to the rotor-slot harmonics caused by the inter-turn short circuit. This type of analysis will not be repeated for the other search coils implemented in the simulations, since this is the only case where the indications for healthy operation are non-zero. First, this table presents the magnitude of the frequencies of interest with reference to the fundamental for the case of both healthy and abnormal operation, respectively. After that, the difference between these two modes of operation that are supposed to give an indication of the condition of the motor is presented. From these tables it can be seen that the inter-turn short circuit is reflected more clearly for a motor equipped with stator windings of the types "4B" and "SB", respectively.

Table 5.2.1 Changes produced by the inter-turn short circuit to the rotor-slot harmonics captured by a search coil wound around stator tooth [dB].

1840 Hz				2040 Hz				2240 Hz			
"4B","SB"		"NB", "2B"		"4B","SB"		"NB", "2B"		"4B","SB"		"NB", "2B"	
fault	no fault	fault	no fault	fault	no fault	fault	no fault	fault	no fault	fault	no fault
4	-3	1	-3	7	1	3	1	-9	-23	-16	-23
7		4		6		2		14		7	

Full load

1870 Hz				2070 Hz				2270 Hz			
"4B","SB"		"NB", "2B"		"4B","SB"		"NB", "2B"		"4B","SB"		"NB", "2B"	
fault	no fault	fault	no fault	fault	no fault	fault	no fault	fault	no fault	fault	no fault
4	-3	-1	-3	7	-1	2	-1	-12	-27	-20	-27
7		2		8		3		15		7	

Half load

1900 Hz				2100 Hz				2300 Hz			
"4B","SB"		"NB, "2B"		"4B","SB"		"NB", "2B"		"4B","SB"		"NB", "2B"	
fault	no fault	fault	no fault	fault	no fault	fault	no fault	fault	no fault	fault	no fault
3	-4	-1	-4	5	-3	1	-3	-12	-31	-20	-31
7		3		8		4		19		11	

No load

SEARCH COIL PLACED AROUND TWO POLE PITCHES

Fig. 5.2.5 presents, both from the measurements and simulations, the time-domain representation of the voltages induced in the search coil placed around two pole pitches of the test motor in the case of the inter-turn short circuit in the stator winding. The measured waveform corresponding to the healthy operation was not included in this figure since it looks almost identical with the one corresponding to the studied fault. It is observed that the inter-turn short circuit in the stator winding is reflected in a different manner for various stator winding configurations.
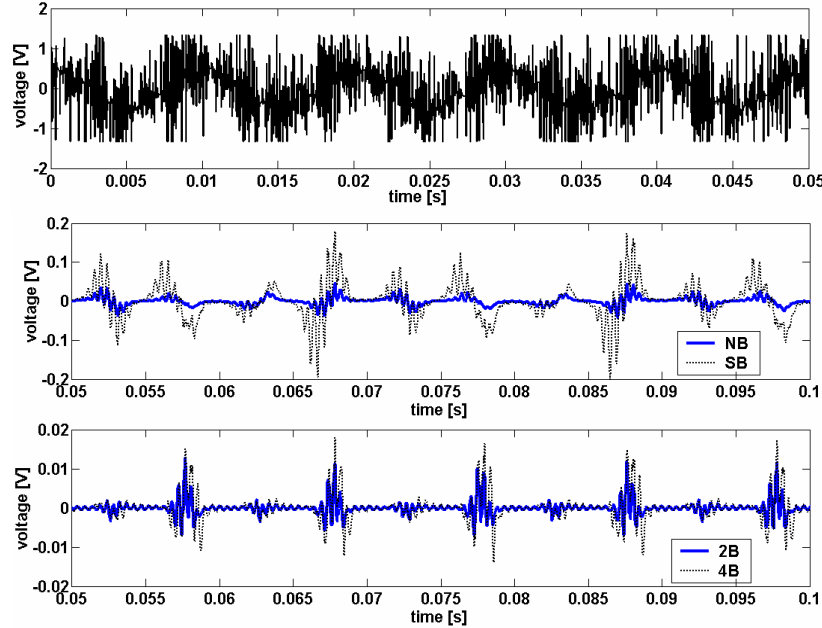
Fig. 5.2.5 Time-domain representation of the voltages induced in the search coil placed around two pole pitches of the test motor – inter-turn short circuit – measurements (topmost figure) and simulations taken at half load.

Fig. 5.2.6 shows the frequency-domain representation of the voltages induced in the search coil wound around two pole pitches following the inter-turn short circuit. These representations correspond to various stator winding configurations implemented in the simulations.
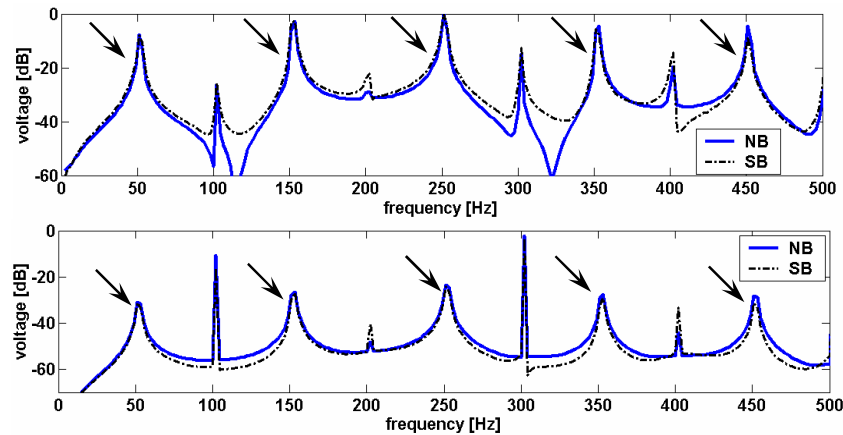

Fig. 5.2.6 Frequency-domain representation of the voltages induced in the search coil wound around two pole pitches – inter-turn short circuit – simulations at full load (top) and no load (bottom).

The relevant frequencies for detecting this fault are according to Eq. 3.10 (Melero et al. 2003, Penman et al. 1994). The frequency components of 250 Hz and 500 Hz for operation at full load and no load, respectively, were chosen as references for the dB representation (these frequencies were characterised by the highest amplitude).

For the winding configurations of the types "2B" and "4B", the inter-turn short circuit does not produce any new characteristic frequency sideband components to be captured by a search coil wound around two pole pitches. This is in accordance with the results extracted from the measurements, where the only sign of a possible fault was represented by an increment in the fundamental frequency of about 9 dB and 14 dB in half-load and no-load testing, respectively.

New characteristic fault sideband frequency components are found in the cases of stator winding configurations of the "NB" and "SB" types. Of these two winding configurations, the "SB" type is observed to be slightly more sensitive to the inter-turn short circuit than the "NB". At no load, the potential information about the fault is found to be considerably diminished.

In the high-frequency range, the experimental turn-to-turn short circuit that was implemented is reflected in a relatively slight increment in the rotor-slot harmonics of about 4 dB in comparison with healthy operation. It was not possible to analyse such modifications from the simulations, since in healthy operation, because of the perfect machine symmetry, the signal captured by this coil is ideally zero.

SEARCH COIL "*p*-1"

Fig. 5.2.7 presents, both from the measurements and simulations, the time-domain representation of the voltages induced in the search coil "*p*-1" for the case of the inter-turn short circuit in the stator winding.

Fig. 5.2.8 shows the frequency-domain representation of the voltages induced in the "*p*-1" search coil following the inter-turn short circuit. These representations correspond to various stator winding configurations implemented in the simulations.

Similarly to the previous cases, new characteristic fault sideband frequency components are introduced by the fault to the stator winding of the "NB" and "SB" types. The "SB" configuration is also reflected by the indication of this search coil as being more sensitive to the inter-turn short circuit than the "NB" one.

Fig. 5.2.9 presents the magnitudes of the new characteristic fault sideband frequency components for the cases of stator winding configurations of the "NB" and "SB" types. These figures are with reference to the rotor-slot harmonics (2040 and 2100 Hz for operation at full load and no load, respectively). The relevant frequencies for detecting this fault are according to Eq. 3.10.
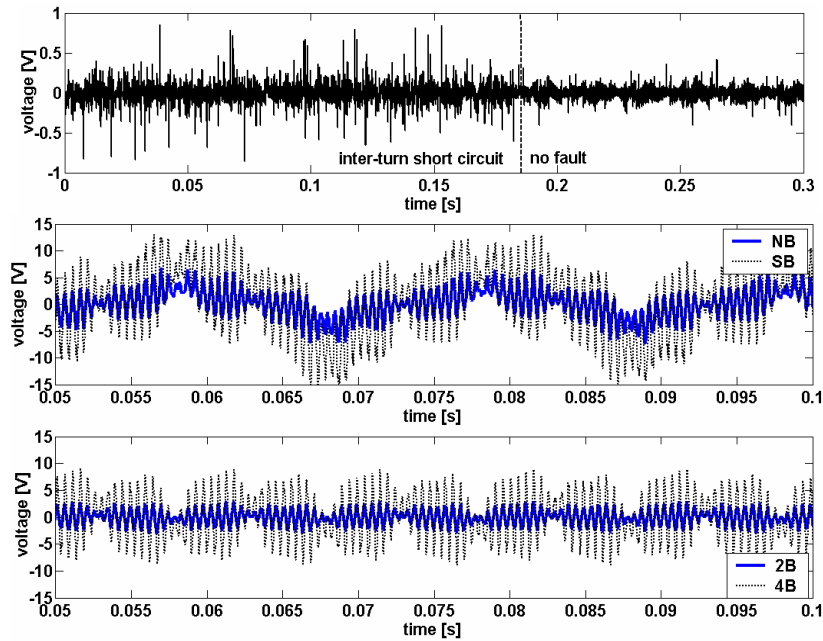
Fig. 5.2.7 Time-domain representation of the voltages induced in search coil "p-1" – inter-turn short circuit – measurements (topmost figure) and simulations taken at half load.
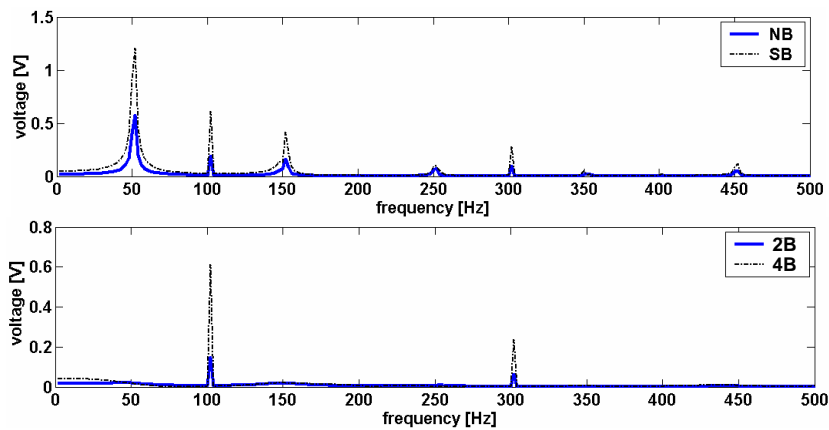
Fig. 5.2.8 Frequency-domain representation of the voltages induced in the "p-1" search coil – inter-turn short circuit – simulations at half load.
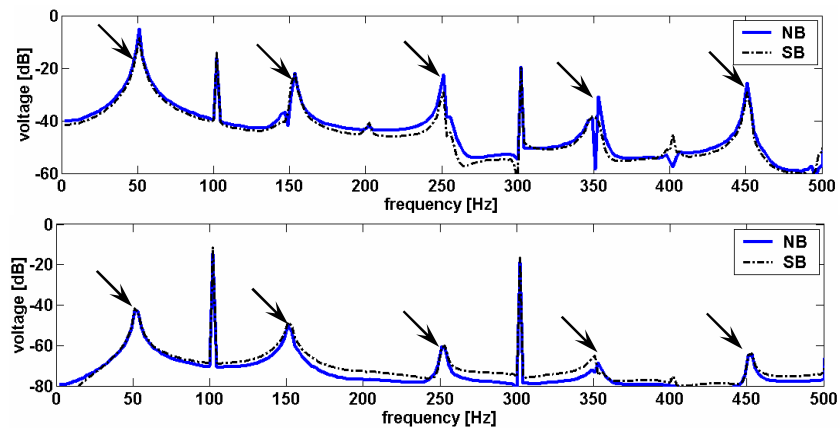
Fig. 5.2.9 Characteristic frequency sidebands produced by the inter-turn short circuit in the indications provided by "p-1" search coil – simulations at full load (top) and no load (bottom).

Using a "*p*-1" search coil, for a motor equipped with winding configurations of the "NB" and "SB" types, the inter-turn short circuit in the stator winding is relatively easy to identify at half load (the magnitudes of the new frequency components are of the same magnitude as the ones presented in Fig. 5.2.9) but not in no load operation, where there is a major reduction of 35 dB in the magnitude of these new components.

Relying on the measurements, Table 5.2.2 presents the main changes produced by the inter-turn short circuit to those frequency components also found during healthy operation. The only modification to be noticed is the increase in the magnitude of the 3rd harmonic, and therefore this is the only one shown in the table.

Table 5.2.2 Changes produced by the inter-turn short circuit – measurements [dB].

f [Hz]	Half load			No load		
	"*p*-1"			"*p*-1"		
	fault - no fault	fault	no fault	fault - no fault	fault	no fault
300 Hz	19	-6	-25	19	-1	-20

SEARCH COILS "*p*+1"

Fig. 5.2.10 presents, both from the measurements and simulations, the time-domain representation of the voltages induced in the search coil "*p*+1" for the case of the inter-turn short circuit in the stator winding.

Fig. 5.2.11 presents the frequency-domain representation of the voltages induced in the studied search coils from the measurements.

Relying on the measurements, the main changes produced by the inter-turn short circuit in comparison with healthy conditions may be found in:
- the magnitude of the fundamental frequency: increments of 12 dB and 16 dB for operation at half load and no load, respectively.
- the magnitude of the 3rd harmonic: increments of about 24 dB, irrespective of the motor operation point.

Fig. 5.2.12 shows the frequency-domain representation of the voltages induced in the "*p*+1" search coil following the inter-turn short circuit. These representations correspond to various stator winding configurations implemented in the simulations at half load.
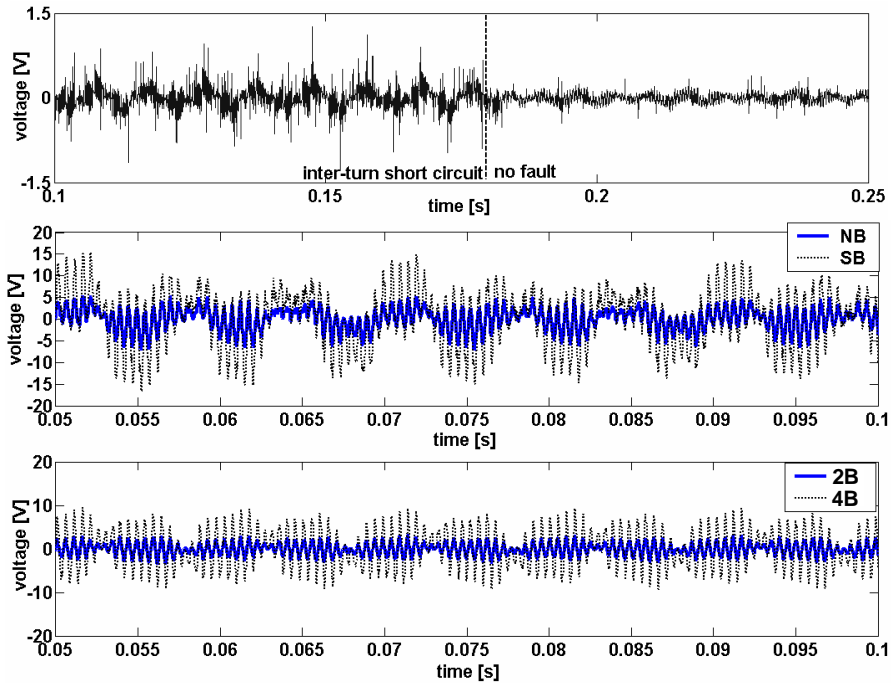
Fig. 5.2.10 Time-domain representation of the voltages induced in search coil "p+1" during the inter-turn short circuit – measurements (topmost figure) and simulations taken at half load.
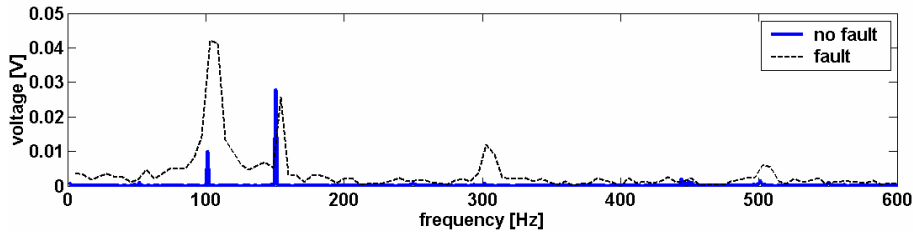
Fig. 5.2.11 Frequency-domain representation of the voltages induced in search coil "p+1" during the inter-turn short circuit – measurements taken at half load.
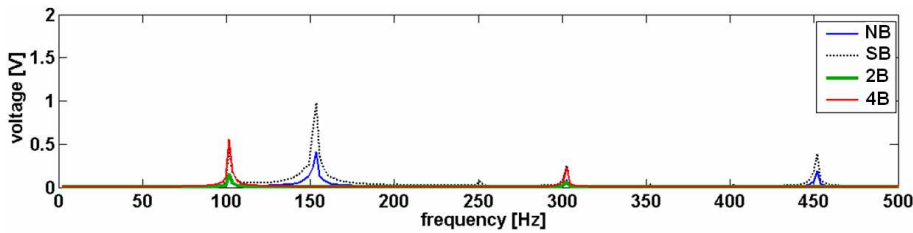
Fig. 5.2.12 Frequency-domain representation of the voltages induced in the "p+1" search coil during the inter-turn short circuit – simulations at half load.

The new characteristic fault sideband frequency components introduced by the stator winding configurations of the "NB" and "SB" types are presented in Fig. 5.2.13. These representations are with reference to the rotor-slot harmonics. The relevant frequencies for detecting this fault are according to Eq. 3.10.
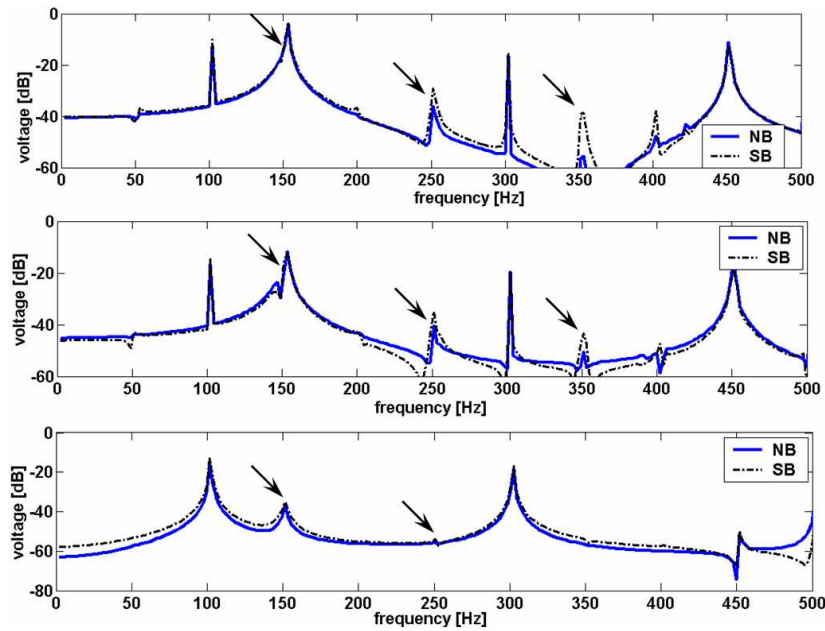
Fig. 5.2.13 Characteristic frequency sidebands produced by the inter-turn short circuit in the indications provided by "p+1" search coil – simulations at full load (topmost figure), half load (middle figure), and no load (bottom figure).

Using a "*p+1*" search coil for winding configurations of the "NB" and "SB" types, the inter-turn short circuit in the stator winding is relatively easy to identify, even at half load. In no load operation, however, the potential fault information becomes very poor (major reduction in the magnitude of some frequency side-band components).

SEARCH COILS AROUND THE SHAFT AND AT THE NON-DRIVE END (NEAR VENTILATOR)

Fig. 5.2.14 presents the time-domain representation of the voltages induced in the search coils placed around the motor shaft and at the non-drive end of the motor for the case of the inter-turn short circuit in the stator winding. Fig. 5.2.15 shows the frequency-domain representation of the voltage induced during the inter-turn short circuit in the search coil positioned around the motor shaft at a half load motor operation. Simulations are not available in these cases as the 2D simulation tool is not able to take into account the 3D effects.

The inter-turn short circuit in the stator winding, irrespective of the motor loading, does not produce any new components in the spectral content of the voltage induced in a search coil placed at the non-drive end of the motor. In the current work, the only sign of a fault is represented by a major increase in the magnitude of the fundamental frequency (approximately 10 times, irrespective of load). For the case of a search coil wound around the shaft this increase was found to be about 7 times and 4 times for the operations at half-load and no load, respectively. Important information about the fault may also be extracted from the magnitude of the 3rd harmonic.

For the search coil placed at the non-drive end of the test motor, the rotor slotting harmonics increased by only 4 dB in half-load operation, in comparison with healthy operation, while in no-load operations no change in the magnitude of this frequency component was found.

In the high-frequency range, a turn-to-turn short circuit in the stator winding is reflected only in the indications provided by the search coil around the shaft by an increment of around 6-8 dB in the magnitude of the rotor-slot harmonics at half-load and no load, respectively.
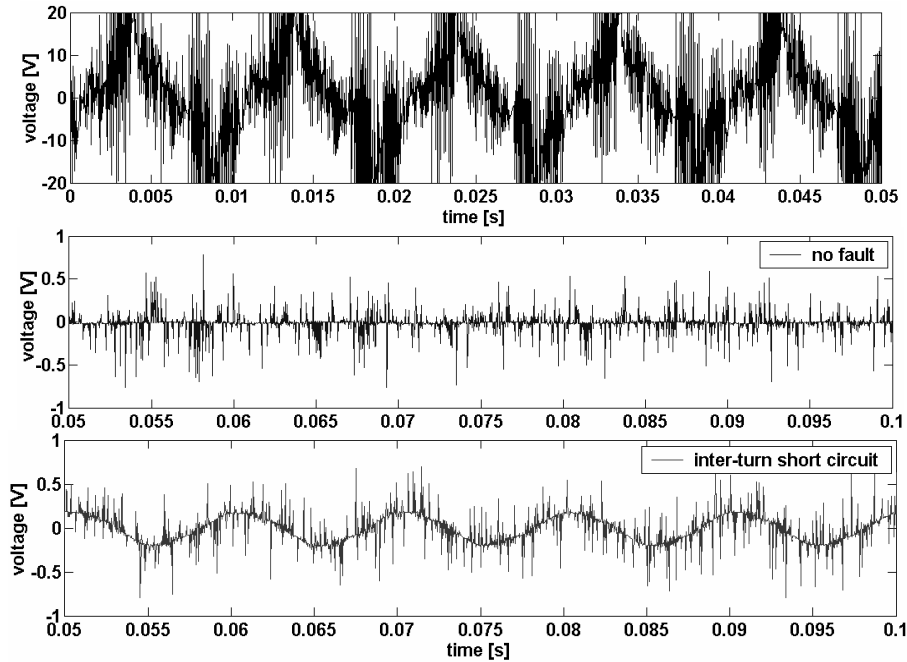
Fig. 5.2.14 Time-domain representation of the voltages induced during the inter-turn short circuit in search coils positioned around the motor shaft and at the non-drive end of the motor (topmost figure) – measurements at half load.
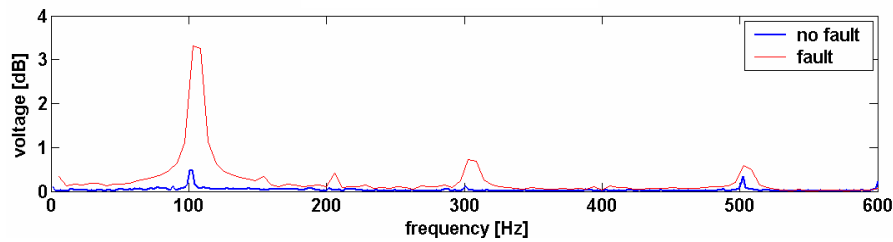
Fig. 5.2.15 Frequency-domain representation of the voltage induced during the inter-turn short circuit in the search coil positioned around the motor shaft – measurements at half load.

Discussion

First of all, it is important to notice from the simulations that for a machine equipped with winding configurations of the types "2B" and "4B", the inter-turn short circuit does not produce any new characteristic frequency sideband components to be captured by the search coils being studied. The measurements that were carried out only for the case of the motor equipped with a stator winding consisting of 2 parallel branches ("2B") pointed out that the new relevant frequency signatures for detecting shorted turns from electromagnetic flux are not observed in the search coils being studied.

Search coil around stator tooth: From the measurements, the only significant changes in comparison with healthy operation were observed at 500 Hz (10-dB increase at half load and 6-dB at no load) and at 900 Hz (10-dB increase both at half load and no load). In the high-frequency range, no modifications were found in the amplitudes of the rotor-slot harmonics, as opposed to the modifications of around 6 dB that were observed in the branch current (Section 5.1.1). The simulations indicated the difficulty of finding clear fault signatures in a motor equipped with stator winding configurations of the types "2B" and "4B". However, the changes caused by the inter-turn short circuit to the rotor-slot harmonics that are captured by a

search coil wound around a stator tooth were found to be more important (7-15 dB) than the ones found in the branch current (2-3 dB, according to the results presented in Section 5.1.1).

Search coil wound around two pole pitches: From the measurements, the only sign of a possible fault was represented by an increment of the fundamental frequency of about 9 dB and 14 dB in half-load and no-load testing, respectively. This is in agreement with the simulations where, for the winding configurations of the types "2B" and "4B", the inter-turn short circuit did not produce any new characteristic frequency sideband components. In the high-frequency range, the experimental implemented turn-to-turn short circuit is reflected in a relatively slight increment in the rotor-slot harmonics of about 4 dB in comparison with healthy operation.

Search coil "p+1". From the measurements, the major increments in the amplitude of the fundamental frequency (12-16 dB) and in the magnitude of the 3rd harmonic (24 dB) are higher than the ones produced by this fault for other fault indicators. It is also very probable that other faults will not be reflected in a similarly major manner in the indications of this coil. For the winding configuration of the "2B" and "4B" types, the simulations (supposed to point out only those frequency components caused by the fault) also indicate the fundamental and the 3rd harmonic as being responsible for providing important information about the inter-turn short circuit.

Search coil "p-1". Relying on the measurements, the major changes produced by the inter-turn short circuit to the 3rd harmonic (19 dB both for half load and no load operation) are noteworthy. This fault signature may also be considered important since it is expected that other faults will not be reflected in a similarly major manner in the indications of this coil. For the winding configurations of the "2B" and "4B" types, the simulations also indicate the 3rd harmonic as a carrier of important information about the inter-turn short circuit.

The **search coils around the shaft** and at the **non-drive end of the machine** offer useful information about a winding fault, especially by capturing the major modification produced in the magnitude of the fundamental frequency component. The severity of these modifications may be considered a unique signature for this type of fault.

Following the previous discussion, it becomes clear that most of the search coils that were studied are able to sense an inter-turn fault, relying mostly on the indications provided by the behaviour of the fundamental and 3rd harmonic frequency component. Major modifications in the magnitudes of the frequency components, as suggested by Eq. 3.10, were identified in the simulations only for those machines equipped with a stator winding configuration of the "NB" and "SB" types.

It is important to mention that it is quite difficult to compare the results presented in this thesis with those presented by other authors, since most of their contributions do not provide additional information about the stator winding configurations of the motors being studied, i.e. parallel/not parallel branches (Melero et al. 2003, Villada et al. 2003, Yazidi et al. 2004, Assaf et al. 2004, Thailly et al. 2005). However, Henao et al. (2003, 2004) and Penman et al. (1994) clearly specify the parallel winding configurations used in their works.

Melero et al. (2003) concluded that the harmonic component at the frequency f_s-f_r (according to Eq. 3.10) may provide useful information about a minimal stator winding turn-to-turn short circuit and the greatest change (28 dB) may be found in the final state of the fault, when the motor is close to catastrophic failure. This final condition was found after 33 cycles (1 cycle = starting-up – running a full load for ten minutes – stopping; T = 220°C). In comparison with the investigations carried out on the behaviour of the air-gap torque harmonics and negative-sequence impedance during such a fault, the increases of the axial leakage flux showed a

more linear trend. Moreover, the total increase between the healthy state and the final phase of the failure was the largest, so this method could be more suitable for predicting how far the motor was from the end of its useful life.

The advantage of using a detection technique relying on flux monitoring was also suggested by Henao et al. (2003). This detection technique was found to be more reliable than the MCSA, which provided no useful information about the fault being studied. The case of an induction machine with six turns short-circuited in phase tested at standstill and when the machine was rotating without load torque and at the rated torque, both under sinusoidal power supply and voltage source inverter was investigated. For the induction machine at standstill, the stray flux was affected by an increase in the magnitude of harmonics 3 and 9, with more than 20 dB for the third and 10 dB for the ninth. For the machine rotating without load torque, the effect that made possible the detection of the fault was localised in harmonics 5 and 7, which were excited, increasing their magnitude to around 10 dB. When the induction machine rotated at the rated speed with short-circuited turns, the only frequency component showing sensitivity to the short circuit was at 450 Hz (9th harmonic) with an increase of around 10 dB in its magnitude.

Penman et al. (1994) detected changes in the harmonics with the lowest nk product (Eq. 3.10) for a motor in which two of the copper turns were short-circuited. This motor was equipped with a wound rotor and tests were carried out at no load and at 48 kW, respectively. The maximum ratio between the induced voltages in the search coil for the unshorted and shorted conditions, respectively, was around 1.2, irrespective of the motor loading

For an 11-kW cage induction motor, as a consequence of a short-circuited section of 12.5% of one phase full winding, Thailly et al. (2005) found considerable increments in the magnitudes of the rotor-slot harmonics. It is claimed that by monitoring the amplitude of these harmonics one may obtain useful information for the detection of an inter-turn short circuit in the stator winding. The results of the simulations carried out in this work for the search coil wound around a stator tooth are in accordance with these conclusions, but the results obtained from the measurements are not.

Relying on the experimental results obtained from the testing of an 11-kW induction motor, Assaf et al. (2004) presented a sensitivity analysis of the recorded axial leakage flux in the presence of 1% and 6% short circuits of the total turn number for various operating conditions. In full-load operation, the harmonics components affected the most by the fault (15-22 dB) were the ones corresponding to the frequencies $3f_s$-$3f_r$, f_s+$3f_s$, $5f_s$+f_r, and $5f_s$+$3f_r$.

Villada et al. (2003) conducted a series of tests on 5-hp and 3-hp induction motors in order to verify the ability of the axial leakage flux to detect shorted turns. Once more, Eq.3.10 was found suitable to provide a good agreement between the spectra of the flux leakage signal and the portion of the winding under fault.

5.2.2. Rotor cage-related faults

SEARCH COIL AROUND STATOR TOOTH

Relying on both the measurements and simulations, Fig. 5.2.16 presents the time-domain representation of the voltages induced in a search coil placed around the stator tooth for the case of a major rotor cage fault, such as three broken rotor bars.
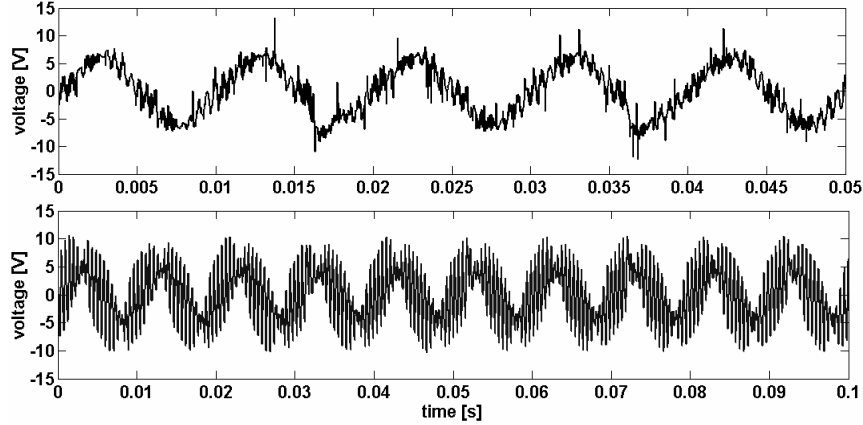

Fig. 5.2.16 Time-domain representation of the voltages induced in the search coils placed around stator tooth – 3 broken rotor bars – measurements (top) and simulations (bottom) taken at half load.

Fig. 5.2.17 shows the frequency-domain representation of the voltages induced in the search coil around stator tooth during a rotor cage-related fault. These representations are based on measurements at half load and stand only for the original stator-winding configuration consisting of 2 parallel branches. From the measurements repeated with no load, the breakage of three rotor bars remains easily visible (the results corresponding to this test are very similar to those presented in Fig. 5.2.17), but the breakage of one rotor bar is harder to detect (based on the presence of the fault-specific frequency sideband components used, to be indicated by arrows in the following figures).

Fig. 5.2.18 shows the frequency-domain representation of the voltages induced during a rotor cage fault. These representations correspond to various stator-winding configurations implemented in the simulations and are with reference to the rotor-slot harmonics. At half load, it is possible to visualise signs characteristic of a rotor cage fault (indicated by the arrows). In average, these signals are around 10 dB lower in comparison with those corresponding to the full load. However, at no load it is more difficult to detect this type of fault, on average, the signals are around 15 dB lower than the ones corresponding to the full load. The minimum rotor cage-related fault that was studied, 1 broken rotor bar, is almost impossible to detect at no load.

A comparison based on Figs. 5.2.17 and 5.2.18 points out a good agreement in terms of new characteristic fault frequency sideband components produced by a rotor cage fault and obtained from the measurements and simulations respectively (see the arrows indicating the frequencies of interest for the detection of a rotor cage-related fault according to the predictions given by Eq. 3.2: 47.7, 50.7, 146.3, 149.3 Hz, and so on for various values of *k*).
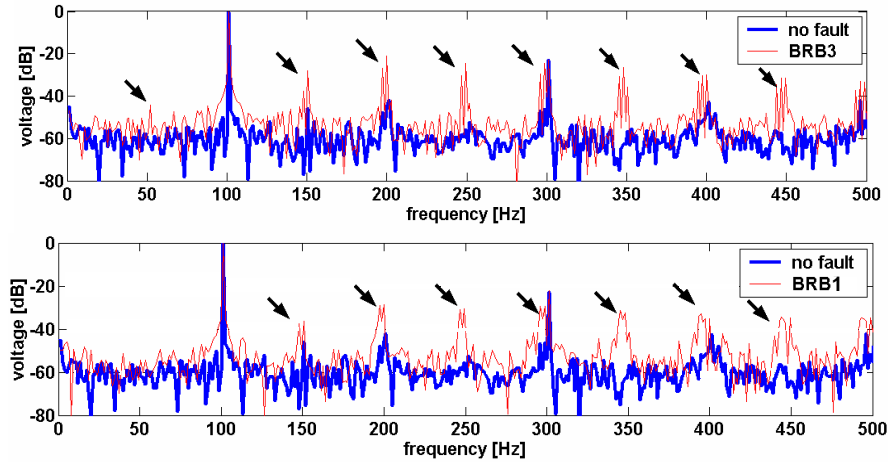
Fig. 5.2.17 Frequency-domain representation of the voltages induced in the search coil around stator tooth during rotor cage-related faults – 3 broken rotor bars (top) and 1 broken rotor bar (bottom) – measurements at half load.
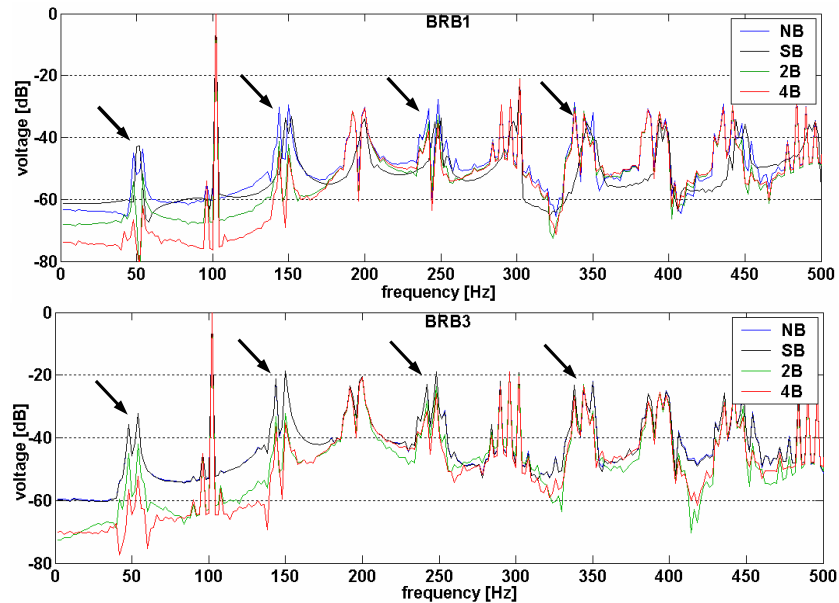
Fig. 5.2.18 Frequency-domain representation of the voltages induced in the search coil wound around a stator tooth – 1 broken rotor bar (top) and 3 broken rotor bars (bottom) – simulations taken at half load.

SEARCH COIL PLACED AROUND TWO POLE PITCHES

Relying on both the measurements and simulations, Fig. 5.2.19 presents the time-domain representation of the voltages induced in a search coil placed around two pole pitches of the test motor for the case of a motor operating with three broken rotor bars. Fig. 5.2.20 shows the frequency-domain representation of the voltages induced in the search coil wound around two pole pitches from the simulations. The representation of the characteristic fault sidebands is with reference to the rotor-slot harmonics. The results from all the load operation points that were studied are included in order to point out the capability of this search coil to sense various degrees of a fault at various loads.
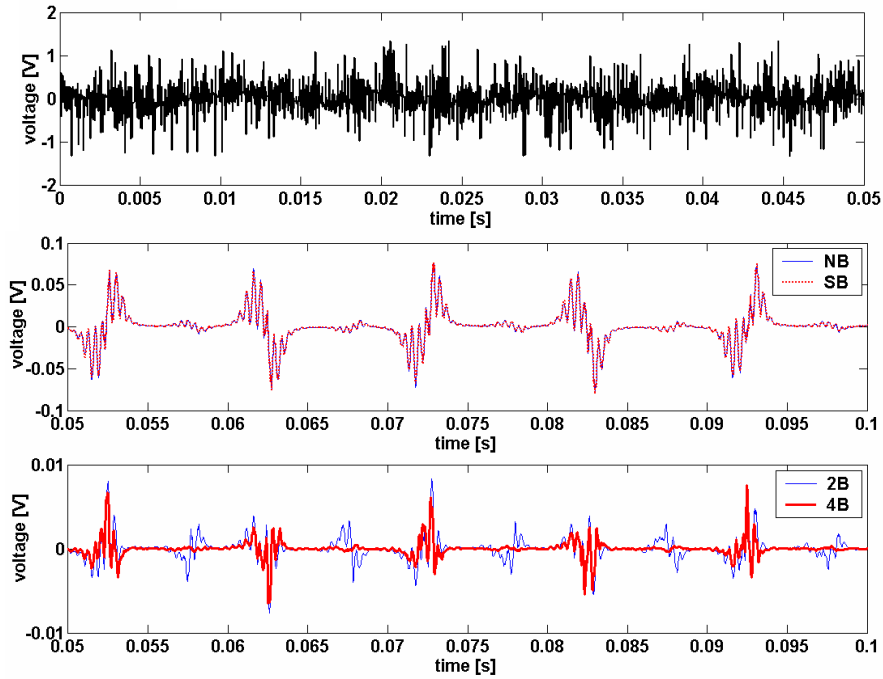
Fig. 5.2.19 Time-domain representation of the voltages induced in the search coil placed around two pole pitches – 3 broken rotor bars – measurements (topmost figure) and simulations taken at half load.
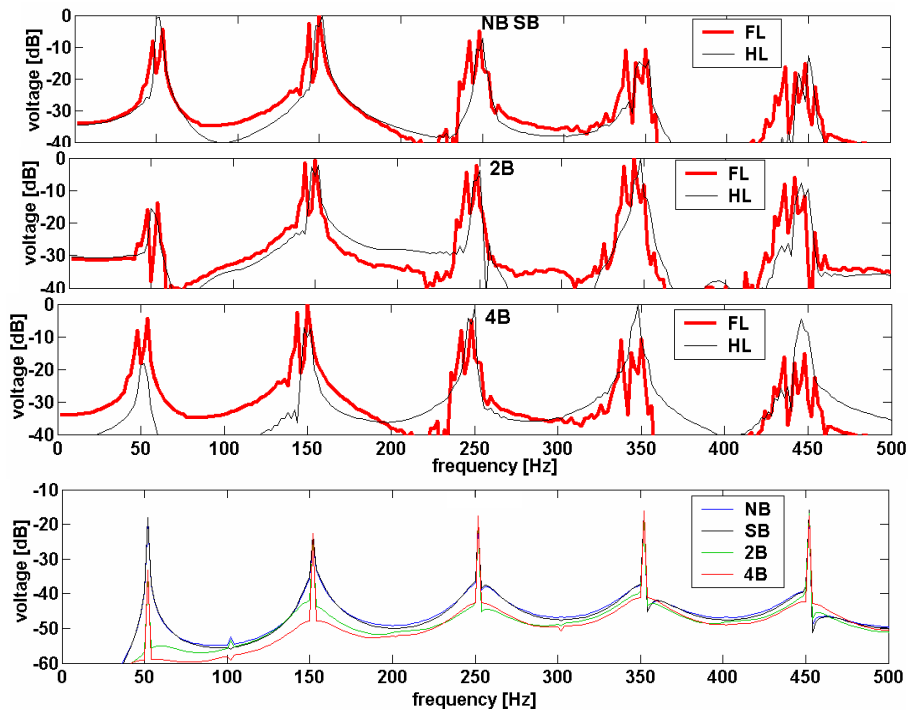
Fig. 5.2.20 Frequency-domain representation of the voltages induced in the search coil wound around two pole pitches – 3 broken rotor bars – simulations at full load and half load (topmost three figures) and no load (bottom figure).

In terms of new frequency sideband components, the rotor cage-related fault is reflected in a similar manner for a motor equipped with any of the stator winding configurations that were studied. In terms of distortion magnitudes, for all the loading points under study, but especially at lower loadings, a motor equipped with stator windings of the types "NB" and "SB" is observed to exhibit more important changes.

Figs. 5.2.21 and 5.2.22 show the frequency-domain representation and the characteristic frequency sidebands produced by rotor cage-related faults of various levels of severity in the indications provided by the search coil wound around two pole pitches from measurements at full load. The ability of this search coil to sense the degree of severity of the rotor cage fault is noteworthy.
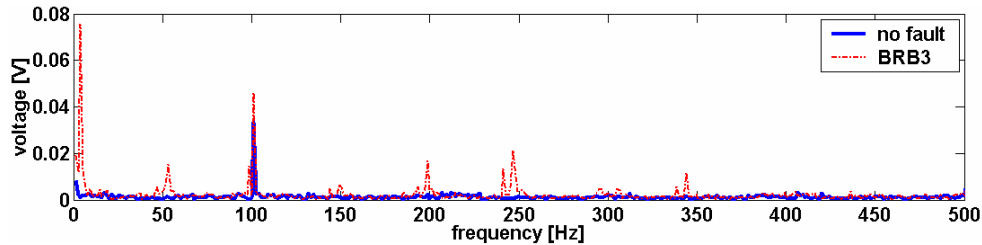

Fig. 5.2.21 Frequency-domain representation of the voltages induced in the search coil wound around two pole pitches – 3 broken rotor bars – measurements at full load.
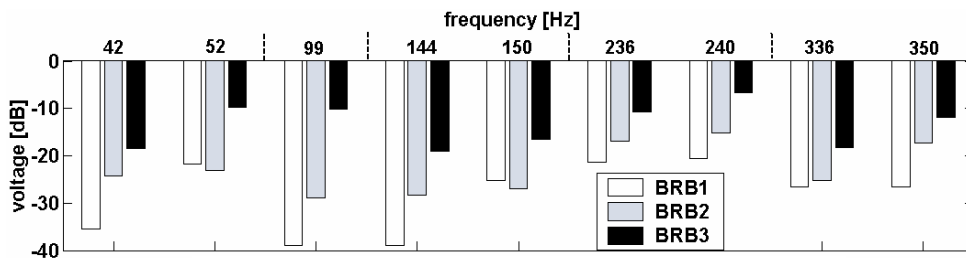
Fig. 5.2.22 Characteristic frequency sidebands produced by various rotor cage-related faults in the indications provided by the search coil placed around two pole pitches – measurements at full load.

A rotor cage-related fault may also be detected from measurements at half load; on average, the magnitude of the previous exposed frequencies is reduced by about 10-15 dB in comparison with those corresponding to the full load operation point. However, the sideband component situated in the immediate vicinity of the fundamental is no longer detectable at this operation point.

From a no load measurement, the rotor cage related-faults become relatively difficult to detect since some of the previously mentioned sideband components disappear and the remaining ones are characterised by magnitudes 20-25 dB lower than the ones corresponding to the full load operation point.

In addition to the frequency components observed in Fig. 5.2.21 and summarised in Fig. 5.2.22, it is important to notice the very low-frequency component situated at around 3 and 2 Hz for the full-load and half-load operation points, respectively. The origin of this sideband may be one of those suggested by Kliman et al. (1988). In this contribution, a frequency component given by sf_s, was associated with the signature produced by a broken end-ring fault, but the same component was also found in the cases of rotor and voltage source asymmetry. The conclusion is that this frequency can be used for condition monitoring, but the possibility of other fault modes has to be taken into account.

Fig. 5.2.23 presents, both from the measurements and simulations, the time-domain representation of the voltages induced in the search coil "*p*-1" for the case of a motor operating with 3 broken rotor bars.

Relying on the simulations, Fig. 5.2.24 shows the frequency-domain representation of the voltages induced in the "*p*-1" search coil. The magnitude of the new frequency sideband components characteristic of a rotor cage fault are found to be higher for the motor equipped with windings of the "NB" and "SB" types. At no load, important signs of cage fault are lost and the condition of the motor may become difficult to assess, even in the case with 3 broken rotor bars. The fault signatures found from a motor equipped with the "SB" and "4B" winding configurations were not included in this figure, since they look similar to the ones corresponding to the "NB" case. The dB representations are with reference to the 150-Hz component, since this was found to have the highest amplitude.
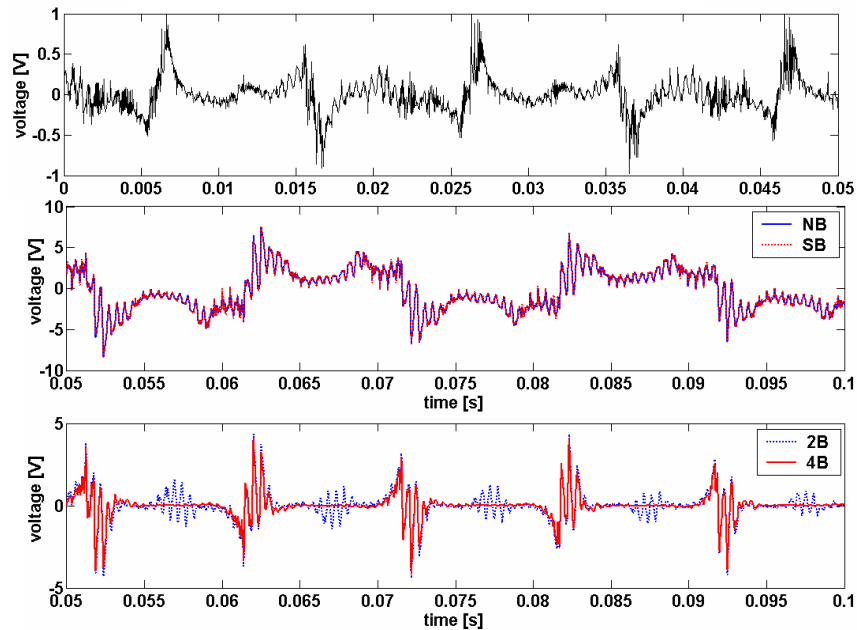
Fig. 5.2.23 Time-domain representation of the voltages induced in the search coil "p-1" – 3 broken rotor bars – measurements (top) and simulations taken at half load.

Based on the measurements, Fig. 5.2.25 shows the frequency-domain representation of the voltages induced in the search coil "*p*-1" for the case of a broken rotor bar. The clear agreement between the measurements and simulations in terms of characteristic frequency sidebands components found responsible for the detection of such abnormalities is obvious. This picture also points out the reduced ability to detect faults of measurements at lower motor loadings; a broken bar is undetected. The dB representation is with reference to the 150-Hz component.
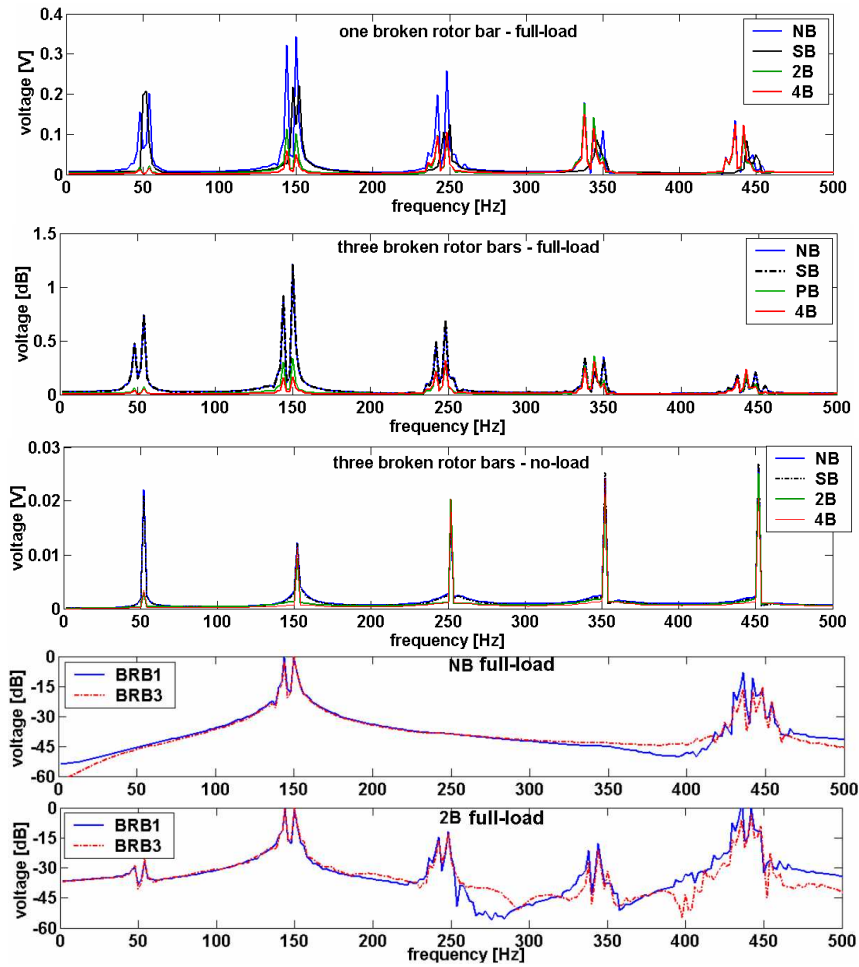
Fig. 5.2.24 Frequency-domain representation of the voltages induced in the "p-1" search coil during various cage-related faults – simulations at various loads.
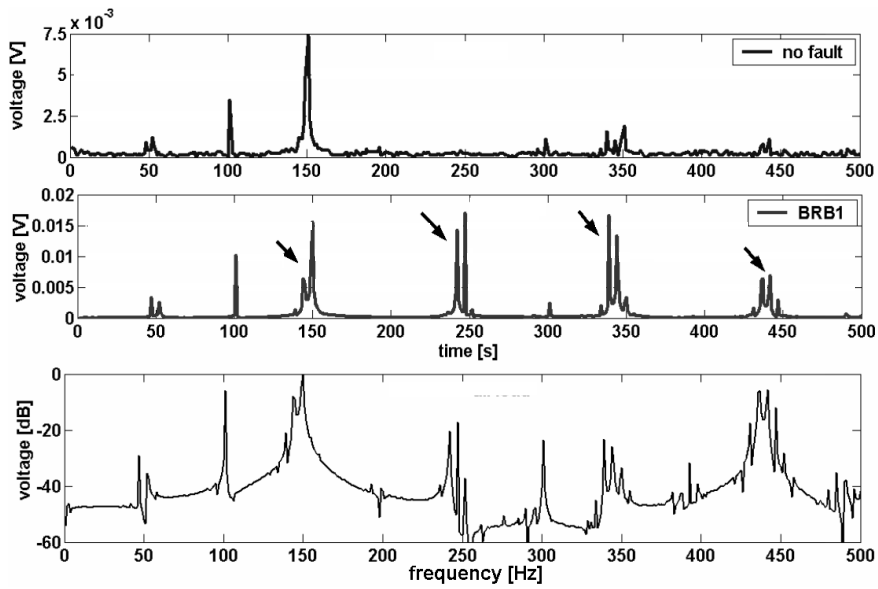
Fig. 5.2.25.a Frequency-domain representation of the voltages induced in the "p-1" search coil – one broken rotor bar – measurements at full load.
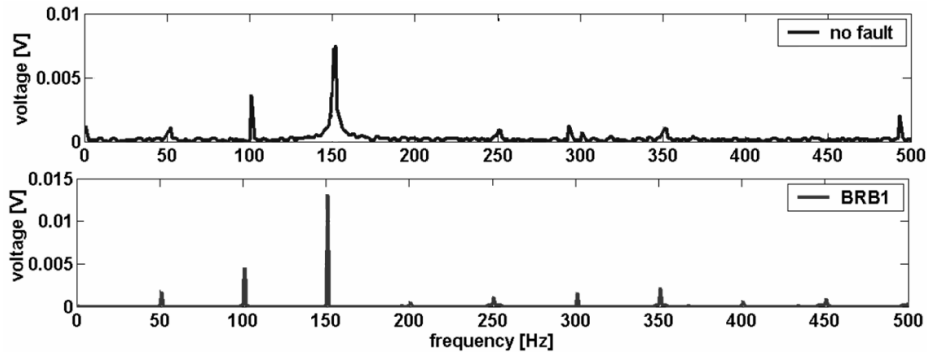
*Fig. 5.2.25.b Frequency-domain representation of the voltages induced in the "p-1" search coil – measurements at no load.*

SEARCH COIL "*p*+1"

Fig. 5.2.26 presents, both from the measurements and simulations, the time-domain representation of the voltages induced in the search coil "*p*+1" for the case of a motor operating with three broken rotor bars.
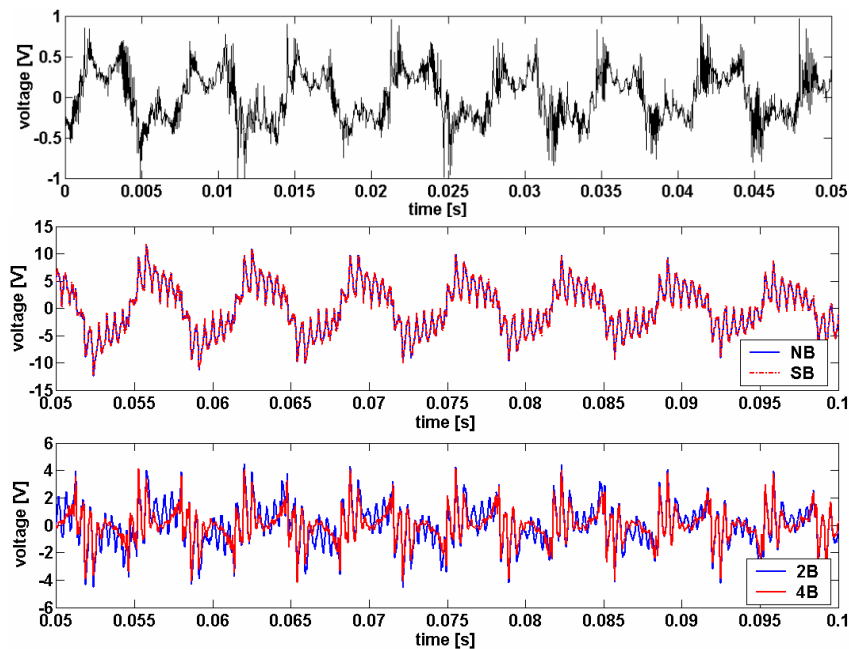

Fig. 5.2.26 Time-domain representation of the voltages induced in the search coil "p+1" – three broken rotor bars – measurements (top) and simulations at half load.

Relying on the simulations, Fig. 5.2.27 shows the frequency-domain representation of the voltages induced in the "*p*+1" search coil. The magnitude of the new frequency sideband components characteristic of a rotor cage fault are found to be higher for the motor equipped with a stator winding of the types "NB" or "SB". Similarly to the case of the "*p*-1" search coil, at no load, important signs of cage fault are lost and the condition of the motor may become difficult to assess, even in the case of three broken rotor bars.

Based on the measurements, Fig. 5.2.28 shows the frequency-domain representation of the voltages induced in the search coil "*p*+1" for various rotor cage faults. The agreement between the measurements and simulations in terms of the characteristic frequency sideband components found responsible for the detection of such abnormalities is very clear.
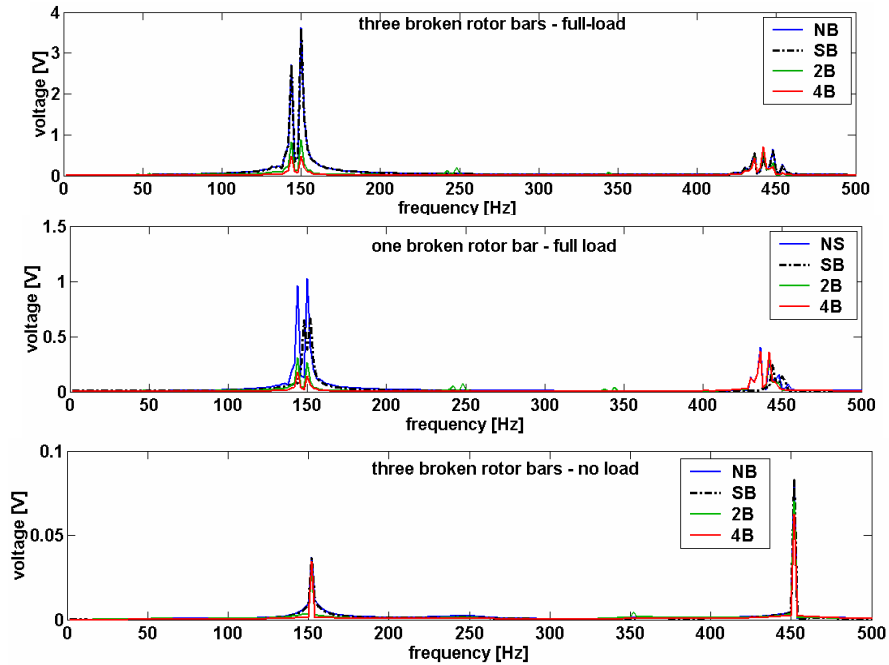
Fig. 5.2.27 Frequency-domain representation of the voltages induced in the "p+1" search coil during various cage-related faults – simulations at various loads.
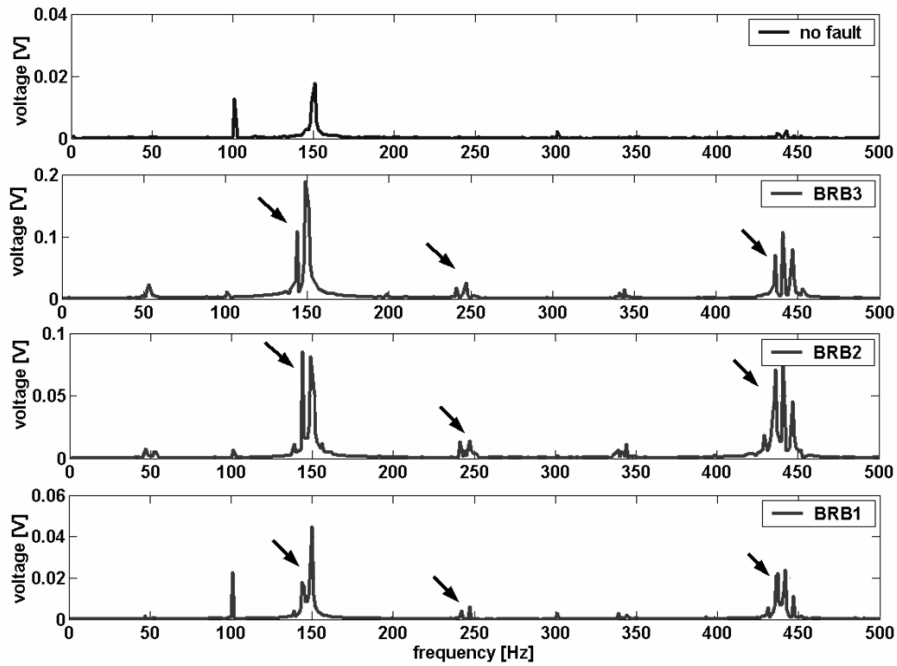

Fig. 5.2.28.a Frequency-domain representation of the voltages induced in search coil "p+1" during various cage-related faults – measurements at full load.
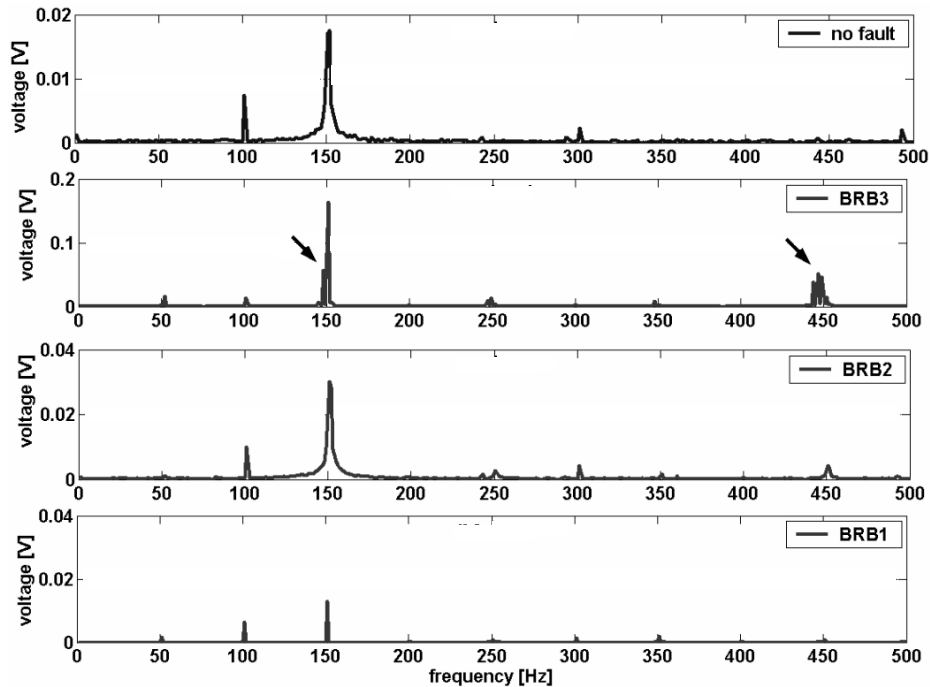
Fig. 5.2.28.b Frequency-domain representation of the voltages induced in search coil "p+1" during various cage-related faults – measurements at no load.

SEARCH COILS AT THE NON-DRIVE END AND AROUND THE MOTOR SHAFT

Fig. 5.2.29 presents the time-domain representation of the voltages induced in the search coils located at the non-drive end of the motor and around the motor shaft, respectively for an operation of the test motor characterized by 3 broken rotor bars. For these cases, simulations are not available. The dB representations are with reference to the fundamental frequency.

Fig. 5.2.30 points out the characteristic frequency sideband components produced by rotor cage-related faults in the indications provided by a search coil placed at the non-drive end of the test motor.
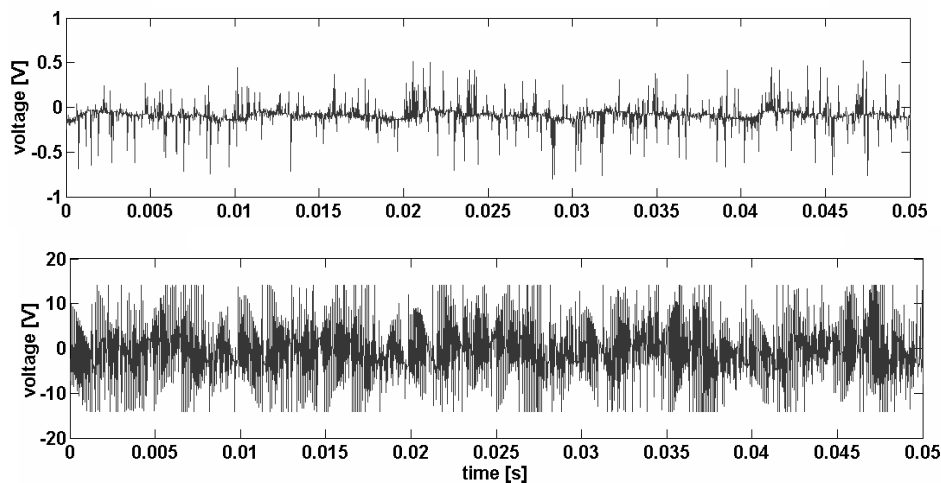
Fig. 5.2.29 Time-domain representation of the voltages induced during a cage-related fault in the search coils located at the non-drive end of the motor near the ventilator (top) and around the motor shaft (bottom) – measurements at full load.
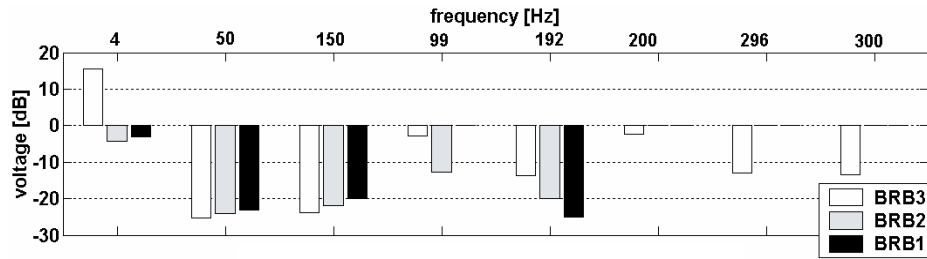
Fig. 5.2.30 Characteristic frequency sidebands produced by a rotor cage-related fault in the indications provided by the search coil placed at the non-drive end of the motor – measurements at full load.

For lower loadings of the test motor, the useful fault indications decrease drastically. The only frequency sidebands to provide potential information about fault remain the ones at a very low frequency and in the vicinity of the fundamental (diminished by approx. 5 dB for the case of three broken rotor bars). At half load and no load, only the case with three broken rotor bars is detectable.

Fig. 5.2.31 presents the frequency-domain representation of the voltages induced in the search coil placed around the motor shaft. For a healthy machine operation, these components are non-existent. In contrast to the search coil intended to sense the flux in the non-drive area of the test motor, this search coil is able to provide useful information about a fault with the same accuracy at half load. However, at no load only the case with three broken bars remains relatively visible, but with a lower sensitivity (on average the magnitudes of the characteristic fault sidebands are about 10 dB lower).
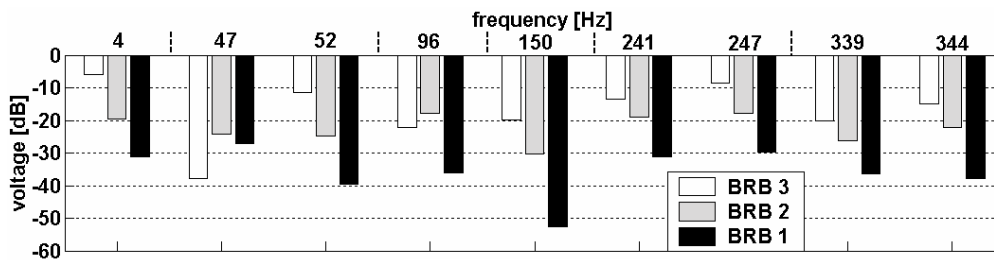
Fig. 5.2.31 Characteristic frequency sidebands produced by various rotor cage-related faults in the indications provided by the search coil placed around the motor shaft – measurements at full load.

Discussions

According to the initial expectations, a large supply current was required to flow in order to facilitate successful detection of rotor faults during steady-state operation. This large current is obtained whilst the motor is running under full load and half load conditions.

At least for a motor operating at full and half loads, the rotor cage-related faults that were studied were reflected in well-defined associated fault frequency components (given by Eq. 3.11) in all of the search coils under study. This is in opposition to the results obtained from the case of the branch current monitoring, where a cage-related fault was reflected in this manner (Eq. 3.2) only for those motors equipped with a stator winding configuration of the types "2B" and "4B".

The distortions in the branch current resulting from a cage fault given by Eq. 3.1 were found in all of the cases that were studied, but such signatures may not be confidently used for rotor cage fault detection purposes since they may also appear as a consequence of some non-faulty operating conditions, such as pulsating loads, interactions between the motor and the train equipment, and particular rotor designs.

Following the discussion previously presented, the benefits of using search coils for detecting rotor cage-related faults become obvious.

5.3.   Static eccentricity, dynamic eccentricity, bearing fault

SEARCH COIL AROUND STATOR TOOTH

Based on the measurements and simulations, respectively, Figs. 5.3.1 and 5.3.2 present the time-domain representation of the voltages induced in the search coil located around a stator tooth of the test motor under various operating conditions. For this search coil, the dB representations shown in Figs. 5.3.3 and 5.3.4 are with reference to the fundamental frequency.

From the measurements, it was found that a bearing fault and static eccentricity could not be detected from the indications provided by this search coil. For the case of static eccentricity, the same conclusion was drawn after analysing the simulation data corresponding to the motor equipped with the original winding configuration of type "2B" and "4B" (see Fig. 5.3.4).

The most important changes produced by the dynamic eccentricity are shown in Figs. 5.3.3 and 5.3.4 and, for both the measurements and simulations, the changes corresponding to various motor loadings are summarised in Table 5.3.1. In contrast to the case of static eccentricity, the dynamic eccentricity is observable for a motor equipped with all the stator winding configurations. It is observed that the magnitude of the new frequency component indications provided by this search coil are higher at a lower loading for a motor equipped with stator winding configurations of the "NB" and "SB" types. This conclusion is in agreement with the one drawn by Dorrell (1993b), who claimed that the UMP resulting from dynamic eccentricity decreases as the motor is loaded from no-load.
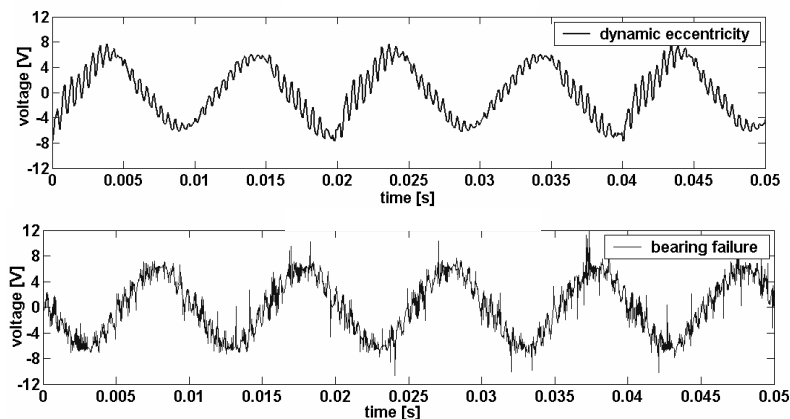
Fig. 5.3.1 Time-domain representation of the voltages induced in the search coil placed around a stator tooth – bearing failure, dynamic eccentricity – measurements at half load.
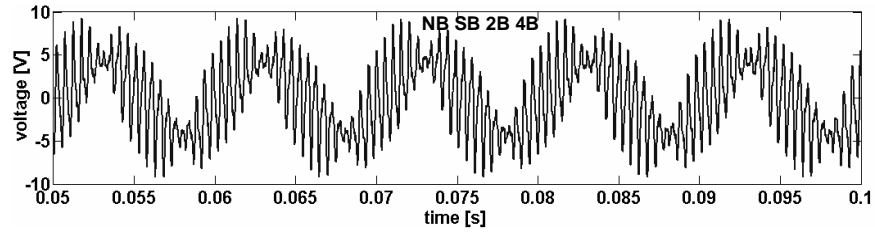
Fig. 5.3.2 Time-domain representation of the voltages induced in the search coil placed around a stator tooth – static eccentricity – simulations at half load.
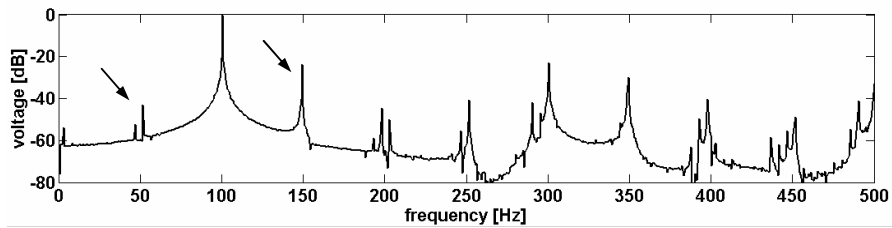
Fig. 5.3.3 Frequency-domain representation of the voltages induced in a search coil placed around a stator tooth – dynamic eccentricity – measurements at half load.
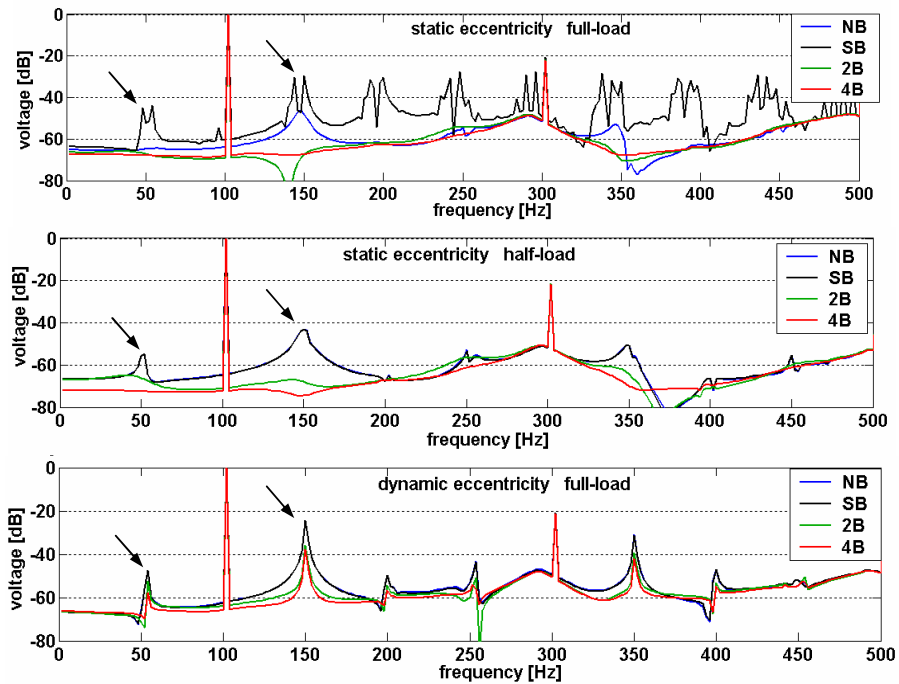
Fig. 5.3.4 Frequency-domain representation of the voltages induced in the search coil placed around a stator tooth – simulations at various loads.

Table 5.3.1 Amplitudes of the sideband frequencies characteristic of dynamic eccentricity [dB].

f [Hz]	Full load				Half load				No load			
	Simul.			Meas.	Simul.			Meas.	Simul.			Meas.
	'NB' 'SB'	'4B'	'2B'	'2B'	'NB' 'SB'	'4B'	'2B'	'2B'	'NB' 'SB'	'4B'	'2B'	'2B'
51,5 50,7 50	-47	-57	-52	-43	-45	-65	-56	-50	-35	-65	-54	-47
148,5 149,2 150	-25	-38	-36	-24	-24	-39	-36	-23	-22	-37	-34	-23
1991.5 1918.5 1949.5	-26	-27	-28	-28	-26	-24	-24	-28	-21	-21	-20	-39
2088.5 2118.5 2149.5	-19	-19	-18	-27	-31	-31	-33	-28	-31	-33	-31	-37

Fig. 5.3.5 presents the characteristic frequency sideband components produced by the static eccentricity in the indications provided by a search coil placed around a stator tooth of a motor equipped with stator windings of the types "NB" and "SB". At a lower loading of the machine, some of the sidebands important for assessing the condition of the motor are lost and, on average, the level of magnitude for all the remaining characteristic fault sidebands diminishes by about 10-15 dB. This behaviour is in agreement with the results presented by other researchers (Dorrell 1993a), stating that as a result of static eccentricity the UMP increases rapidly as the motor is loaded from no load.
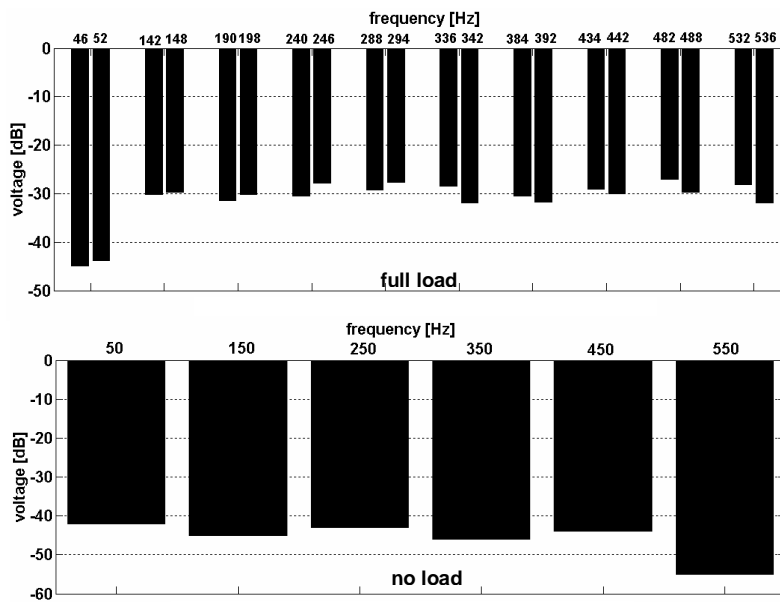
Fig. 5.3.5 Characteristic frequency sidebands produced by static eccentricity in the indications provided by the search coil placed around a stator tooth – simulations.

In the high-frequency range, the experimentally implemented dynamic eccentricity was reflected in the rotor-slot harmonics by increasing their magnitudes by around 3 dB irrespective of the machine loading in comparison with healthy operation. Such modifications are not found in the simulations in any of the stator winding configurations.

Slightly higher changes (5-7 dB) are to be found for the experimentally implemented static eccentricity, while no changes in the amplitude of the rotor-slot harmonics are to be found from the simulations.

In the high-frequency range, the experimental implemented bearing fault was very poorly reflected in the rotor-slot harmonics, increasing their magnitudes only by around 1-2 dB, irrespective of the machine loading in comparison with healthy operation.

SEARCH COIL PLACED AROUND TWO POLE PITCHES

Based on the measurements and simulations, respectively, Figs. 5.3.6 and 5.3.7 present the time-domain representation of the voltages induced in the search coil located around two pole pitches of the test motor under various operating conditions.
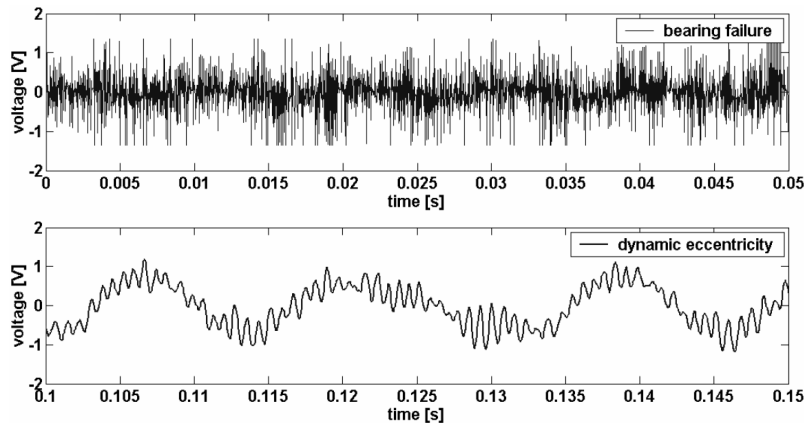

Fig. 5.3.6 Time-domain representation of the voltages induced in the search coil placed around two pole pitches – bearing fault, dynamic eccentricity – measurements at half load.
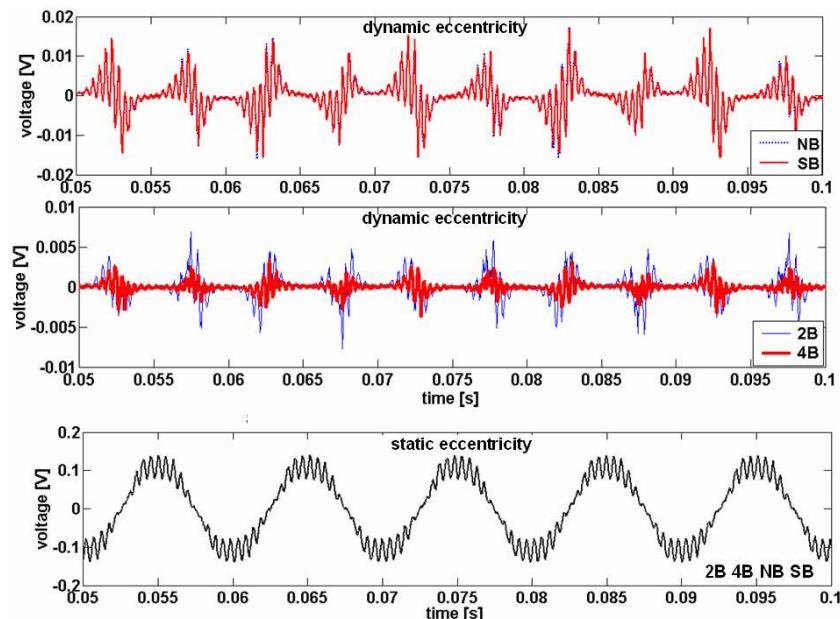

Fig. 5.3.7 Time-domain representation of the voltages induced in the search coil placed around two pole pitches – simulations at half load.

According to the measurements, only the dynamic eccentricity may be detected via an external search coil placed around two pole pitches (Fig. 5.3.8). The frequencies that offer possible information about this fault are marked by arrows and are according to Eq. 3.7.

It is relatively clear that at a lower motor loading, the dynamic eccentricity appears clearer in the flux spectrum provided by this search coil.

From the simulations it was found that new frequency components characteristic of static eccentricity appear only in the cases of a motor equipped with stator winding configurations of the "NB" and "SB" types (Figs. 5.3.9 and 5.3.10).

For dynamic eccentricity, it was found that new frequency sideband components appear, irrespective of the stator winding configuration, and the asymmetry becomes clearer for a motor operating at a lower loading (Fig. 5.3.9). This is in accordance with the results obtained from the measurements and presented in Fig. 5.3.8.

The magnitudes of these new fault frequency sideband components are presented with reference to the rotor slot frequencies (2040 Hz and 2100 Hz for operation at full load and no load, respectively). It is important to notice that even at a lower loading, the magnitudes of the new frequency sidebands resulting from static eccentricity do not diminish.
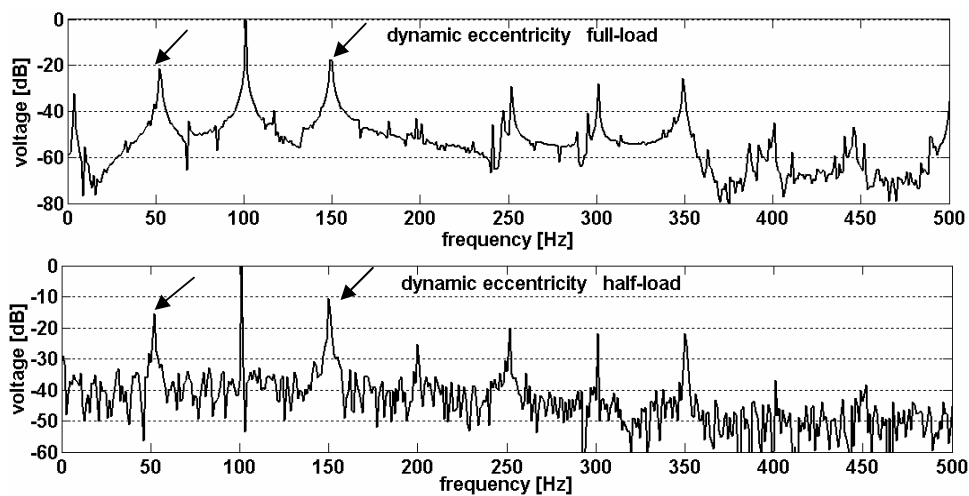

Fig. 5.3.8 Frequency-domain representation of the voltages induced in a search coil placed around two pole pitches – dynamic eccentricity – measurements at various loads.

The simulation tool in which the dynamic eccentricity was implemented is able to predict the same new frequency sideband components as the ones found in the measurements. The signatures produced by the dynamic eccentricity in this search coil are identical to the ones found in the current spectrum (Section 5.1) and summarised in Table 5.3.2.
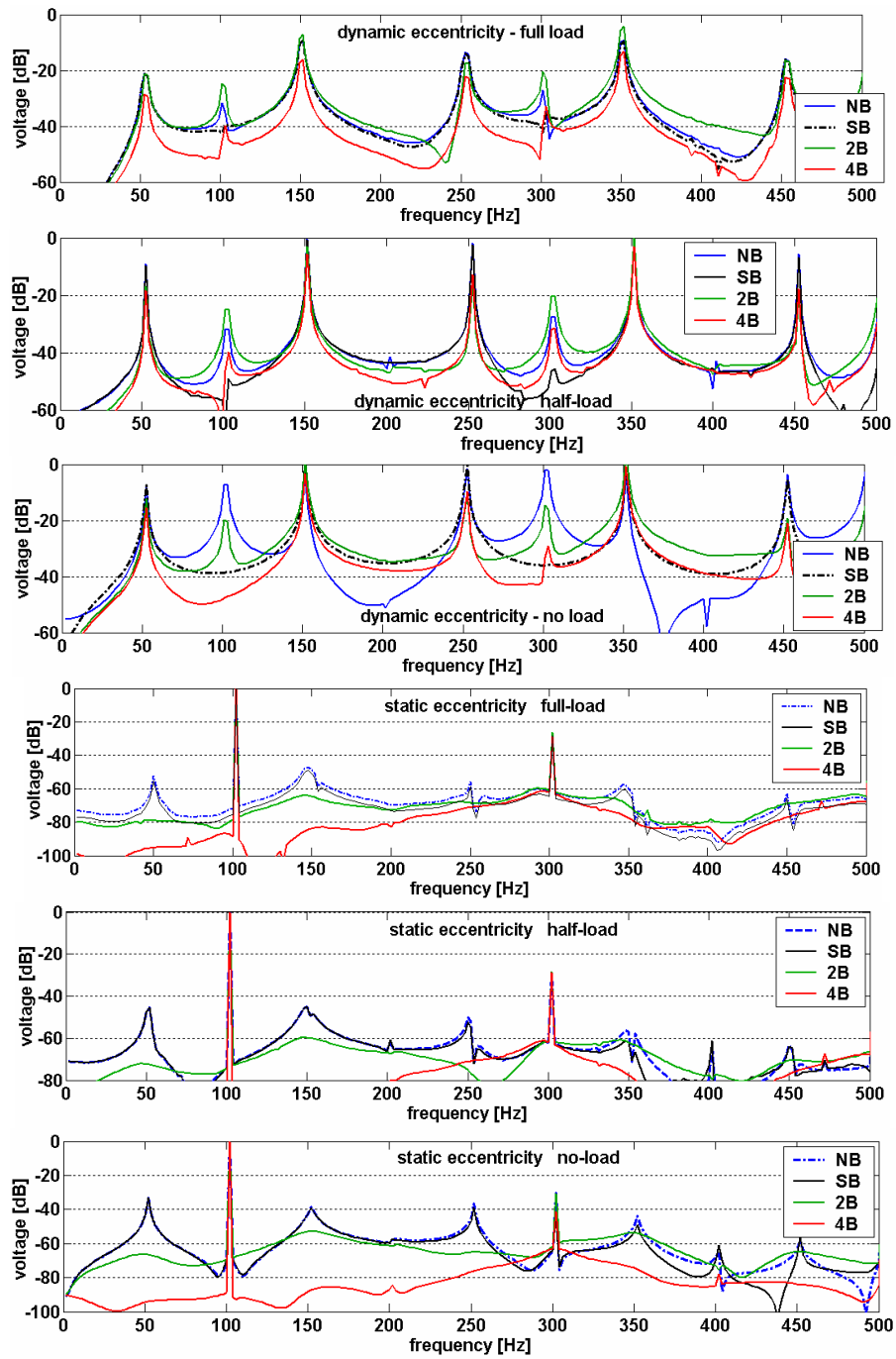
Fig. 5.3.9 Frequency-domain representation of the voltages induced in the search coil placed around two pole pitches – static eccentricity, dynamic eccentricity – simulations at various loads.
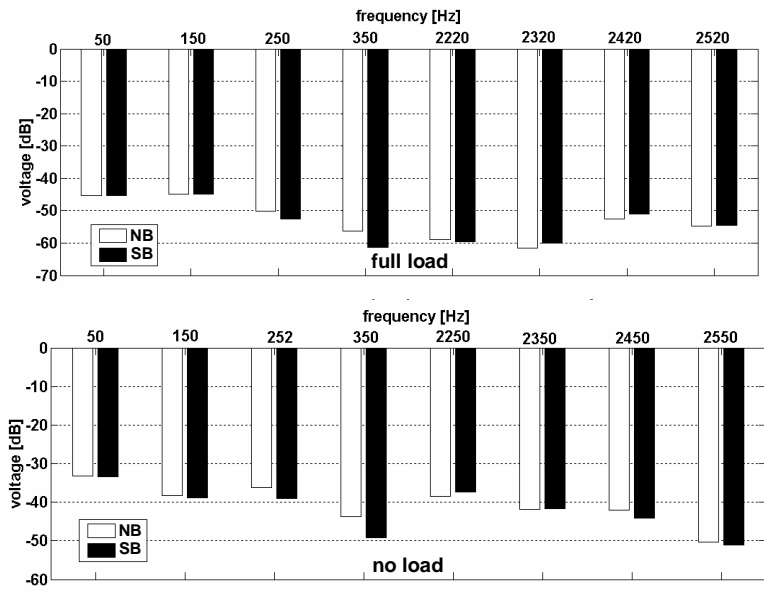
Fig. 5.3.10 *Characteristic frequency sidebands produced by static eccentricity in the indications provided by the search coil placed around two pole pitches of the test motor – simulations at various loads.*

Table 5.3.2 Amplitudes of the sideband frequencies characteristic of dynamic eccentricity [dB].

f [Hz]	Full load					Half load					No load				
	Simul.				Me-as.	Simul.				Me-as.	Simul.				Me-as.
	'NB'	'SB'	'4B'	'2B'	'2B'	'NB'	'SB'	'4B'	'2B'	'2B'	'NB'	'SB'	'4B'	'2B'	'2B'
51,5	-21	-21	-28	-21	-21										
50,7						-10	-10	-18	-18	-15					
50											-8	-8	-16	-12	-15
148,5	-8	-8	-16	-8	-18										
149,2						-1	-1	-6	-3	-11					
150											-5	-1	-3	2	-12
1991.5	-11	-11	-8	-2	-20										
1918.5						-18	-18	-14	-10	-16					
1949.5											-12	-30	-12	-2	-20
2088.5	-4	-4	-1	-9	-35										
2118.5						-5	-5	-2	-20	-14					
2149.5											-9	-5	-4	-12	-13

In the high-frequency range, the experimentally implemented dynamic eccentricity was reflected in the rotor-slot harmonics by increasing their magnitudes by around 2 dB in full-load motor operation in comparison with healthy operation. No such signs were found for the half-load and no-load motor operation points. From the simulations, such modifications could not be analysed, since in healthy operation the signal captured by this coil is ideally zero.

Slightly higher modifications (3-5 dB) are to be found for the experimental implemented static eccentricity, irrespective of the motor loading, while from the simulations such modifications could not be analysed, since in healthy operation the signal captured by this coil is ideally zero.

In the high-frequency range, the experimentally implemented bearing fault was very poorly reflected in the rotor-slot harmonics, increasing their magnitudes by around only 2 dB only at half-load in comparison with healthy operation.

SEARCH COIL "_p_+1"

Based on the measurements and simulations, respectively, Figs. 5.3.11 and 5.3.12 present the time-domain representation of the voltages induced in the "_p_+1" search coil under various operating conditions.
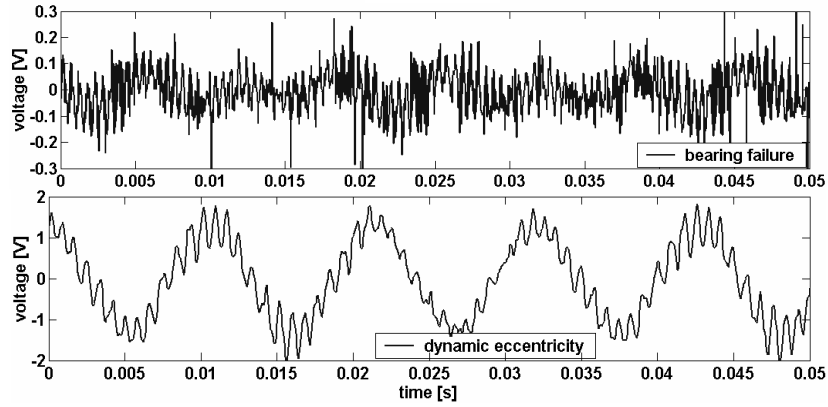
*Fig. 5.3.11 Time-domain representation of the voltages induced in search coil "p+1" – bearing fault, dynamic eccentricity – measurements at half load.*
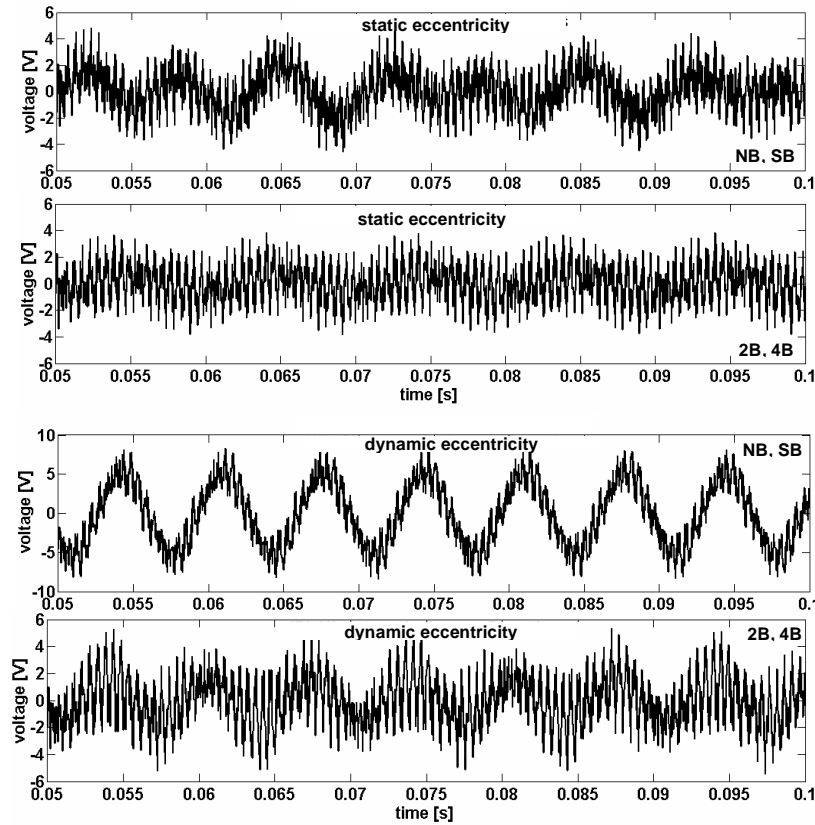

Fig. 5.3.12 Time-domain representation of the voltages induced in search coil "p+1" – static eccentricity, dynamic eccentricity – simulations at half load.

Based on the measurements and simulations at half load, Figs. 5.3.13 and 5.3.14 show the frequency-domain representation of the voltages induced in the search coil "p+1" for the case of static eccentricity. A summary of the most important changes offering potential information about the static eccentricity for all of the motor loadings that were studied may be found in Tables 5.3.3 and 5.3.4. The dB representation is with reference to the 150-Hz component in the case of the measurements and with reference to the rotor-slot harmonics for the simulations (full load 1840 Hz, half load 1870 Hz, no load 1900 Hz).
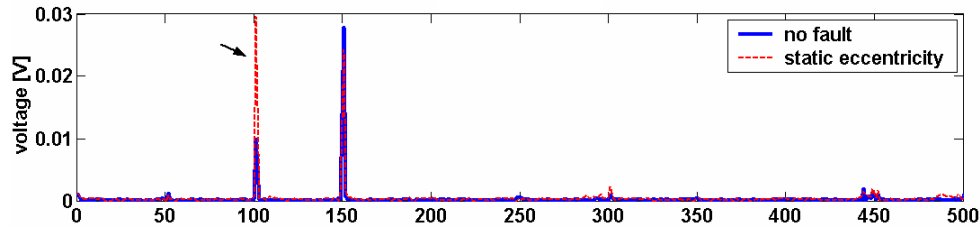
Fig. 5.3.13 Frequency-domain representation of the voltage induced in the "p+1" search coil – static eccentricity – measurements at half load.

Table 5.3.3 Main changes produced by the static eccentricity in the indications provided by the "p+1" search coil – measurements [dB].

f [Hz]	$U_{\text{static eccentricity}}-U_{\text{healthy}}$		
	100	300	rotor-slot harmonics
full load	11	1	7-15
half load	13	10	5-9
no load	14	2-4	5-7
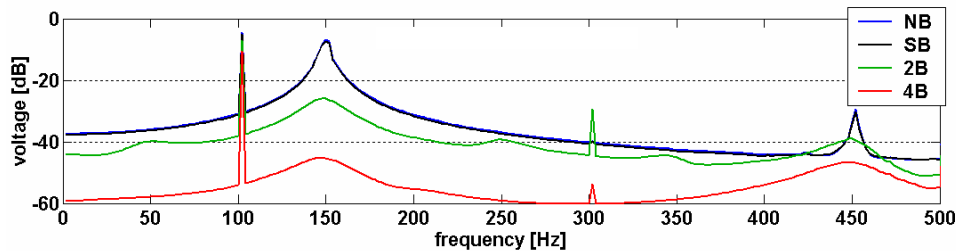
Fig. 5.3.14 Frequency-domain representation of the voltage induced in the "p+1" search coil – static eccentricity – simulations at half load.

Table 5.3.4 Main changes produced by the static eccentricity in the indications provided by the "p+1" search coil – simulations at various loads [dB].

f [Hz]	100				150				50	300
winding config.	'NB'	'SB'	'2B'	'4B'	'NB'	'SB'	'2B'	'4B'	'2B'	'2B'
full load	-5	-5	-8	-11	-10	-10	-30	-45	-42	-30
half load	-5	-5	-7	-11	-7	-7	-26	-45	-40	-30
no load	-8	-8	-8	-12	-12	-12	-21	-46	-38	-30

It is important to notice that the magnitude of the frequency components of interest for the detection of static eccentricity is inversely proportional to the number of parallel branches to be found in the stator winding of the test motor.

Based on the measurements and simulations at half load, Figs. 5.3.15 and 5.3.16 show the frequency-domain representation of the voltages induced in the search coil "p+1" for the case of dynamic eccentricity. A summary of the most important modifications offering potential information about the dynamic eccentricity for all of the motor loadings that were studied may be found in Tables 5.3.5 and 5.3.6. The dB representation is with reference to the rotor-slot harmonics for both the simulations and measurements.
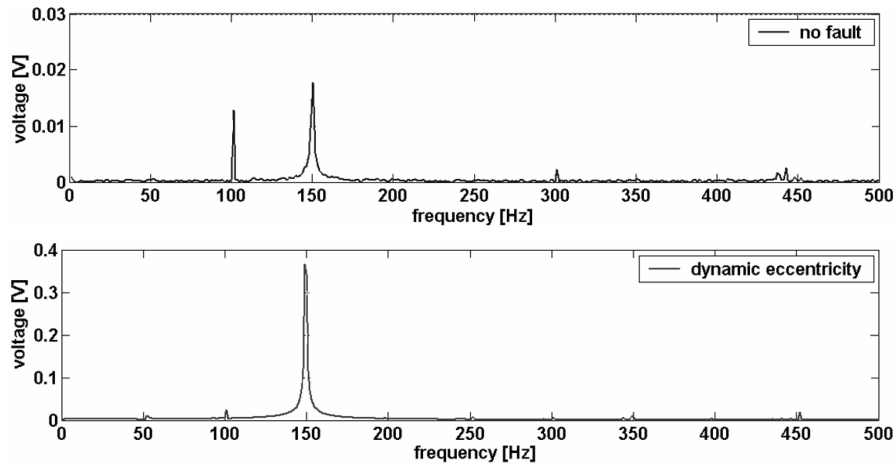
Fig. 5.3.15 Frequency-domain representation of the voltage induced in the "p+1" search coil – dynamic eccentricity – measurements at full load.
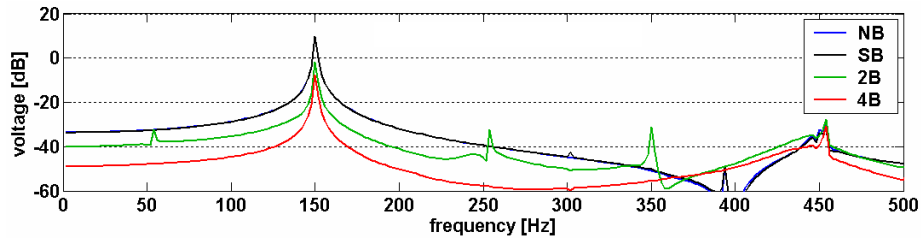
Fig. 5.3.16 Frequency-domain representation of the voltages induced in the "p+1" search coil – dynamic eccentricity – simulations at full load.

Table 5.3.5 Main changes produced by the dynamic eccentricity – measurements at various loads [dB].

f [Hz]	50	150	250
full load	6	8	8
half load	2	4	11
no load	12	16	21

Table 5.3.6 Main changes produced by the dynamic eccentricity in the indications provided by the "p+1" search coil – simulations at various loads [dB].

f [Hz]	148.5 149.2 150				51.5 50.7 50		252	1991.5 1918.5 1949.5			2088.5 2118.5 2149.5			
winding config.	'NB'	'SB'	'2B'	'4B'	'2B'	'2B'	'2B'	'NB'	'4B'	'SB'	'2B'	'NB'	'4B'	'SB'
full load	10	10	-2	-7	-32	-32	-18	-	-	-	-9	-	-	-
half load	12	12	-1	-7	-32	-31	-16	-	-	-	-7	-	-	-
no load	9	9	-2	-8	-34	-30	-2	-12	-12	-30	-12	-8	-4	-6

It is observed that at lower levels of motor loading, the magnitude of the frequency component that exhibits the most important change (150 Hz) is higher. This behaviour was also observed from the simulations (Table 5.3.6).

Concerning the behaviour of the sideband components responsible for the detection of the dynamic eccentricity in the case of a motor equipped with various stator winding configurations, a similar effect to the one observed with static eccentricity is found.

A comparative analysis between the measurements and simulations points out a very good agreement and the ability of the simulation tool to predict the same new frequency sideband components.

A bearing fault may not be detected from the indications provided by this search coil. In the high-frequency range, the maximum modifications of the rotor-slot harmonic magnitudes do not exceed the level of 2-3 dB, irrespective of the motor loading.

In comparison with the previous search coils, both static and dynamic eccentricity may be detected more easily with the use of a search coil purposely intended to capture the harmonics of the order "$p+1$" (Table 5.3.7).

Table 5.3.7 Changes to be found in the magnitude of the rotor-slot harmonics – measurements at various loads [dB].

Static eccentricity			Dynamic eccentricity		
$U_{static\ eccentricity} - U_{healthy}$			$U_{dynamic\ eccentricity} - U_{healthy}$		
Full load	Half-load	No load	Full load	Half load	No load
6-13	4-11	6-12	12-24	8-22	8-17

SEARCH COIL "p-1"

Based on the measurements and simulations, respectively, Figs. 5.3.17 and 5.3.18 present the time-domain representation of the voltages induced in the "p-1" search coil under various operating conditions.
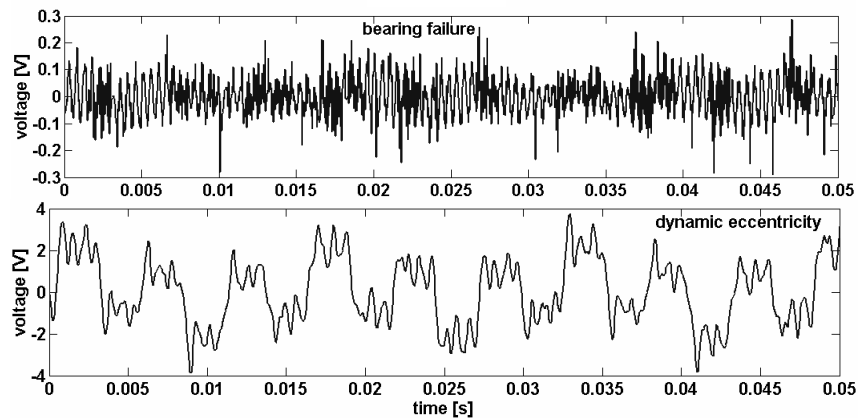
Fig. 5.3.17 Time-domain representation of the voltages induced in search coil "p-1" – bearing fault, dynamic eccentricity – measurements at half load.
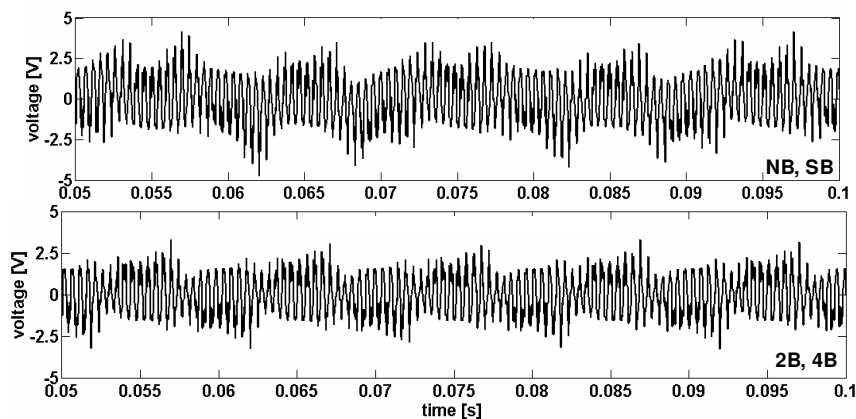
*Fig. 5.3.18.a Time-domain representation of the voltages induced in search coil "p-1" – static eccentricity – simulations at half load.*
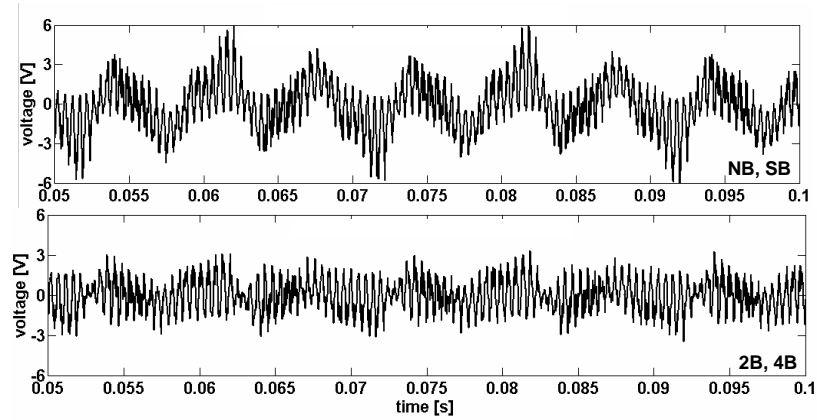
Fig. 5.3.18.b Time-domain representation of the voltages induced in search coil "p-1" – dynamic eccentricity – simulations at half load.

Based on the measurements and simulations, respectively, Figs. 5.3.19 and 5.3.20 show the frequency-domain representations of the voltages induced in the search coil "*p*-1" for the cases of static and dynamic eccentricity. The dB representations are presented with reference to the rotor slot frequencies for the simulations and with reference to the 150-Hz component for the measurements. Tables 5.3.8-5.3.12 present a summary of the most important modifications offering potential information about the static eccentricity for all of the loadings under study.
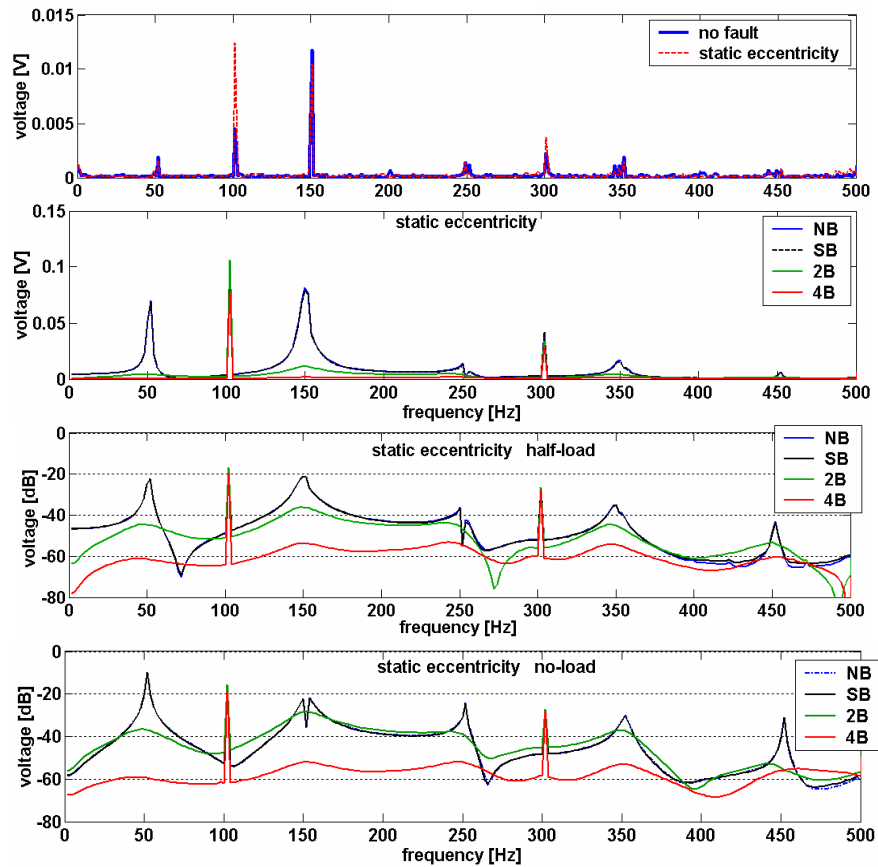
Fig. 5.3.19 Frequency-domain representation of the voltages induced in the "p-1" search coil – healthy and static eccentricity – measurements (topmost figure) and simulations with various loads.
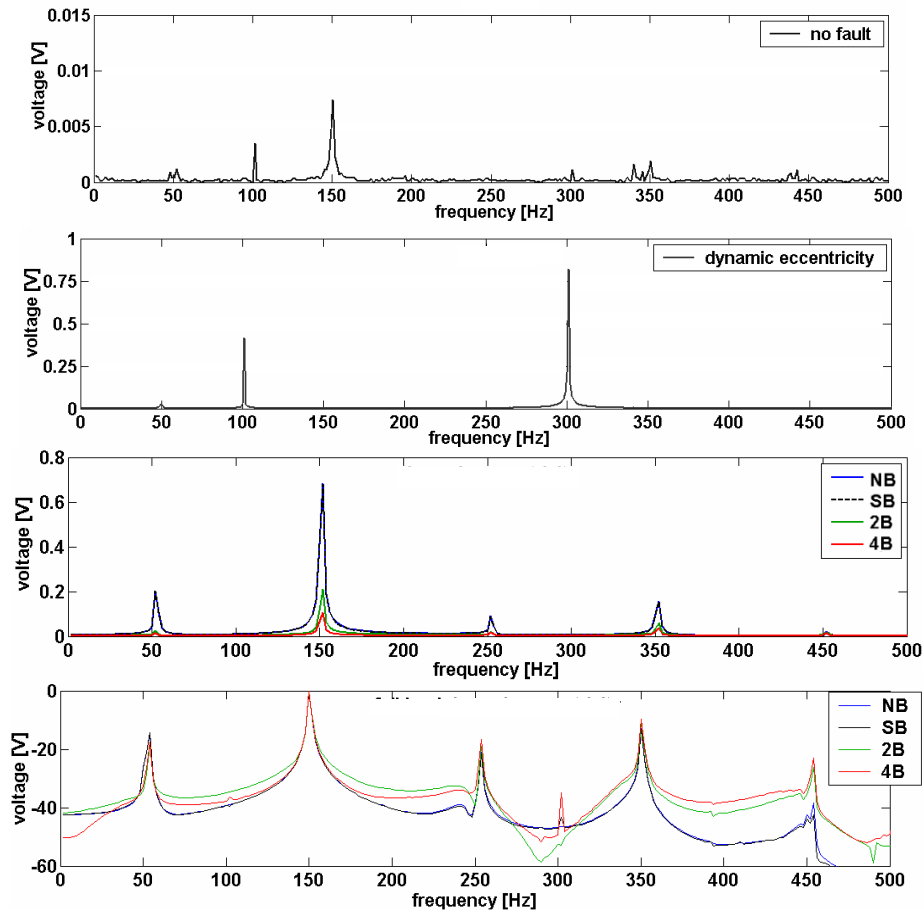
Fig. 5.3.20 Frequency-domain representation of the voltages induced in the "p-1" search coil – healthy and dynamic eccentricity – measurements (two topmost figures) and simulations at full load.

Table 5.3.8 Main changes produced by the static eccentricity in the indications provided by the "p-1" search coil – measurements [dB].

	$U_{static\ eccentricity} - U_{healthy}$	
f [Hz]	100	300
full load	15	10
half load	14	10
no load	15	20

Table 5.3.9 Main changes produced by the static eccentricity in the indications provided by the "p-1" search coil – simulations [dB].

f [Hz]	50				150			
winding config.	'NB'	'SB'	'2B'	'4B'	'NB'	'SB'	'2B'	'4B'
full load	-27	-27	-49	-60	-22	-24	-41	-60
half load	-22	-22	-44	-61	-21	-21	-36	-54
no load	-10	-10	-36	-60	-22	-22	-28	-52

Table 5.3.10 Behaviour of the 3rd harmonic for the case of dynamic eccentricity in the indications provided by the "p-1" search coil – measurements.

	$U_{\text{static eccentricity}} / U_{\text{healthy}}$
full load	2
half load	1.4
no load	0.25

Table 5.3.11 Main changes produced by the dynamic eccentricity in the indications provided by the "p-1" search coil – simulations [dB].

f [Hz]	50				150			
winding config.	**'NB'**	**'SB'**	**'2B'**	**'4B'**	**'NB'**	**'SB'**	**'2B'**	**'4B'**
full load	-16	-16	-28	-31	-1	-1	-9	-14
half load	-10	-10	-26	-29	2	2	-7	-12
no load	0	0	-23	-28	3	3	-4	-10

Table 5.3.12 Changes in the magnitude of the rotor-slot harmonics observed in the indications provided by the "p-1" search coil – measurements [dB].

	Static eccentricity			Dynamic eccentricity		
	$U_{\text{static eccentricity}} - U_{\text{healthy}}$			$U_{\text{dynamic eccentricity}} - U_{\text{healthy}}$		
Search coil	**Full load**	**Half load**	**No load**	**Full load**	**Half load**	**No load**
"p-1"	4-6	5-6	4-6	14-26	12-20	8-20

A comparative analysis between the measurements and simulations in terms of measured and predicted specific frequency components points out a very good agreement for the case of static eccentricity.

In the high-frequency range, it is almost impossible to detect bearing fault with this search coil. The maximum modifications of the rotor-slot harmonic magnitudes do not exceed the level of 3-4 dB, irrespective of the motor loading.

In comparison with the previous search coils, both static and dynamic eccentricity may be detected more easily via the use of a search coil purposely intended to capture the harmonics of the order "p-1" (Table 5.3.12).

SEARCH COILS LOCATED AROUND THE SHAFT AND AT THE NON-DRIVE END OF THE MOTOR

Figs. 5.3.21 and 5.3.22 present the time-domain representation of the voltages induced in the search coil located around the motor shaft and at the non-drive end of the motor, respectively. For this search coils, simulations are not available and the dB representations are with reference to the fundamental frequency.

From the frequency-domain representation of the voltages induced in these search coils (Figs. 5.3.23 and 5.3.24) it was found that:

- a search coil wound around the shaft and purposely intended to sense the axial flux is able to indicate a fault in the bearing. The measurements carried out for this work show that this was the clearest means to observe new frequency components resulting from this fault. However, this signature is almost similar to the one obtained from the static eccentricity;
- a dynamic eccentricity is easily detected by a search coil positioned around the motor shaft at any motor loading
- the search coil placed externally at the non-drive end of the motor is able to indicate the dynamic eccentricity even from measurements at no load but is not able to sense the cases of static eccentricity and bearing fault.
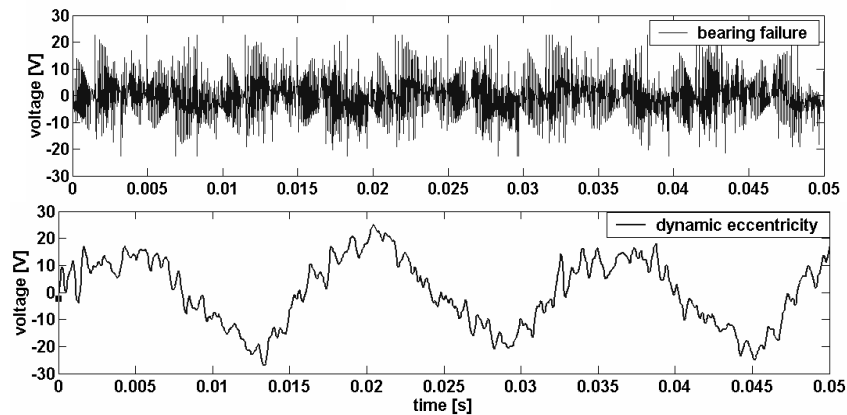
Fig. 5.3.21 Time-domain representation of the voltages induced in the search coil located around the shaft – bearing fault, dynamic eccentricity – measurements at half-load.
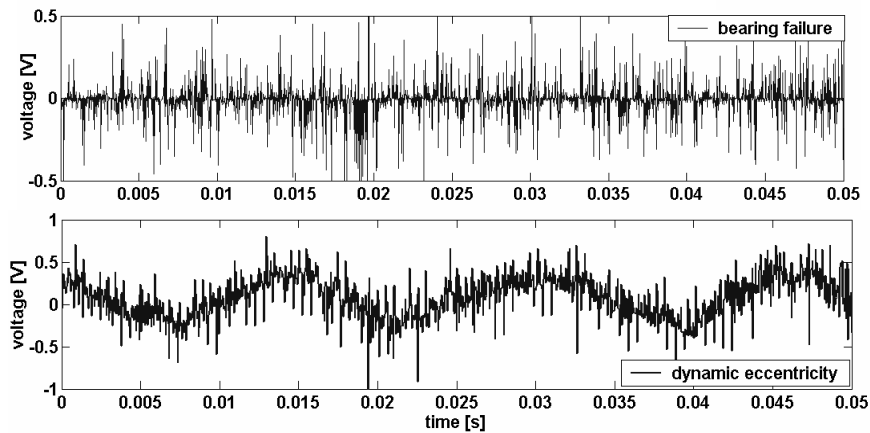
Fig. 5.3.22 Time-domain representation of the voltages induced in the search coil positioned at the non-drive end of the motor – bearing fault, dynamic eccentricity – measurements at half-load.
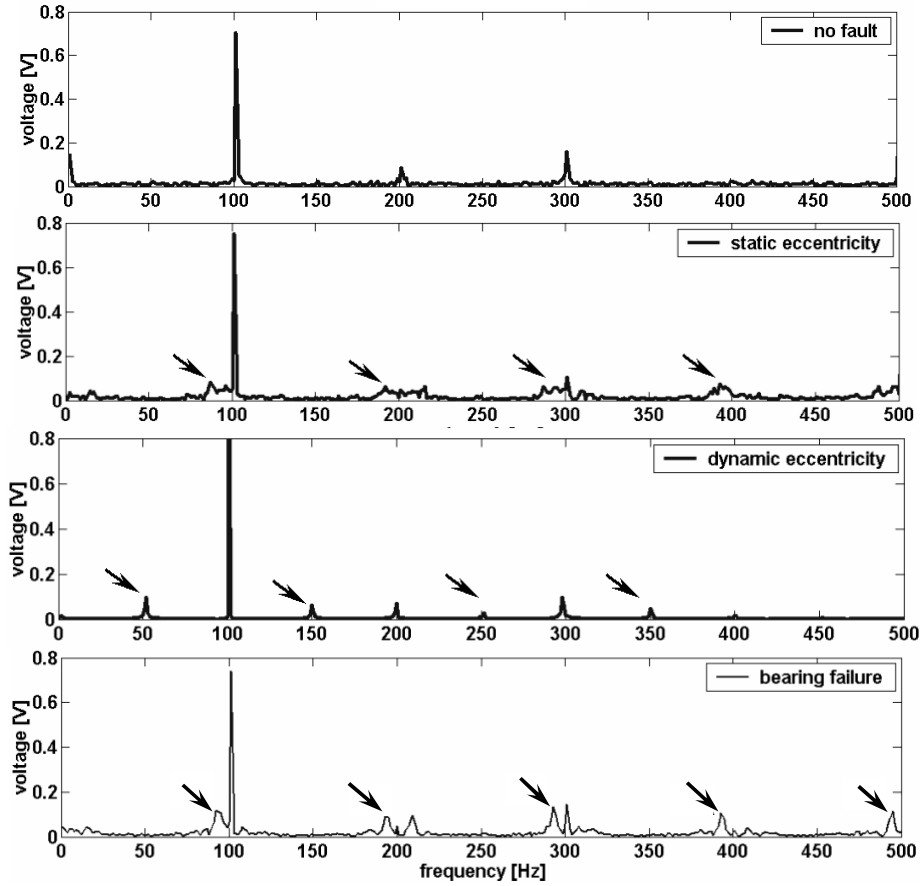
Figs. 5.3.23 Frequency-domain representation of the voltages induced in a search coil placed around the motor shaft – static eccentricity, dynamic eccentricity, bearing fault – measurements at half load.
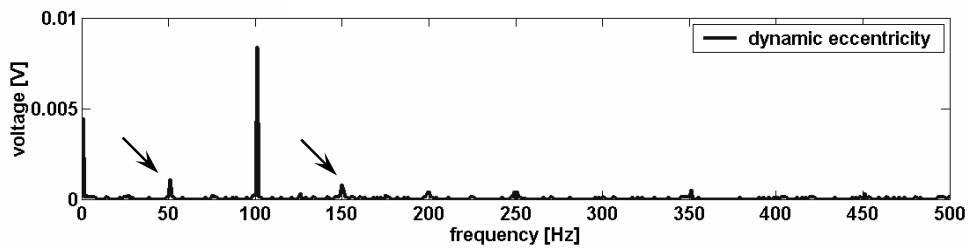
Fig. 5.3.24 Frequency-domain representation of the voltage induced in a search coil placed at the non-drive end of the test motor – dynamic eccentricity – measurements at half load.

Figs. 5.3.25-5.3.28 summarise the characteristic frequency sideband components produced by the faults presented in Figs. 5.3.23 and 5.3.24 and also present similar results obtained from other motor loadings.
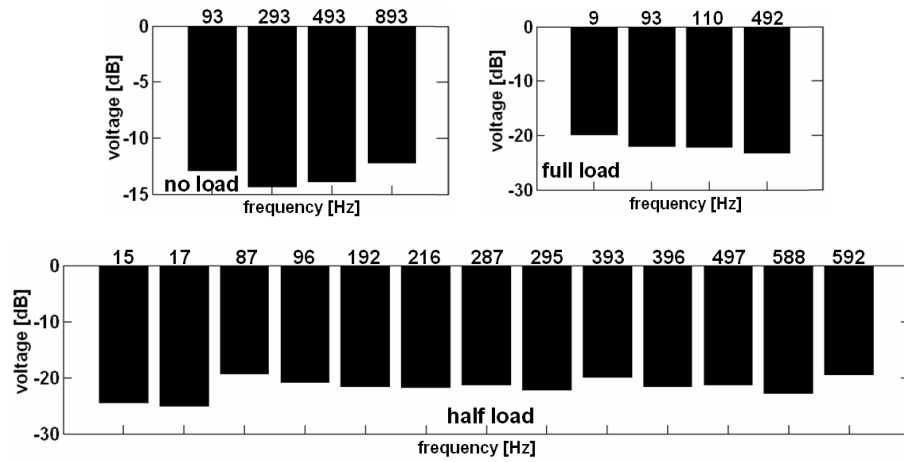
Fig. 5.3.25 Characteristic frequency sideband components produced by the static eccentricity in the indications provided by the search coil wound around the motor shaft – measurements.
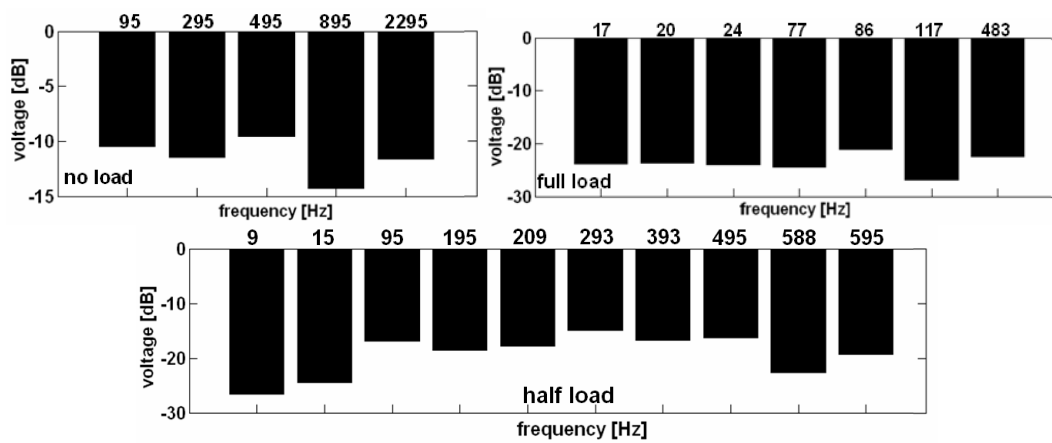
Fig. 5.3.26 Characteristic frequency sideband components produced by bearing fault in the indications provided by the search coil wound around the motor shaft – measurements at various loads.
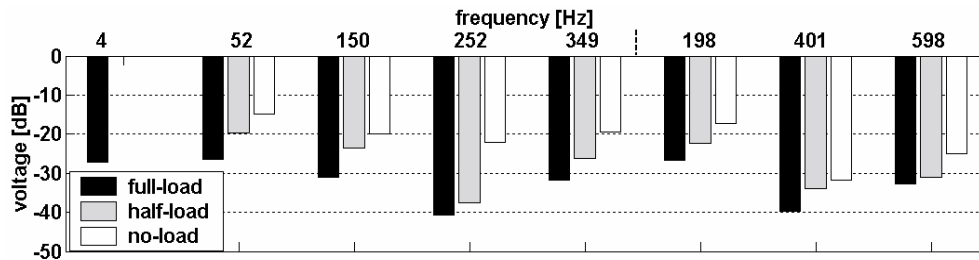
Fig. 5.3.27 Characteristic frequency sideband components produced by the dynamic eccentricity in the indications provided by the search coil wound around the motor shaft – measurements at various loads.
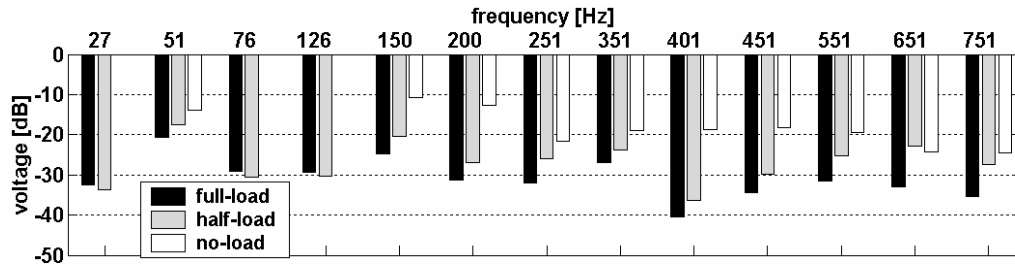
Fig. 5.3.28 Characteristic frequency sideband components produced by the dynamic eccentricity in the indications provided by the search coil placed at the non-drive end of the motor – measurements at various loads.

In the high-frequency range, the bearing fault is relatively more clearly reflected in the indications provided by the search coil around the shaft. An increment of around 10 dB in the magnitude of the rotor-slot harmonics at full load seems to be more important than the similar modifications produced by the same fault and by various faults in other search coil indications. For a half-load and no load, the same modifications are about 7 and 4 dB, respectively.

For the search coil around the shaft, in the high-frequency range, the experimental implemented static eccentricity was reflected in the rotor-slot harmonics by increasing their magnitudes with around 8-10 dB in full load motor operation in comparison with healthy operation. For the half-load and no-load motor operating points, these indications decrease to levels of 4 and 3 dB, respectively.

The dynamic eccentricity is not reflected in any modifications of the rotor-slot harmonics, irrespective of the motor loading for both of these search coils.

Discussion

Since it has been shown that the dynamic eccentricity may be easily observed in all of the fault indicators that were studied, in this section the focus will be mainly on a critical analysis of the means to detect the static eccentricity and a bearing fault.

Search coil around stator tooth. From the measurements, it was found that it was not possible to detect a bearing fault or the static eccentricity from the indications provided by this search coil. For the case of static eccentricity, the same conclusion was drawn after analysing the simulation data corresponding to the motor equipped with the original winding configuration (type "2B"). Since not even the rotor-slot harmonics offer an important hint about the static eccentricity, it becomes clear that other means of detecting this type of eccentricity are needed.

Search coil around two pole pitches. On the basis of the measurements and simulations, only the dynamic eccentricity may be detected via an external search coil placed around two pole pitches. In the high-frequency range, the experimental implemented dynamic eccentricity was not reflected very clearly in the magnitude of the rotor-slot harmonics (the increase in the magnitude of the rotor-slot harmonics was only 2 dB in full-load motor operation, in comparison with healthy operation, and smaller for lower loadings). From the simulations, it was not possible to analyse such modifications, since in healthy operation the signal captured by this coil is ideally zero. Slightly higher modifications (3-5 dB) are to be found for the experimental implemented static eccentricity, irrespective of the motor loading, while from the simulations such modifications could not be analysed, since in healthy operation the signal captured by this coil is ideally zero. However, one may not confidently rely on such modifications to claim the ability to detect a static eccentricity, since such modifications are common to other faults/asymmetries (i.e. turn-to-turn short circuit in the stator winding). In the high-frequency range, the experimental implemented bearing fault was very poorly reflected in the rotor-slot harmonics, increasing their magnitudes by around only 2 dB only at half-load in comparison with healthy operation.

Search coil "p+1". From the measurements, the static eccentricity is clearly revealed in the information provided by the changes in the magnitude of the following frequency components in comparison with healthy operation:
- fundamental: increments between 11-14 dB,
- 3rd harmonic: increments between 2-10 dB,
- rotor-slot harmonics: increments between 5-15 dB (irrespective of the loading)

Search coil "p-1". Relying on the measurements, the static eccentricity is clearly revealed in the information provided by the changes in the magnitude of the following frequency components in comparison with the healthy operation:
- fundamental: increments of around 15 dB (irrespective of the loading),
- 3rd harmonic: increments between 10-20 dB (getting higher at lower loads),
- rotor-slot harmonics: increments between 4-6 dB (irrespective of the loading).

It was not possible to detect a bearing fault from the "p±1" search coils, since only a small change in the magnitude of the rotor-slot harmonics (increment of 2-3 dB) in comparison with healthy operation was found. Moreover, such minor changes in the magnitude of the rotor-slot harmonics were also found for other types of faults, and therefore, such an indication is not even suitable for achieving discrimination between them.

Search coil wound around the shaft. A search coil purposely intended to sense the axial flux was found to be able to indicate a fault in the bearing, this being the clearest means to observe a signature produced by this fault. However, this signature was found to be almost similar to the one obtained from the static eccentricity, which, in terms of the appearance of new frequency components, was also invisible in the indications of the search coils previously mentioned. In the high-frequency range, the bearing fault was relatively more clearly reflected in the indications provided by this search coil; an increment of around 10 dB in the magnitude of the rotor-slot harmonics at full load seems to be more important than the similar modifications produced by the same fault and by various faults in other search coil indications. For the half-load and no load, the same modifications were about 7 and 4 dB, respectively.

The static eccentricity was also reflected in the rotor-slot harmonics, increasing their magnitudes by 8-10 dB in full-load motor operation in comparison with healthy operation. For the half-load and no-load motor operating points, these indications decrease to levels of 4 and 3 dB, respectively.

Search coil placed externally at the non-drive end of the motor. This search coil was not able to sense the cases of static eccentricity and bearing fault. Potential indicators about these faults, if there were any, were very small and were probably covered by the noise floor. However, even with this poor performance in detecting static eccentricity and a bearing fault, such an external search coil is able to indicate the dynamic eccentricity even from measurements at no load.

5.4. Core fault

The study of the stator winding currents and branch currents does not provide any useful sign of the core faults under study in any of the stator winding configurations that were investigated.

Electromagnetic flux monitoring

Since, in the simulations, the test motor is considered to be perfect symmetrical, in healthy operation the only non-zero indications are provided by the search coil around a stator tooth. The indications provided by this coil for the healthy condition remain unchanged, irrespective of both the various stator winding configurations that were studied and the core faults that were implemented. The same findings were also found to be valid for the search coil placed around two pole pitches of the test motor.

The only signs found to be suitable for the detection of such types of fault were the ones provided by the search coils "p-1" and "p+1". However, the indications provided by these search coils do not show important changes for the various degrees of the faults that were studied (core fault "cf" 1-9; see Figs. 4.2-4.3).

Fig. 5.4.1 presents the time-domain representation of the voltages induced in the "p-1" and "p+1" search coils in motor operation with the most severe core fault that was studied.
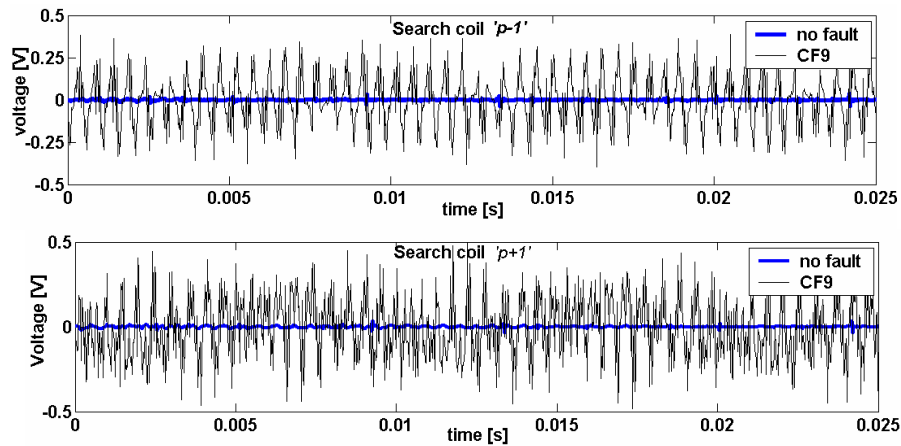
Fig. 5.4.1 Time-domain representation of the voltages induced in the "p-1" (top) and "p+1" (bottom) search coils in motor operation with a core fault – simulations.

Next, the possibility of sensing core fault in each of the winding configurations that were studied is presented.

Stator winding configuration of type "4B"

This fault is not characterised by any new characteristic fault frequency sidebands. The magnitude of the fundamental frequency, which decreases with the progress of the fault degree, is the only sign of a core fault problem.

Table 5.4.1 Modifications in the magnitudes of the fundamental frequency captured by search coil "p-1" (left) and "p+1" (right).

cf1/cf9	cf1/cf6	cf1/cf3	cf1/cf9	cf1/cf6	cf1/cf3
1.85	1.4	1.1	0.3	-	-

Stator winding configuration of type "2B"

No considerable change in the magnitude of the fundamental component was found for the motor equipped with a stator winding consisting of two parallel branches.

Table 5.4.2 Modifications in the magnitudes of the fundamental frequency captured by the search coils "p-1" (left) and "p+1" (right).

cf1/cf9	cf1/cf6	cf1/cf3	cf1/cf9	cf1/cf6	cf1/cf3
1.1	-	-	0.3	-	-

Stator winding configuration of types "SB" and "NB"

Table 5.4.3 Modifications in the magnitudes of the fundamental frequency captured by the search coils "p-1" (left) and "p+1" (right) – winding configuration of "SB" type.

cf1/cf9	cf1/cf6	cf1/cf3	cf1/cf9	cf1/cf6	cf1/cf3
2	1.4	-	0.28	0.8	-

Table 5.4.4 Modifications in the magnitudes of the fundamental frequency captured by the search coils "p-1" (left) and "p+1" (right) – winding configuration of "NB" type.

cf1/cf9	cf1/cf6	cf1/cf3	cf1/cf9	cf1/cf6	cf1/cf3
2	1.3	-	0.31	0.75	-

Some new frequency sideband components are found at the frequencies of 50 Hz and 150 Hz, respectively. Their magnitudes with reference to the one at the fundamental frequency are represented in Table 5.4.5. New sideband components at these frequencies were also found as a result of the simulated inter-turn short circuit in the stator winding.

Table 5.4.5 Magnitudes of the frequency components considered potential fault indicators for the detection of core fault [dB].

"p-1" "NB"			"p+1" "NB"	
f [Hz]	50	150	*f* [Hz]	150
cf 6	-20	-23	cf 6	-16
cf 9	-14	-15	cf 9	-18

"p-1" "SB"			"p+1" "SB"	
f [Hz]	50	150	*f* [Hz]	150
cf 6	-24	-19	cf 6	-14
cf 9	-13	-13	cf 9	-17

6. FINAL DISCUSSION

This section is intended to gather and concentrate all the important conclusions presented at the end of each subsection dealing with the analysis of the experimental and simulated data. In this respect, the reader should expect from this section a more qualitative critical analysis rather than a quantitative one.

First of all, the ability of the phase current to detect specific faults was tested, since monitoring this parameter is the most convenient and cheapest way to sense a fault.

In principle, any rotor cage-related fault is clearly seen from stator currents when checking the specific sideband frequency components extracted from the well-known equations presented in the literature.

As observed from both the measurements and simulations, a turn-to-turn short circuit in the stator winding was best reflected in the unbalance of the stator winding phase currents and in the rise in magnitude of some frequency components which already exist in the line current spectra of a healthy motor.

Relying on both experiments and simulations, this work concludes that the static eccentricity does not bring about any major distortion in the spectral content of the branch current. A similar conclusion was found for the experimentally implemented bearing and core fault, respectively.

Since the stator winding phase of the test induction motor consists of two half-phases (branches) connected in parallel and these phases are accessible from outside the motor, the analysis of the differential circulating current between the half-phases was performed with the purpose of fault detection. The measured and simulated waveforms of the circulating currents between stator winding parallel branches for healthy machine operation and for the faults under study were presented. It was observed that a major rotor fault (such as 3 broken rotor bars), a stator-related fault (such as a turn-to-turn short circuit), and the dynamic eccentricity can clearly be seen by monitoring the circulating currents. However, by relying only on the indications provided by the circulating current, it appears difficult to discriminate between various fault conditions. Moreover, the cases of static eccentricity and bearing fault are not possible to detect as abnormal conditions on the sole basis of monitoring only the magnitudes of the circulating currents. Taking into account the drawbacks characteristic of a monitoring method relying on the stator current, it was further proceeded to study the ability of the electromagnetic fluxes captured in various motor locations to sense the same faults.

From the measurements, it was found that the indications provided by the search coil purposely intended to sense the electromagnetic flux around a stator tooth are not of much use when aiming to detect a stator winding fault. The inability of the information provided by this search coil refers both to the absence of new frequency sideband components characteristic of a stator fault and to major changes in the magnitude of the frequency components produced by the slotting.

However, an external coil over two pole pitches may provide more useful information about the inter-turn short circuit, giving an increment in the fundamental frequency of about 3 and 5 times in half load and no load testing.

When aiming to detect a stator winding fault, the search coils purposely intended to sense the air-gap harmonics of the order "$p\pm1$" provided richer information about this fault, in comparison with the other search coils implemented in the simulations. A "p-1" search coil is useful in that it is able to detect important changes in the magnitudes of the 3rd, 5th, and rotor-

slot harmonics, while the "$p+1$" search coil is able to sense important changes in the magnitude evolution of the fundamental frequency. Such important changes in the magnitude of the fundamental frequency were also found in those search coils implemented only in the measurements: around the shaft and at the non-drive end.

From the simulations it was important to notice that new characteristic fault sideband frequency components are introduced by the stator winding configurations "NB" and "SB" during the inter-turn short circuit. Unfortunately, none of these winding configurations was studied experimentally in order to validate this effect. Usually, a motor equipped with an "SB" type stator winding configuration is observed to be more sensitive to the inter-turn short circuit than one equipped with an "NB" configuration.

A rotor cage-related fault is the most easily detected abnormality in an induction motor and it was no surprise to find out that all of the search coils that were studied were found to be able to provide useful information about such faults. A good agreement between the data obtained from the measurements and simulations was found. This agreement is in terms of the new characteristic fault frequency sideband components produced by a rotor cage fault.

For a rotor-cage related fault, the richness of the information provided by the search coils that were studied is proportional to the loading level at which the test motor is operated. At a no-load operation, for instance, important signs of the cage fault are lost and the motor condition may become difficult to assess.

A search coil wound around the shaft and purposely intended to sense the axial flux was able to indicate a fault in the bearing and it appeared that this was the clearest means to observe a modification introduced by this fault. However, this signature is almost similar to the one obtained from the static eccentricity.

In terms of new frequency sideband components produced by a static eccentricity, the search coil around the shaft is the only one to sense such modifications. The static eccentricity is reflected in the indications of the "$p+1$" and "$p-1$" search coil only by increments in the magnitudes of specific frequency sideband components. The search coils around the stator tooth and over two pole pitches are of no great use when trying to sense a static eccentricity.

A search coil placed externally at the non-drive end of the motor is able to indicate the dynamic eccentricity even from measurements at no load, but is not able to sense cases of static eccentricity and bearing fault.

The case of dynamic eccentricity is detected without any difficulty, irrespective of the motor loading, by all of the search coils that were studied. It is important to notice that for lower levels of motor loading, the magnitude of these frequency components is higher.

A comparative analysis between the measurements and simulations for the case of dynamic eccentricity points out a good agreement in terms of predicted and measured new frequency sideband components responsible for the detection of this asymmetry (excepting the case of the "$p+1$" search coil).

The study of the stator winding currents and branch currents does not provide any useful sign for the case of a core fault in any of the stator winding configurations that were investigated. The only signs found suitable for the detection of such types of fault were the ones provided by the search coils "$p-1$" and "$p+1$". However, the indications provided by these search coils do not show important changes for the various degrees of the faults under study. Unfortunately, no measurements with an artificially implemented core fault are available in order to validate these claims.

An interesting conclusion drawn from the simulations is that for a motor equipped with a stator winding of the "NB" or "SB" type, all of the faults under study were reflected in a similar way in the indications provided by various fault indicators. It is important to notice this, since these configurations are different ("NB" stator winding consisting of no parallel branches, "SB" stator winding consisting of two parallel branches, but with a special configuration - see Appendix II). Therefore, it is concluded that not only the number of parallel branches but also the internal connections of the winding affects the fault indications.

Table 6.1 presents a summary of the results concerning the suitability of each of the fault detection methods that were studied for the detection of specific faults. This table is purposely intended, mainly, to offer a general view of those faults that are difficult to detect and/or need special attention because of this.

The criteria used for ranking a method are not general for all of the cases and the reader is recommended to carefully address each of the previous chapters for a clearer understanding of those given here. For example, in the case of the inter-turn short circuit in the stator winding, the phase branch current was ranked as a good fault indicator considering the unbalance introduced by such a fault to the branch currents. The increase in the amplitudes of the specific frequency sideband component of the branch current was also considered an important symptom for ranking this parameter as a good fault indicator. On the other hand, when ranking the phase current as a good fault indicator for a rotor cage fault, the presence of new frequency components in its spectrum was relied on.

When claiming that a parameter offers poor/ambiguous information about a fault, the possibility of finding similar indications for other faults is considered. However, this type of classification was also used for the case of the core fault in order to distinguish between the richness of the information provided by the "$p\pm1$" search coils for various stator winding configurations.

In addition, Table 6.1 is intended to offer a starting point and some suggestions for further work on various issues such as:

- investigations to be carried out using 3D simulation tools, thus making it possible to take advantage of the important fault signatures (as observed from the measurements), provided by the electromagnetic fluxes circulating along the axial direction of the machine,
- experimental implementation of the core faults and the subsequent measurements for verifying the findings obtained from the simulations.

Important advances to this thesis may also be found in the investigations of other cage induction machines and, finally, different machine types. Such an investigation would allow some general conclusions to be drawn that would be of great help for the industry, which is always interested in having a generalised strategy for the condition monitoring and fault diagnosis of various types of electrical machines.

A challenging task for future research would be, for example, the study of rotor faults in permanent magnet machines, since it was found that such research is very rare and such studies are essential nowadays because of the increasing interest in the use of permanent magnet machines.

Table 6.1. Faults versus recommended methods for detecting faults – summary.

Studied faults / Fault detection methods		phase current	circulating current	Search coil locations for sensing the electromagnetic fluxes					
				stator tooth	2 pole pitches	shaft	non-drive end	"p+1"	"p-1"
Inter-turn short circuit in stator winding	Simul. NB		-						
	Simul. SB					-	-		
	Simul. 4B								
	Simul. 2B								
	Meas.								
Rotor-cage related faults	Simul. NB		-						
	Simul. SB					-	-		
	Simul. 4B								
	Simul. 2B								
	Meas.								
Dynamic eccentricity	Simul. NB		-						
	Simul. SB					-	-		
	Simul. 4B								
	Simul. 2B								
	Meas.								
Static eccentricity	Simul. NB		-						
	Simul. SB					-	-		
	Simul. 4B								
	Simul. 2B								
	Meas.								
Bearing fault	Simul.	-	-	-	-	-	-	-	-
	Meas.								
Core fault	Simul. NB								
	Simul. SB					-	-		
	Simul. 4B								
	Simul. 2B								
	Meas.	-	-	-	-	-	-	-	-

Legend:

□ Inability to detect fault   ░ Poor/ambiguous fault information   ■ Good ability to detect fault   - Not available

7 CONCLUSIONS

This research work was mainly concerned with the analysis of the electromagnetic flux patterns supposed to contain potential useful information about a fault in a cage induction machine. Other electrical parameters used for fault detection such as stator phase current and circulating currents between the parallel branches of the stator winding, were used as comparative means to asses the usefulness of this parameter in fault detection.

The relevant fault signatures of the electrical parameters that were studied were mostly derived both from the measurements and from numerical electromagnetic field simulations in a steady state.

When and where possible, the accuracy of different fault signatures derived from numerical electromagnetic field simulations was verified by experiments. For fault detection purposes, the interest was focused more on qualitative than exact quantitative results, i.e. more focused on finding how the monitored parameter behaves as a function of time and not so much in magnitude. In this respect, despite various differences in the magnitudes of some simulated and measured parameters, the agreement between the measurements and simulations was considered as "good" in terms of the ability to detect fault characteristic frequency components introduced by specific faults.

A rotor cage-related fault is the most easily detected abnormality in an induction motor and it was no surprise to find out that by monitoring both the stator current and electromagnetic flux at all the search coil locations one may obtain useful information about such faults. For a rotor-cage related fault, the richness of the information provided by the search coils that were studied is proportional to the loading level at which the test motor is operated.

A turn-to-turn short circuit in the stator winding was best reflected in the unbalance of the stator winding phase currents. In terms of characteristic fault frequency components, observed from the experiments, a turn-to-turn short circuit in the stator winding was reflected only in a rise in magnitude of a few frequency components already present in the line current spectra of a healthy motor. The search coils purposely intended to capture the harmonics of the order "$p\pm1$" provide more useful information about a stator winding fault. No useful information about static eccentricity and bearing faults was found in the stator current.

It was observed that a major rotor fault (such as a rotor bar breakage), a stator-related fault (such as a turn-to-turn short circuit), and the dynamic eccentricity are clearly seen by monitoring the circulating currents but such information is not good enough to discriminate between various fault conditions. Moreover, it is not possible to detect the cases of static eccentricity and bearing fault as abnormal conditions on the sole basis of monitoring the magnitudes of the circulating currents.

The usefulness of the search coils purposely intended to capture the harmonics of the order "$p\pm1$" may be found especially when trying to detect static and dynamic eccentricities. However, the information provided by these coils is of no great significance when trying to detect a bearing fault. A search coil intended to sense the axial flux and wound around the shaft was found to be the only means to provide a relatively clear modification because of this fault. However, the fault signatures provided by this coil are found to be almost similar to the ones produced by the static eccentricity.

The case of dynamic eccentricity was also detected without any difficulty, irrespective of the motor loading, by all the fault indicators that were studied. Moreover, for lower levels of motor loading, the magnitude of the frequency components responsible for the detection of

such asymmetries is higher. This is in contrast with the case of the other faults studied, excepting the inter-turn short circuit, where when the motor was operated at lower loadings the sensitivity of the fault detection procedure diminished.

The study of the stator winding currents and branch currents does not provide any useful signs in the case of a core fault in any of the stator winding configurations investigated. The only signs found suitable for the detection of such types of fault were the ones provided by the search coils "p-1" and "p+1". However, the indications provided by these search coils do not show important changes in the various degrees of the faults being studied.

The experimental and computational research contained in this thesis was carried out only for a cage induction machine of 35 kW but, for some faults common to other types of electrical machines, such as inter-turn short circuits in the stator winding, bearing faults, and various types of eccentricity, it is possible to generalise these results. However, this thesis also contains a few references concerning the use of the fault indicators under study for other types of motor and their specific faults.

Finite element analysis was found, according to the initial expectations, to be a flexible tool when studying faulty machines, as practically all the electromagnetic faults could be analysed using the same basic tool.

Other advances that could be made on the basis of this work lie mainly in the area of the experimental validation of those findings concerning the various effects that a stator winding may have on the ability of various indicators to detect faults. The experimental implementation of the core fault and verification of the claims obtained from the simulations may provide the industrial environment with a new and efficient means of monitoring core conditions.

ASSESMENT ON THE MATTER OF ACHIEVING THE INITIAL OBJECTIVES OF THE THESIS

At the very end, it may be claimed that most of the research objectives set in the beginning of the research were achieved. Especially, the electromagnetic flux was found able to provide precious information about possible means to detect all of the faults under study; this was not always the case with the stator current.

When and where possible, the accuracy of different fault signatures issuing from numerical electromagnetic field simulations was validated by experiments. However, due to the constraints imposed by the software (lack of a 3D simulation tool) and by the lack of test motors equipped with various stator winding configurations, the validation procedure could not be fully completed. This procedure represents a challenging task for a further work.

I believe that:

- the wide variety of the electrical parameters that were studied purposely intended to detect various faults;
- the study on the ability of the electromagnetic flux eccentricity harmonics of order "p±1" for detecting faults other than various types of eccentricity, and,
- the comparative analysis of the multitude of results provided by measurements and by a specific time-stepping finite element approach that allows an unlimited access to the physical quantities from the test machine,

will give the reader the impression of something new in the broad field of fault diagnosis and condition monitoring for electrical machines.

References

Anderson, A., 'A note on generator core failures'. Available on web at: http://www.antony-anderson.com/failure1.htm.

Arkkio, A., 1987, 'Analysis of induction motors based on the numerical solution of the magnetic field and circuit equations', Helsinki, *Acta Polytechnica Scandinavica, Electrical Engineering Series No. 59*, ISBN 951-666-250-1, 97 p. Available on web at: http://lib.hut.fi/Diss/list.html#1980.

Arkkio, A., 1988, 'Time stepping finite element analysis of induction motors', *8th International Conference on Electrical Machines–ICEM '88*, Pisa, Italy, Sept. 12-14, 1998, pp. 275-281.

Arkkio, A., 1996, 'Unbalanced magnetic pull in cage induction motors–dynamic and static eccentricity', *12th International Conference on Electrical Machines–ICEM'96*, Vigo, Spain, Sept. 10-12, 1996, pp. 192-197.

Arkkio A., Anttila, M., Pokki, K., Lantto, E., 2000, 'Electromagnetic force on a whirling cage rotor', *IEE Proceedings Electrical Power Applications*, Vol. 147, No. 5, pp. 353-360.

Assaf, T., Henao, H., Capolino, G.-A., 2004, 'Simplified axial flux spectrum method to detect incipient stator inter-turn short-circuits in induction machine', *IEEE International Symposium on Industrial Electronics*, May 4-7, 2004, Vol. 2, pp. 815-819.

Barbour, A., Thomson, W.T., 1997, 'Finite element study of rotor slot designs with respect to the current monitoring for detecting static airgap eccentricity in squirrel-cage induction motor', *The 1997 IEEE Industry Applications Society Conference: The 32nd IAS Annual Meeting,* New Orleans, Louisiana, Oct. 5-8, 1997, pp. 112-119.

Barker, S., 2000, 'Avoiding premature bearing failure with inverter fed induction motors', *Power Engineering Journal*, Vol. 14, Issue 4, pp. 182-189.

Bellini, A., Filippetti, F., Franceschini, G., Tassoni, C., Kliman, G.B., 2000, 'Quantitative evaluation of induction motor broken bars by means of electrical signature analysis', *The 2000 IEEE Industry Applications Society Conference: The 35th IAS Annual Meeting*, Rome, Italy, Oct. 8-12, 2000, Vol. 1, pp. 484-491.

Benbouzid, M.E.H., Vieira, M., Theys, C., 1999, 'Induction motors faults detection and localisation using stator current advanced signal processing techniques', *IEEE Transactions on Power Electronics,* Vol. 14, Issue 1, pp. 14-22.

Benbouzid, M.E.H., 1999, 'Bibliography on induction motors faults detection and diagnosis', *IEEE Transactions on Energy Conversion*, Vol. 14, Issue 4, pp.1065-1074.

Benbouzid, M. E. H., 2000, 'A review of induction motors signature analysis as a medium for faults detection', *IEEE Transactions on Industrial Electronics*, Vol. 47, Issue 5, pp. 984-993.

Benbouzid, M. E. H., Kliman, G. B., 2003, 'What stator current processing-based technique to use for induction motor rotor faults diagnosis ?', *IEEE Transactions on Energy Conversion*, Vol. 18, No. 2, pp.238-244.

Berman, M., Erlicki, M.S., 1991, 'Behaviour of an induction motor with equalizing connections in the stator winding', *Proceedings of the 17th Convention of Electrical and Electronics Engineers in Israel*, March 5-7, 1991, pp. 324-327.

Binns, K.J., Lawrenson, P.J., Trowbridge, C.W., 1992, '*The analytical and numerical solution of electric and magnetic fields*', John Wiley & Sons Publishers, 1992, ISBN: 0-471-92460-1, 486 p.

Bowers, S.V., Piety, K.R., 2001, 'Proactive motor monitoring through temperature, shaft current and magnetic flux measurements', Emerson Process Management–CSI. Available on web at: http://www.compsys.com.

Burnett, T., 2002 'Principles of flux diagnostics', Emerson Process Management–CSI MotorView. Available on web at: http://www.compsys.com/.

Burnett, R., Watson, J. F., Elder, S., 1995, 'The application of modern signal processing techniques to rotor fault detection and location within three-phase induction motors', *Conference on Instrumentation and Measurement Technology,* Apr. 24-26, 1995, pp. 426.

Burnett, R., Watson, J.F., 1995, 'The current analysis program-a software tool for rotor fault detection in three phase induction motors', *7th International Conference on Electrical Machines and Drives* (*Conference Publication No. 412*), Durham, UK, Sept. 11-13, 1995, pp. 156-160.

Busse, D.F., Erdman, J.M., Kerkman, R.J., Schlegel, D.W., Skibinski, G.L., 1997, 'An evaluation of the electrostatic shielded induction motor: a solution for rotor shaft voltage buildup and bearing current', *IEEE Transactions on Industry Applications*, Vol. 33, Issue 6, pp. 1563-1570.

Cameron, J.R., Thomson, W.T., Dow, A.B., 1986, 'Vibration and current monitoring for detecting air-gap eccentricity in large induction motors', *IEE Proceedings*, Vol. 133, pt. B, No. 3, May, pp. 155-163.

Cardoso, A.J.M., Saraiva, E.S., 1993, 'Computer-aided detection of air-gap eccentricity in operating three-phase induction motors by Park's Vector Approach', *IEEE Transactions on Industry Applications*, Vol. 29, No. 5, pp. 897-901.

Cardoso, A.J.M., Cruz, S.M.A., Fonseca, D.S.B., 1997, 'Inter-turn stator winding fault diagnosis in three-phase induction motors by Park's Vector approach', *IEEE International Electric Machines and Drives Conference─IEMDC '97*, Milwaukee-WI, USA, May 18-21, 1997, pp. MB1/5.1-MB1/5.3

Chari, M.V.K., Silvester, P., 1971, 'Finite element analysis of magnetically saturated d.c machines', *IEEE Transactions*, PAS-90, pp. 2362-2368.

Chari, M.V.K., Konrad, A., Palmo, M.A., Angelo, J.D., 1982, 'Three dimensional vector potential analysis for machine field problems', *IEEE Transactions on Magnetics*, Vol. MAG-18, No. 2, pp. 436-446.

Chow, M.-Y.; Sharpe, R.N.; Hung, J.C., 1993, 'On the application and design of artificial neural networks for motor fault detection', *IEEE Transactions on Industrial Electronics,* Vol. 40, Issue 2, pp. 181-188.

Chow, T.W.S., 1996, 'Condition monitoring of electric machines using third-order spectrum analysis', *The 1996 IEEE Industry Applications Society Conference: The 31st IAS Annual Meeting*, San Diego-CA, USA, Oct. 6-10, 1996, Vol. 1, pp. 679-686.

Chow, M-Y., 2000, 'Guest editorial special section on motor fault detection and diagnosis' *IEEE Transactions on Industrial Electronics*, Vol. 47, issue 5, pp. 982-983.

Clough, R., 1960, 'Finite elements in plane stress analysis', *Proceedings of the 2nd Conference on Electronic Computation*, ASCE, 1960.

Connolly, H.M., Lodge, L., Jackson, R.J., Roberts, I., 1985, 'Detection of inter-turns short-circuits in generator rotor windings using air-gap search coils', *Conference on Electrical Machines Design and Applications*, 1985, pp. 11-15.

Coulomb, J. L., 1983, 'A methodology for the determination of global electromechanical quantities from the finite element analysis and its application to the evaluation of magnetic forces, torques and stiffness', *IEEE Transactions on Magnetics*, Vol. 19, Issue 6, pp. 2514-2519.

Courant, R., 1943, 'Vibrational method for the solution of problems of equilibrium and vibrations', *Bulletin of the American Mathematical Society*, Vol. 49.

Crawford, D. E., 1975, 'A mechanism of motor failures', *12th IEEE Electrical and Electronics Insulation Conference*, Institute of Electrical and Electronics Engineers, Inc., New York, NY, pp. 126-129.

Cruz, S.M.A., Cardoso, A.J.M., 2004, 'Diagnosis of stator inter-turn short circuits in DTC induction motor drives', *IEEE Transactions on Industry Applications*, Vol. 40, Issue 5, pp. 1349-1360.

Deleroi W., 1982, 'Squirrel cage motor with broken bar in the rotor - physical phenomena and their experimental assessment', *5ᵗʰ International Conference on Electrical Machines–ICEM '82*, Budapest, Hungary, 1982, pp. 767-770.

Dorrell, D. G., 1993a, '*Calculation of unbalanced magnetic pull in cage inductlon machines*', Ph.D. Dissertation, University of Cambridge, U.K, 1993.

Dorrell, D. G., 1993b, ,The effects of dynamic rotor eccentricity in cage induction motors', in *Proceedings UPEC'94,* University College Galway, Galway, Ireland, 1994, pp. 402-405.

Dorrell, D.G., Thomson, W.T., Roach, S., 1995,' Combined effects of static and dynamic eccentricity on airgap flux waves and the application of current monitoring to detect dynamic eccentricity in 3-phase induction motors', *7ᵗʰ International Conference on Electrical Machines and Drives Conference –EMD '95*, Durham, U.K, Sept. 11-13, 1995, pp. 151-155.

Dorrell, D.G. , Thomson, W.T., Roach, S., 1997, 'Analysis of airgap flux, current, vibration signals as a function of the combination of static and dynamic eccentricity in 3-phase induction motors', *IEEE Transactions on Industry Applications,* Vol. 33, No. 1, pp. 24-34.

Douglas, H., Pillay, P., Ziarani, A.K., 2005, 'Broken rotor bar detection in induction machines with transient operating speeds', *IEEE Transactions on Energy Conversion*, Vol. 20, Issue 1, pp. 135-141.

Driesen, J., 2000, 'Coupled electromagnetic-thermal problems in electrical energy transducers', Doctoral Thesis, Leuven, May, 2000, 216 p.

Duque, O., Pérez, M., Moríñigo, D., 2004, 'Practical application of the spectral analysis of line current for the detection of mixed eccentricity in cage induction motors fed by frequency converter', *16ᵗʰ International Conference on Electrical Machines–ICEM '04*, Sept. 5-8, 2004, Krakow, Poland. Available on CD, No. 444, 6 p.

Elder, S., Watson, J.F., Thomson, W.T., 1989, 'Fault detection in induction motors as a result of transient analysis', *4ᵗʰ International Conference on Electrical Machines and Drives*, London, UK, Sept. 13-15, 1989, Vol. 1, pp. 182-186.

EPRI, 1982, 'Improved Motors for Utility Applications', *Publication EL-2678*, Vol. 1, 1763-1, final report, October, 1982.

Elkasabgy, N.M., Eastham, A.R., Dawson, G.E., 1992, 'Detection of broken bars in the cage rotor on an induction machine', *IEEE Transactions. on Industry Applications*, Vol. IA-22, No. 6, pp. 165-171.

Filippetti, F., Franceschini, G., Tassoni, C., Vas, P., 1996, 'AI techniques in induction machines diagnosis including the speed ripple effect', *The 1996 IEEE Industry Applications Society Conference: The 31ˢᵗ IAS Annual Meeting*, San Diego, Oct. 6–10, 1996, pp. 655-662.

Filippetti, F., Grellet, G., Salles, G., Franceschini, G., Tassoni, C., 1998, '**Monitoring of induction machines load torque disturbances: an alternative NN-based method**', *The 1998 IEEE Industry Applications Society Conference: The 33ʳᵈ IAS Annual Meeting*, St. Louis-MO, USA, Oct. 12-16, 1998, pp. 103-110.

Filippetti, F., Franceschini, G., Gentile, G.*,* Meo, S., Ometto, A., Rotondale, N., Tassoni, C., 1999, '1989-1998: State of art of model based diagnostic procedures for induction machines stator inter-turn short circuits', *IEEE lnternational Symposium on Diagnostics for Electrical Machines, Power Electronics and Drives - SDEMPED*, Gijon, Spain, Sept. l-3, 1999, pp 19-31.

Filippetti, F., Gentile, G.*,* Meo, S., Ometto, A. and Rotondale, N., 2000a, 'High order current spectral components utilisation to improve induction machine diagnostics', *14ᵗʰ International Conference on Electrical Machines—ICEM 2000*, Helsinki, Finland, Aug. 28-30, 2000, pp. 941-945.

Filippetti, F., Franceschini, G., Tassoni, C., Vas, P., 2000b, 'Recent developments of induction motor drives fault diagnosis using AI techniques', *IEEE Transactions on Industrial Electronics*, Vol. 47, Issue 5, pp. 994-1004.

Filippetti, F., Franceschini, G., Tassoni, C., 2005, 'Neural networks aided on-line diagnostics of induction motor rotor faults', *IEEE Transactions on Industry Applications*, Vol. 31, Issue 4, pp. 892-899.

Foggia, A., Torlay, J-E., Corenwinder, C., Audoli, A., Herigault, J.,1999, 'Circulating current analysis in the parallel-connected windings of synchronous generators under abnormal operating conditions', *International Conference on Electric Machines and Drives–IEMDC '99*, Seattle-WA, USA, May 9-12, pp. 634-636.

Früchtenicht, J., Jordan, H., Seinch, H., 1982, 'Exzentnzitätsfelder als Urache von Laufinstabilitäten bei Asynchronmachinen', Parts 1 and 2, *Arkiv fur Electroteknik*, Vol. 65, pp. 271-292.

Gaylard, A., Meyer, A., Landy, C., 1995, 'Acoustic evaluation of faults in electrical machines', *7th International Conference on Electrical Machines and Drives*, Durham, UK, Sept. 11-13, pp. 147-150.

Gentile, G., Meo, S., Ometto, A., 2003, 'Induction motor current signature analysis to diagnostics, of stator short circuits', *4th IEEE International Symposium on Diagnostics for Electric Machines, Power Electronics and Drives–SDEMPED '03*, Atlanta-GA, USA, Aug. 24-26, 2003, pp. 47-51.

Green, V., Sasic, M., Wright, B., 2005, 'Summary of industry practices, guides and standards related to on-line partial discharge monitoring of stator insulation condition', *Industry Applications Society 52nd Annual Petroleum and Chemical Industry Conference*, Sept. 12-14, pp. 359-365.

Hargis, C., Gaydon, B. G., Kamish, K., 1982, 'The detection of rotor defects in induction motors', *Proceedings IEE - EMDA Conference*, London, 1982, pp. 216-220.

Henao, H. Demian, C. Capolino, G.-A., 2003, 'A frequency-domain detection of stator winding faults in induction machines using an external flux sensor', *IEEE Transactions on Industry Applications*, Vol. 39 , Issue 5, pp. 1272-1279.

Henao, H. Martis, C. Capolino, G.-A., 2004, 'An equivalent internal circuit of the induction machine for advanced spectral analysis', *IEEE Transactions on Industry Applications*, Vol. 40, Issue 3, pp. 726-734.

Hirvonen, R., 1994, 'On-line condition monitoring of defects in squirrel cage motor', *11th International Conference on Electrical Machines–ICEM '94*, Paris, France, Vol.2, pp. 267-272.

Hsu, J.S., 1995, 'Monitoring of defects in induction motors through air-gap torque observation', *IEEE Transactions on Industry Applications*, Vol. 31, Issue 5, pp. 1016-1021.

Huang, X., Habetler, T.G.; Harley, R.G., 2004, 'Detection of rotor eccentricity faults in closed-loop drive-connected induction motors using an artificial neural network', *IEEE 35th Annual Power Electronics Specialists Conference–PESC*, Aachen, Germany, June 20-25, Vol. 2, pp. 913-918.

IEEE, 1985, 'Motor reliability working group. Report of large motor reliability survey of industrial and commercial installations', *IEEE Transactions on Industry Applications*, 1985, 1A. (4), Part I & II.

IEEE, 1994, 'IEEE recommended practice for instrumentation: specifications for magnetic flux density and electric field strength meters-10 Hz to 3 kHz', *IEEE Std. 1308-1994*.

IEEE, 2004, 'IEEE standard test procedure for polyphase induction motors and generators', *Electric Machinery Committee of the IEEE Power Engineering Society, IEEE Std. 112-2004* (Revision of IEEE Std 112-1996), 2004.

Jianming, J., 1993, '*The finite element method in electromagnetics*', Wiley, New York, 1993, ISBN: 0-471-43818-9, 784 p.

Joksimovic, G.M., Penman, J., 2000, 'The detection of inter-turn short circuits in the stator windings of operating motors', *IEEE Transactions on Industrial Electronics*, Vol. 47 , Issue 5 , pp. 1078-1084.

Joksimovic, G.M., Durovic, M.D., Penman, J., Arthur, N., 2000, 'Dynamic simulation of dynamic eccentricity in induction machines-finding function approach', *IEEE Transactions on Energy Conversion*, Vol. 15, Issue 2, pp. 143-148.

Jover Rodriguez, P., Arkkio, A., 2003, 'Induction motor stator fault detection using fuzzy logic', *International Conference on Circuits, Signal and Systems–IASTED ' 03*, Cancún, Mexico, May 19-21, 2003, pp. 96-100.

Karmaker, H.C., 2003, 'Broken damper bar detection studies using flux probe measurements and time-stepping finite element analysis for salient-pole synchronous machines', *4th IEEE International Symposium on Diagnostics for Electric Machines, Power Electronics and Drives–SDEMPED '03*, Atlanta-GA, US, Aug. 24-26, 2003, pp. 193-197.

Kerszenbaum, I., 1992, 'Shaft currents in electric machines fed by solid-state drives', *IEEE Conference on Industrial and Commercial Power Systems*, Pittsburgh-PA, USA, May 4-7, 1992, pp. 71-79.

Kim, K., Parlos, A.G., Mohan Bharadwaj, R., 2003, 'Sensorless fault diagnosis of induction motors', *IEEE Transactions on Industrial Electronics*, Vol. 50, Issue 5, pp. 1038-1051.

Kliman, G.B., Koegl, R. A., Stein, J., Endicott, R. D., Madden, M. W., 1988, 'Noninvasive detection of broken rotor bars in operating induction motors', *IEEE Transactions on Energy Conversion*, Vol. 3 Issue: 4, pp. 873-879.

Kliman, G.B., Stein, J., 1990, 'Induction motor fault detection via passive current monitoring', *9th International Conference in Electrical Machines–ICEM'90,* Boston-MA, Aug. 13-15, 1990, pp. 13-17.

Kliman, G.B., Premerlani, W. J., Koegl, R.A., Hoeweler, D., 1996, 'A new approach to on-line fault detection in ac motors', *The 1996 IEEE Industry Applications Society Conference: The 30th IAS Annual Meeting*, San Diego-CA, USA, Oct. 6-10, 1996, pp. 687-693.

Kliman, G.B., Premerlani, W.J., Yazici, B., Koegl, R.A., Mazereeuw, J., 1997, 'Sensorless, online motor diagnostics', *IEEE Computer Applications in Power*, Vol. 10, No.2, pp. 39-43.

Kliman, G.B., Sang Bin Lee, Shah, M.R., Lusted, R.M., Nair, N.K., 2004, 'A new method for synchronous generator core quality evaluation', *IEEE Transactions on Energy Conversion*, Vol. 19, Issue 3, pp. 576-582.

Kohler, J.L., Sottile, J., Trutt, F.C., 2002, 'Condition monitoring of stator windings in induction motors. I. Experimental investigation of the effective negative-sequence impedance detector', *IEEE Transactions on Industry Applications*, Vol. 38, Issue 5, pp. 1447-1453.

Kokko, V., 2003, '*Condition monitoring of squirrel-cage motors by axial magnetic flux measurements*', Doctoral thesis, Oulun Yliopisto, Oulu 2003, ISBN 951-42-6938-1, p. 157. Available on web at: http://herkules.oulu.fi/isbn9514269381.

Kral, C., Habetler, T.G., Harley, R.G., 2004, 'Detection of mechanical imbalances of induction machines without spectral analysis of time-domain signals', *IEEE Transactions on Industry Applications*, Vol. 40, Issue 4, pp. 1101-1106.

Lee, S.B., Kliman, G.B., Shah, M.R., Nair, N.K., Lusted, R.M., 2005, 'An iron core probe based inter-laminar core fault detection technique for generator stator cores', *IEEE Transactions on Energy Conversion*, Vol. 20 , Issue 2, pp. 344-351.

Legowski, S.F., Sadrul Ula, A.H.M., Trzynadlowski, A.M., 1996, 'Instantaneous power as a medium for the signature analysis of induction motors', *IEEE Transactions on Industry Applications,* Vol. 32, Issue 4, pp. 904-909.

Lenz, J.E., 1990, 'A review of magnetic sensors', *Proceedings of the IEEE*, Vol. 78, Issue 6, pp. 973-989.

Leonard R A , Thomson W. T, 1986, "Vibration and stray flux monitoring for unbalanced supply and inter-turn winding fault diagnosis in induction motors", *British Journal of NDT*, July, pp. 211-215.

Li, B., Chow, M-Y., Tipsuwan, Y., Hung, J.C., 2000, 'Neural-network-based motor rolling bearing fault diagnosis', *IEEE Transactions on Industrial Electronics*, Vol. 47, No. 5, pp. 1060-1069.

Li, J. C., Ma, J., Hwang, B., 1995, 'Bearing localized defect detection by bicoherence Analysis of Vibrations', *Journal of Engineering for Industry, American Society of Mechanical Engineers*, New York, USA, Vol. 117, No. 4, pp. 625-629.

Lindh, T., Ahola, J., Kamarainen, J. K., Kyrki, V., Partanen, J., 2003, 'Bearing damage detection based on statistical discrimination of stator current', *4th IEEE International Symposium on Diagnostics for Electric Machines, Power Electronics and Drives–SDEMPED '03*, Atlanta-GA, USA, Aug. 24-26, 2003, pp.177-181.

Liu, Z., Yin, X., Zhang, Z., Chen, D., Chen, W., 2004, 'Online rotor mixed fault diagnosis way based on spectrum analysis of instantaneous power in squirrel cage induction motors', *IEEE Transactions on Energy Conversion,* Vol. 19, Issue 3, pp. 485-490.

Malinowski, J., McCormick, J., 2002, 'AC induction motor specifications-an update on currently available procedures and options', *Conference Record of the 2002 Annual Pulp and Paper Industry Technical Conference*, Toronto-ON, Canada, June 17-21, 2002**,** pp. 181-189.

Maxwell, J. C., 1865, 'A dynamical theory of the electromagnetic field', *Philosophical Transactions of the Royal Society of London* 155, 459-512 (1865). (This article accompanied a December 8, 1864 presentation by Maxwell to the Royal Society).

McCormick, A. C., Nandi, A. K., 1999, 'Bispectral and trispectral features for machine condition diagnosis', *IEEE Proceedings of Visual Image Signal Processing*, Vol. 146, No. 5, pp. 229-234.

Melero, M.G., Cabanas, M.F., Rojas, C., Orcajo, G.A., Cano, J.M., Solares, J., 2003, 'Study of an induction motor working under stator winding inter-turn short circuit condition', *4th IEEE International Symposium on Diagnostics for Electric Machines, Power Electronics and Drives–SDEMPED '03*, Atlanta-GA, USA, Aug. 24-26, pp. 52-57.

Meireles, M.R.G., Almeida, P.E.M., Simoes, M.G., 2003, 'A comprehensive review for industrial applicability of artificial neural networks', *IEEE Transactions on Industrial Electronics*, Vol. 50, Issue 3, pp. 585-601.

Muhlhaus, J., Ward, D. M., Lodge, I., 1985, 'The detection of shorted turns in generator rotor windings by measurement of circulating stator currents', *Proceedings of the 2nd International Conference on Electrical Machines Design and Applications–EMDA '85, IEE Publications, Vol. 254*, London, pp. 100-103.

Mäki-Ontto, P., 2006, '*Modeling and reduction of shaft voltages in AC motors fed by frequency converters*', Doctoral thesis, ISBN 951-22-8141-4, p. 140. Available on web at: http://lib.tkk.fi/Diss/2006/isbn9512281414.

Nandi, S., Toliyat, H.A., Parlos, A.G., 1997, 'Performance analysis of a single phase induction motor under eccentric conditions', *The 1997 IEEE Industry Applications Society Conference: The 32nd IAS Annual Meeting*, New Orleans-LA, USA, Vol. 1, Oct. 5-9, 1997, pp. 174-181.

Nandi, S., Toliyat, H.A., 1998, 'Detection of rotor slot and other eccentricity related harmonics in a three phase induction motor with different rotor cages', *Conference Proceedings of International Conference on Power Electronic Drives and Energy Systems for Industrial Growth–PEDES '98*, Perth, Australia, Nov. 30-Dec. 3, 1998, Vol. 1, pp. 135-140.

Nandi, S., Toliyat, H.A., 1999, 'Condition monitoring and fault diagnosis of electrical machines-a review', *The 1999 IEEE Industry Applications Society Conference: The 34th IAS Annual Meeting*, Phoenix-AZ, USA, 3-7 Oct., 1999, Vol. 1, pp. 197-204.

Nandi, S., Toliyat, H.A., 2000, 'Novel frequency domain based technique to detect incipient stator inter-turn faults in induction machines', *The 2000 IEEE Industry Applications Society Conference: The 35th IAS Annual Meeting*, Rome, Italy, Vol. 1, Oct. 8-12, 2000, pp. 367- 374.

Nandi, S., Toliyat, H.A., 2002, 'Novel frequency-domain-based technique to detect stator inter-turn faults in induction machines using stator-induced voltages after switch-off', *IEEE Transactions on Industry Applications,* Vol. 38, Issue 1, pp. 101-109.

Nandi, S. Bharadwaj, R.M. Toliyat, H.A., 2002, 'Performance analysis of a three-phase induction motor under mixed eccentricity condition', *IEEE Transactions on Energy Conversion*, Vol. 17, Issue 3, pp. 392-399.

Nandi, S., Toliyat, H.A., Xiaodong Li, 2005, 'Condition monitoring and fault diagnosis of electrical motors-a review', *IEEE Transactions on Energy Conversion*, Vol. 20, Issue 4, pp. 719-729.

Nattrass, D.A., 1993, 'Partial discharge. XVII. The early history of partial discharge research', *IEEE Electrical Insulation Magazine*, Vol. 9, Issue 4, pp. 27-31.

Nau, S.L., Mello, H.G.G., 2000, 'Acoustic noise in induction motors: causes and solutions', *Industry Applications Society 47th Annual Conference on Petroleum and Chemical Industry*, San Antonio-TX, USA, Sept. 11-13, pp. 253-263.

Negrea, M., Arkkio, A., Jokinen, T., Hakuli, M., 2001, 'Thermal analysis of a permanent magnet synchronous motor', *3rd IEEE International Symposium on Diagnostics for Electrical Machines, Power Electronics and Drives–SDEMPED '03*, Grado, Italy, Sept. 1-3, pp. 517-522.

Negrea, M., Pöyhönen, S., Jover, P., Arkkio, A., Hyötyniemi, H., 2002, 'Modelling, simulation and signal processing with application to electric machine fault diagnostics and condition monitoring', *Proceedings of the 7th International Conference on Modeling and Simulation of Electric Machines, Converters and Systems–ELECTRIMACS*, Montreal, Canada, Aug. 18-21, 2002, on CD, 6 p.

Negrea, M., Jover, P., Arkkio, A., 2004, **'**A comparative investigation on the reliability and accuracy of different diagnostic media when attempting to identify specific faults in an induction motor', *Symposium on Power Electronics, Electrical Drives, Automation and Motion–SPEEDAM '04*, Capri, Italy, May 16-18, 2004, pp. 809-814.

Negrea, M., Jover, P., Arkkio, A., 2005 'Electromagnetic flux-based condition monitoring for electrical machines', *5th IEEE International Symposium on Diagnostics for Electric Machines, Power Electronics and Drives–SDEMPED '05*, Wien, Austria, Sept. 7-9, 2005, on CD, 6p.

Negrea, M., Jover, P., Arkkio, 2006, 'A comparative investigation of electrical parameters for fault detection and condition monitoring in induction motors–stator winding current and electromagnetic flux', *17th International Conference on Electrical Machines–ICEM '06*, Sept. 2–5, 2006, Chania, Crete Island, Greece, on CD, 6 p.

Obaid, R.R., Habetler, T.G., Gritter, D.J., 2000, 'A simplified technique for detecting mechanical faults using stator current in small induction motors', *The 2000 IEEE Industry Applications Society Conference: The 35th IAS Annual Meeting,* Rome, Italy, Vol. 1, Oct. 8-12, 2000, pp. 479-483.

Obaid, R. R., Habetler, T. G., Stack, J. R., 2003, 'Stator current analysis for bearing damage detection in induction motors', *4th IEEE International Symposium on Diagnostics for Electric Machines, Power Electronics and Drives–SDEMPED '03*, Atlanta-GA, USA, Aug. 24-26, 2003, pp.182-187.

Obaid, R. R., Habetler, T. G., 2003, 'Effect of load on detecting mechanical faults in small induction motors', *4th IEEE International Symposium on Diagnostics for Electric Machines, Power Electronics and Drives–SDEMPED '03*, 24-26 Aug. 2003, pp. 307-311.

Ocak, H., Loparo, K. A., 2001, 'A new bearing fault detection and diagnosis scheme based on hidden Markov modeling of vibration signals', *Proceedings of IEEE International Conference on Acoustics, Speech, and Signal Processing–ICASSP '01*, Salt Lake City-UT, USA, Vol. 5, May 7-11, 2001, pp. 3141-3144.

Ong, R., Dymond, J.H., Findlay, R.D., 1997, 'Comparison of techniques for measurement of shaft currents in rotating machines', *IEEE Transactions on Energy Conversion*, Vol. 12 Issue 4, pp. 363-367.

Ong, R., Dymond, J.H., Findlay, R.D., 2000, 'Bearing damage analysis in a large oil-ring-lubricated induction machine', *IEEE Transactions on Industrial Electronics,* Vol. 47, Issue 5, pp. 1085-1091.

Parlos, A.G., Kim, K., 2001, 'Development and experimental demonstration of a model-based fault detection system for electromechanical systems', *Proceedings of the 2001 American Control Conference*, Arlington-VA, USA, June 25-27, 2001, Vol. 5, pp. 3866-3871.

Paterson, N., 1998, '*The analysis and detection of faults in three-phase induction machines using finite element techniques*', Doctoral Thesis, Robert Gordon University, Wetherby British Library, Aberdeen, UK, 180 p .

Payne, B.S., Husband, S.M., Ball, A.D., 2002, 'Development of condition monitoring techniques for a transverse flux motor', *International Conference on Power Electronics, Machines and Drives–PEMD '02 (IEE Conference Publication No. 487)*, Bath, UK, June 4-7, 2002, pp. 139-144.

Penman, J., Dey, M.N., Tait, A.J., Bryan, W.E., 1986, 'Condition monitoring of electrical drives', *IEE Proceedings*, Vol. 133, pt. B, No. 3, pp. 142-148.

Penman, J., Sedding, H. G., Lloyd, B. A., Fink, W. T., 1994. 'Detection and location of interturn short circuits in the stator windings of operating motors', *IEEE Transactions on Energy Conversion*, Vol. 9, No. 4, pp 652-658.

Penman, J., Jiang, H., 1996, 'The detection of stator and rotor winding short circuits in synchronous generators by analysing excitation current harmonics', *International Conference on Opportunities and Advances in International Electric Power Generation*, Durham, UK, Mar. 18-20, 1996, pp. 137-142.

Pöyhönen S., Negrea M., Arkkio A., Hyötyniemi H. and Koivo H., 2002a, 'Support vector classification for fault diagnostics of an electrical machine', *6th International Conference on Signal Processing–ICSP '02*, Beijing, China, Aug. 26-30, 2002, Vol. 2, pp. 1719-1722.

Pöyhönen S., Negrea M., Arkkio A., Hyötyniemi H. and Koivo H., 2002b, 'Fault diagnostics of an electrical machine with multiple support vector classifiers', *17th IEEE International Symposium on Intelligent Control–ISIC '02*, Vancouver-BC, Canada, Oct. 27-30, 2002, Vol. 1, pp. 373-378.

Pöyhönen, S., Negrea, M., Jover, P., Arkkio, A., Hyötyniemi, H., 2003,'Numerical magnetic field analysis and signal processing for fault diagnostics of electrical machines', *The International Journal for Computation and Mathematics in Electrical and Electronic Engineering–COMPEL*, Vol. 22, No. 4, pp. 969-981.

Pöyhönen, S., 2004, '*Support Vector Machine Based Classification in Condition Monitoring of Induction Motors*' Doctoral thesis, Helsinki University of Technology, ISBN: 951-22-7155-9. Available on web at: http://lib.tkk.fi/Diss/2004/isbn9512271559/

Rankin, D.R. , Wilson, I.,1995, 'The use of shaft voltage to detect air gap eccentricity and shorted turns in salient pole alternators', *7th International Conference on Electrical Machines and Drives*, 1995, Durham, UK, Sept. 11–13, 1995, pp. 194-197.

Ramirez-Nino, J., Pascacio, A., 2001, 'Detecting inter-turn short circuits in rotor windings', *IEEE Computer Applications in Power*, Vol. 14, Issue 4, pp. 39-42.

Rienstra, A., Hall, J., 2004, 'Applying acoustic vibration monitoring to predictive maintenance'. Available on web at: http://www.maintenanceworld.com/Articles/rienstraA/ultrasonic.pdf.

Rotating Electrical Machines Part 15, 1995, 'Impulse voltage withstand levels of rotating a.c. machines with form-wound stator coils', *IEC 34-15, 1995.*

Salles, G., Filippetti, F., Tassoni, C., Crellet, G., Franceschini, G., 2000, 'Monitoring of induction motor load by neural network techniques', *IEEE Transactions on Power Electronics*, Vol. 15, Issue 4, pp. 762-768.

Salon, S.J., 1995, '*Finite elements analysis of electrical machines*', Kluwer Academic Publishers, ISBN: 0792395948, 264 p.

Schoen, R.R., Lin, B.K., Habetler, T.G., Schlag, J.H., Farag, S., 1994, 'An unsupervised, on-line system for induction motor fault detection using stator current monitoring', *The 1994 IEEE Industry Applications Society Conference: The 29th IAS Annual Meeting*, Denver-CO, USA, Oct. 3-6, 1994, Vol. 1, pp.103-109.

Schoen, R.R., Habetler, T.G., Kamran, F., Bartfield, R.G., 1995, 'Motor bearing damage detection using stator current monitoring', *IEEE Transactions on Industry Applications*, Vol. 31, Issue 6, pp. 1274-1279.

Schoen, R. R., Habetler, T.G., 1995, 'Effects of time-varying loads on rotor fault detection in induction machines', *IEEE Transactions on Industry Applications*, Vol. 31, Issue 6, pp. 900-906.

Schoen, R. R, Habetler, T. G., 1997, 'Evaluation and implementation of a system to eliminate arbitrary load effect in current-based monitoring of induction machines', *IEEE Transactions on Industry Applications,* Vol. 33, No 6, pp. 1571-1577.

Silvester, P. P., Ferrari, R.L., 1996, '*Finite Elements for Electrical Engineers*', Third edition, Cambridge University Press, 1996, ISBN-13: 9780521449533, ISBN-10: 0521449537, 344 p.

Siau, J., Graff, A, Soong, W., Ertugrul, N., 2003, 'Broken bar detection in induction motors using current and flux spectral analysis', *Australasian Universities Power Engineering Conference–AUPEC2003,*, Christchurch, New Zealand, Sept. 28-Oct. 1, 2003, ISBN 0-473-09867-9. Available on web at: www.itee.uq.edu.au/~aupec/aupec03/papers/086%20Siau%20full%20paper.pdf.

Siddique, A., Yadava, G.S., Singh, B., 2003, 'Applications of artificial intelligence techniques for induction machine stator fault diagnostics: review', *4th IEEE International Symposium on Diagnostics for Electric Machines, Power Electronics and Drives–SDEMPED '03*, Atlanta-GA, USA, Aug. 24-26, 2003, pp. 29-34.

Smith, A.C., Dorrell, D.G., 1996, 'Calculation and measurement of unbalanced magnetic pull in cage induction motors with eccentric rotors. I. Analytical model', *IEE Proceedings on Electric Power Applications*, Vol. 43, Issue 3, May 1996, pp. 193-201.

SpectraQuest, 'Machinery Fault Simulator', *SpectraQuest Inc.*, Available on web at: www.spectraquest.com.

Stack, J. R., Habetler, T. G., Harley, R. G., 2003, 'Fault classification and fault signature production for rolling element bearings in electric machines', *4th IEEE International Symposium on Diagnostics for Electric Machines, Power Electronics and Drives–SDEMPED '03*, Atlanta-GA, USA, Aug. 24-26, 2003, pp. 172-176.

Stack, J.R. Habetler, T.G. Harley, R.G., 2004, 'Bearing fault detection via autoregressive stator current modeling', *IEEE Transactions on Industry Applications*, Vol. 40, Issue 3, pp. 740-747.

Stavrou, A., Sedding, H.G., Penman, J., 2001, 'Current monitoring for detecting inter-turn short circuits in induction motors', *IEEE Transactions on Energy Conversion*, Vol. 16, Issue 1, pp. 32-37.

Stone, G.C., Lloyd, B.A., Campbell, S.R., Sedding, H.G., 1997, 'Development of automatic, continuous partial discharge monitoring systems to detect motor and generator partial discharges', *IEEE International Electric Machines and Drives Conference–IEMDC '97,* Milwaukee-WI, USA, May 18-21, 1997, pp. MA2/3.1-MA2/3.3.

Tallam, R.M., Habetler, T.G., Harley, R.G., Gritter, D.J., Burton, B.H., 2000, 'Neural network based on-line stator winding turn fault detection for induction motors', *The 2000 IEEE Industry Applications Society Conference: The 35th IAS Annual Meeting*, Rome, Italy, Vol. 1, Oct. 8-12, pp. 375-380.

Tallam, R.M., Lee, S.B., Stone, G., Kliman, G.B., Yoo, J., Habetler, T.G., Harley, R.G., 2003, 'A survey of methods for detection of stator related faults in induction machines', *4th IEEE International Symposium on Diagnostics for Electric Machines, Power Electronics and Drives–SDEMPED '03*, Atlanta-GA, USA, Aug. 24-26, 2003, pp. 35-46.

Tavner, P., Penman, J., 1987, '*Condition Monitoring of Electrical Machines*', Research studies press LTD, 1987. ISSN/ISBN: 0-86380-061-0, 302 p.

Tavner, P.J., Anderson, A.F., 2005, 'Core faults in large generators', *IEE Proceedings on Electric Power Applications*, Vol. 152, Issue 6, pp. 1427-1439.

Tenhunen, A., Holopainen, T.P., Arkkio, A., 2003, 'Impulse method to calculate the frequency response of the electromagnetic forces on whirling cage rotors', *IEE Proceedings on Electric Power Applications*, Vol. 150, Issue 6, pp. 752-756.

Thailly, D. Romary, R. Brudny, J.-F., 2005, 'Quantitative analysis of the external radial magnetic field for detection of stator inter-turn short-circuit in induction machines', *European Conference on Power Electronics and Applications–EPE '05*, Dresden, Germany, Sept. 11-14, 2005, Available on CD.

Thomas, V.V., Vasudevan, K., Kumar, V.J., 2003, 'Online cage rotor fault detection using air-gap torque spectra', *IEEE Transactions on Energy Conversion*, Vol. 18, Issue 2, pp. 265-270.

Thomson, W. T., Deans, N. D., Leonard, R. A., Milne, A. J., 1983, 'Monitoring strategy for discriminating between different types of rotor cage faults', *Proceedings of the 18th Universities Power Engineering Conference–UPEC*, University of Surrey, Guildford, U.K., April 1983.

Thomson, W. T., 1992, 'On-line current monitoring–The influence of mechanical loads or a unique rotor design on the diagnosis of broken bars in induction motors', *10th International Conference on Electrical Machines–ICEM '92*, Manchester, U.K., Sept. 15-17, 1992, pp. 1236-1240.

Thomson, W.T., 1994, 'On-line current monitoring to detect electrical and mechanical faults in three-phase induction motor drives', *International Conference on Life Management of Power Plants*, Edinburgh-UK, Dec. 12-14, pp. 66-73.

Thomson, W. T., A Barbour, F Filippetti and C. Tassoni, 1998, 'An appraisal of the MMF-permeance method and finite element models to study static air-gap cccentricity in induction machines', *13th International Conference on Electrical Machines–ICEM '98*, Istanbul, Turkey, Sept. 2-4, 1998, pp. 218-227.

Thomson, W. T., 1999, 'A review of on-line condition monitoring techniques for three-phase squirrel-cage induction motors–past, present and future', *2nd IEEE International Symposium on Diagnostics for Electrical Machines, Power Electronics and Drives–SDEMPED '99,* Gijon, Spain, Sept. 1-3, 1999, pp. 3-17.

Thomson, W. T., 2001, 'On-line MCSA to diagnose shorted turns in low voltage stator windings of 3-phase induction motors prior to failure', *IEEE International Electric Machines and Drives Conference – IEMDC '01,* Cambridge-Massachusetts, USA, Jun. 17-20, pp. 891-898.

Thomson, W. T., Gilmore, R. J., 2003, 'Motor current signature analysis to detect faults in induction motor drives–fundamentals, data interpretation, and industrial case histories' *Proceedings of the 32nd Turbomachinery Symposium*, Houston, TX, USA, Sept. 8-11, pp. 145-156.

Thorsen, O. V., Dalva, M., 1999, 'Failure identification and analysis for high voltage induction molars in the petrochemical industry', *IEEE Transactions on Industry Applications*, Vol. 35, No. 4, pp. 810-818.

Toliyat, H.A., Lipo, T.A., 1995, 'Transient analysis of cage induction machines under stator, rotor bar and end ring faults', *IEEE Transactions on Energy Conversion*, Vol. 10, No. 2, pp. 241-247.

Trutt, F.C., Sottile, J., Kohler, J.L., 2002, 'Condition monitoring of induction motor stator windings using electrically excited vibrations', *The 2002 IEEE Industry Applications Society Conference: The 37th IAS Annual Meeting*, Vol. 4, pp. 2301-2305.

Trzynadlowski, A.M., Ritchie, E., 2000, 'Comparative investigation of diagnostic media for induction motors: a case of rotor cage faults', *IEEE Transactions on Industrial Electronics,* Vol. 47, Issue 5, pp. 1092-1099.

Tsoumas, I.; Mitronikas, E.; Safacas, A.; 2005, 'Induction motor mixed fault diagnosis based on wavelet analysis of the current space vector', *8th International Conference on Electrical Machines and Systems-ICEMS 2005*, Vol. 3, 27-29 Sept., 2005, pp. 2186-2191.

Vas, P., 1993, '*Parameter estimation, condition monitoring, and diagnosis of electrical machines*', Oxford, Clarendon, 1993, ISBN: 0198593759, 378 p.

Vas, P., 1999, '*Artificial-Intelligence-based electrical machines and drives: Application of fuzzy, fuzzy-neural, and genetic-algorithm-based techniques*', New York, Oxford Press, 1999, ISBN: 019859397X, 656 p.

Villada, F., Cadavid, D., Munoz, N., Valencia, D., Parra, D., 2003, 'Fault diagnosis in induction motors fed by PWM inverters', *4th IEEE International Symposium on Diagnostics for Electric Machines, Power Electronics and Drives–SDEMPED' 03,* Atlanta-GA, USA, Aug. 24-26, 2003, pp. 229-234.

Wang, C., Gao, R. X., 2000, 'Sensor placement strategy for in-situ bearing defect detection', *Proceedings of the 17th IEEE Instrumentation and Measurement Technology Conference–IMTC*, Baltimore-MD, USA, May 1-4, Vol. 3, pp. 1463-1467.

Wiedenbrug, E., Frey, G.; Wilson, J., 2003, 'Impulse testing as a predictive maintenance tool', *4th IEEE International Symposium on Diagnostics for Electric Machines, Power Electronics and Drives–SDEMPED '03*, Atlanta-GA, USA, Aug. 24-26, pp. 13-19.

Wieser, R., Kral, C., Pirker, F., Schagginger, M., 1999, 'On-line rotor cage monitoring of inverter-fed induction machines by means of an improved method', *IEEE Transactions on Power Electronics,* Vol. 14, Issue 5, pp. 858-865.

Williamson, S., Mirzoian, P., 1985, 'Analysis of cage induction motor with stator winding faults', *IEEE Transactions on Power Apparatus and Systems*, July 1985, Vol. 104, No. 7, pp. 1838-1842.

Williamson, S., 2004, 'The future of electrical machines', *Proceedings of International Conference on Power Electronics Systems and Applications*, Hong Kong, Nov. 9-11, 2004, pp. 11-12.

Yazidi, A., Thailly, D., Henao, H., Romary, R., Capolino, G.-A., Brudny, J.-F., 2004, 'Detection of stator short-circuit in induction machines using an external leakage flux sensor', *IEEE International Conference on Industrial Technology–ICIT '04,* Dec. 8-10, 2004, Hammamet, Tunisia, Vol. 1, pp 166-169.

Yen, G. G., Lin, K. C., 2000, 'Wavelet Packet Feature Extraction for Vibration Monitoring', *IEEE Transactions on Industrial Electronics*, Vol. 47, Issue 3, pp. 650-667.

Appendix I – Information about the measurement devices

Transient recorder W+W700

Mainframe: Includes measuring computer, 9-inch monochrome display screen, control unit, 3½ inch micro floppy drive for software load and as a mass storage medium for measurement data. Space for 4 single or dual channels. Support for external colour monitor for menu and signal presentation.

Retrofit to AT processor with external keyboard and 42- or 100-MB internal hard disk available.

Expansion Frame: for further 8 single or dual channels. Up to three additional frames can be connected for a total of 32 channels.

Single channels: They include pre-amplifiers with different inputs, 8 bits trigger, for level, window, slew rate, and reference band.
Timeout with linkage possibilities.
Storage up to 256 Kwords, 1Mwords as option.
Dual time base.
Anti-aliasing filter.

Channel types:
50-MHz 8-bit
50-MHz 10-bit
100-MHz 12-bit

Dual channels
They include two pre-amplifiers with differential input,
8 bit trigger, level, window, slew rate.
Timeout with linkage possibilities.
Storage per channel 256 kWords, 1 Mword as option.
Dual time base.
Anti aliasing filter.

Channel types:
20-MHz 8-bit dual
1-MHz 12-bit dual
200-kHz 12-bit dual

-- In the main frame and expansion frame any combination of channels is possible.

Markers
As an option some channels can be equipped with marker inputs. Markers are signals which can only assume the logical states 0 or 1. The number of markers available depends on the bit count of the respective signal inputs:

8-bit 50-MHz   8 Markers
8-bit 20-MHz dual   no Markers
12-bit 10-MHz   4 Markers
12-bit 1-MHz dual 2×4 Markers
12-bit 200-kHz dual 2×4 Markers

The pre-amplifiers are adapted to the maximum sampling rate and the resolution of the channel. The differential outputs are switchable to asymmetric inputs. AC or DC signal coupling can be selected.

The pre-amplifiers are equipped with an anti-aliasing filter of the four-pole vessel type with five selectable frequencies.

Time base

Each channel is equipped with a dual time base with trigger delay selectable from -100% to 400%.

The time elapsed since arming the channel assures the correct time relationship between channels with different trigger timing.

Trigger

The trigger source of a channel can be defined as the main trigger for the whole instrument or as a local trigger for the respective channel. In addition, the trigger method listed below can be combined with the main trigger for the whole instrument: OR/AND/OFF. Triggering from an external source and manual triggering (TRIGGER KEY) are also possible.

For each channel an individual trigger with the following possibilities is available:
---level trigger for rising and falling edge.
---window trigger, in, out.
---slew rate.
---time-out trigger for the forgoing trigger method.
   Trigger is activated if a trigger event does not occur within a specified time frame.
---reference band trigger for the comparison of two signals.

Channel memories

The channels are equipped with a memory of 25 kWords each. A 1-MWord option and, for the 1-MHz and 200-kHz channels, a 64-kW memory option is available.

Signal presentation

On the screen up to 8 channels can be displayed simultaneously in correct relation to the time axis. You can select, move, and zoom the signals with the help of the cursor and control wheel.

The following forms of representation are available:
---Yt: up to 8 signals, amplitude in relation to time.
---DUAL: up to 4 signals with different presentation in two windows.
---Two separately: up to 8 signals in two independent windows with independent manipulation.
---X-Y.
---X-Y-t: in preparation.

Operating

The combination of a pop-up menu and control wheel makes possible the simple and fast handling of the W+W700.

User programming

The inherent versatility of the W+W700 can be further enhanced by user-originated programs written in any desired program language.

Interactive control of the W+W700 by the user program enables the measurements sequences to be automated and the processing of measuring data to be specific to the application involved. For Turbo Pascal, version 5.0 and up, complete program units are available, which makes programming easier.

Norma Wide Band Power analyser

Device configuration: Three configurations are preset by the manufacturer.
One configuration is stored on power-down.
5 configurations can be stored by the customer.

Zero suppression: RMS and Rectified Mean value <1% of range are displayed as 0.
Power values (P, S, Q) <0,01% are displayed as zero.
Integration values below these limits are ignored.

Angular error: between voltage and current:
Angular error influence by current range in Mode AC+DC without LP filter.

Valid for			
Frequency range	0…100Hz	100…1kHz	Add. Error
Range			
50 mV	00.015°	0.020°	0.005 °/kHz
158 mV	0.005°	0.010°	0.005 °/kHz
500 mV	0.005°	0.005°	0.005 °/kHz
1580 mV	0.005°	0.005°	0.005 °/kHz

Channel separation: >5 dB at 100 kHz

Trigger input: TTL signal, overload max. 250 V_{RMS}
Trigger distance> average time B+ 1 s,
Trigger delay: EXT.TRG<100 µs
IEEEBUS *TRG<600 µs

Synchronization: Internal: 10 Hz….10 kHz of CH1…..CH6 resp. CH12
External: 10 Hz…10kHz; 3V…..50 V_{RMS} ;overload max. 250 V_{RMS} ;
Common-mode voltage $\leq 5 V_p$

Real Time Clock: 1 min. per month

Integrator: time error: $\pm 0.0025\% + 10$ µs
The integration time always corresponds to integer multiples of averaging
Period A

Voltage channel

Nominal voltage: max. 1000 V_{RMS}

Measuring voltage: max. 1000 V_{RMS} or 2500 V_p , DC …..1MHz sinusoidal

Bandwidth: DC…2MHz
Sampling rate: 35…70 kHZ
Voltage frequency product: max. 10^9 VHz
Rise time: slew rate max. 10kV/µs

Measuring accuracy: apply to a sinusoidal signal at ≤4% distortion factor and a level of ≥¨10% of range (V_p) in the nominal temperature range for 1 year after calibration at $23 \pm 1K$.

Limits of errors $\pm$ (% of m.v.+% of range)

Frequency range	AC+DC	AC
45Hz…65Hz	$\pm$ (0.05+0.02)	$\pm$ (0.05+0.005)
65Hz….1kHz	$\pm$ (0.12+0.03)	$\pm$ (0.12+0.005)

Current channel

Shunt factor: Is read automatically from EEPROM in shunt.

Measuring voltage: max. 1.1 V_{RMS} or 1,58 V_P. DC…..1MHz sinusoidal.

Bandwidth: DC…..>1.2 Mhz
Sampling rate: 35…70 kHz
Overload Protection up to: 250 V_{RMS} ,350 V_P in all range

Voltage frequency product: max. 10^7
Rise time: slew rate: 30 V/μs

Measuring accuracy: apply to a sinusoidal signal at ≤4% distortion factor and a level of ≥¨10% of range (V_p) in the nominal temperature range for 1 year after calibration at $23 \pm 1K$.

Limits of errors $\pm$ (% of m.v.+% of range)

Frequency range	AC+DC	AC
45Hz…65Hz	$\pm$ (0.05+0.02)	$\pm$ (0.05+0.005)
65Hz….1kHz	$\pm$ (0.12+0.05)	$\pm$ (0.12+0.005)

Appendix II Stator winding configurations

"NB" no parallel branches

1	2	3	4	5	6	7	8	9	10	11	12	13	14	15	16	17	18	19	20	21	22	23	24
A+	A+	A+	A+	C-	C-	C-	C-	B+	B+	B+	B+	A-	A-	A	A-	C+	C+	C+	C+	B-	B-	B-	B-

25	26	27	28	29	30	31	32	33	34	35	36	37	38	39	40	41	42	43	44	45	46	47	48
A+	A+	A+	A+	C-	C-	C-	C-	B+	B+	B+	B+	A-	A-	A-	A-	C+	C+	C+	C+	B-	B-	B-	B-

"2B" Two parallel branches

1	2	3	4	5	6	7	8	9	10	11	12	13	14	15	16	17	18	19	20	21	22	23	24
A1+	A1+	A1+	A1+	C1-	C1-	C1-	C1-	B1+	B1+	B1+	B1+	A1-	A1-	A1-	A1-	C1+	C1+	C1+	C1+	B1-	B1-	B1-	B1-

25	26	27	28	29	30	31	32	33	34	35	36	37	38	39	40	41	42	43	44	45	46	47	48
A2+	A2+	A2+	A2+	C2-	C2-	C2-	C2-	B2+	B2+	B2+	B2+	A2-	A2-	A2-	A2-	C2+	C2+	C2+	C2+	B2-	B2-	B2-	B2-

"SB" Two branches; special

1	2	3	4	5	6	7	8	9	10	11	12	13	14	15	16	17	18	19	20	21	22	23	24
A1+	A1+	A2+	A2+	C1-	C1-	C2-	C2-	B1+	B1+	B2+	B2+	A1-	A1-	A2-	A2-	C1+	C1+	C2+	C2+	B1-	B1-	B2-	B2-

25	26	27	28	29	30	31	32	33	34	35	36	37	38	39	40	41	42	43	44	45	46	47	48
A1+	A1+	A2+	A2+	C1-	C1-	C2-	C2-	B1+	B1+	B2+	B2+	A1-	A1-	A2-	A2-	C1+	C1+	C2+	C2+	B1-	B1-	B2+	B2+

"4B" Four parallel branches

1	2	3	4	5	6	7	8	9	10	11	12	13	14	15	16	17	18	19	20	21	22	23	24
A1+	A1+	A1+	A1+	C1-	C1-	C1-	C1-	B1+	B1+	B1+	B1+	A2-	A2-	A2-	A2-	C2+	C2+	C2+	C2+	B2-	B2-	B2-	B2-
A4+	A4+	A4+	A4+	C4-	C4-	C4-	C4-	B4+	B4+	B4+	B4+	A1-	A1-	A1-	A1-	C1+	C1+	C1+	C1+	B1-	B1-	B1-	B1-

25	26	27	28	29	30	31	32	33	34	35	36	37	38	39	40	41	42	43	44	45	46	47	48
A3+	A3+	A3+	A3+	C3-	C3-	C3-	C3-	B3+	B3+	B3+	B3+	A4-	A4-	A4-	A4-	C4+	C4+	C4+	C4+	B4-	B4-	B4-	B4-
A2+	A2+	A2+	A2+	C2-	C2-	C2-	C2-	B2+	B2+	B2+	B2+	A3-	A3-	A3-	A3-	C3+	C3+	C3+	C3+	B3-	B3-	B3-	B3-

SB

139

4B